GEOLOGIC HISTORY OF WATER ON MARS:

REGIONAL EVOLUTION OF AQUEOUS AND GLACIAL PROCESSES IN THE SOUTHERN HIGHLANDS, THROUGH TIME

Dissertation zur Erlangung des akademischen Grades eines Doktors der Naturwissenschaften (Dr. rer. nat)

vorgelegt als kumulative Arbeit
am Fachbereich Geowissenschaften
der Freien Universität Berlin

von

SOLMAZ ADELI

Berlin, 2016

Erstgutachter: Prof. Dr. Ralf Jaumann
Freie Universität Berlin
Institut für Geologische Wissenschaften
Arbeitsbereich Planetologie
sowie
Deutsches Zentrum für Luft- und Raumfahrt
Institut für Planetenforschung,
Abteilung Planetengeologie

Zweitgutachter: Prof. Dr. Michael Schneider
Freie Universität Berlin
Institut für Geologische Wissenschaften
Arbeitsbereich Hydrogeologie

Tag der Disputation: 22 July 2016

To my mother and my grandmother,
the two strong women who inspired me the most,
to follow my dreams, and to never give up.

تقدیم به مادر و مادر بزرگم
به دو زن قوی که الهام دهنده ی من بودند
تا آرزو هایم را دنبال کنم و هرگز تسلیم نشوم

EIDESSTATTLICHE ERKLAERUNG

Hiermit versichere ich, die vorliegende Arbeit selbstständig angefertigt und keine anderen als die angeführten Quellen und Hilfsmittel benutzt zu haben.

Solmaz Adeli

Berlin, 2016

Acknowledgement

First of all, I would like to thank my supervisor Prof. Dr. Ralf Jaumann for giving me the opportunity of working at the Deutsches Zentrum für Luft- und Raumfahrt (DLR). I wish to thank him particularly for standing behind me in all the ups and downs. Herr Jaumann, I am so deeply grateful for your support and your trust. Danke schön!

This work would have not been achieved without the support of Ernst Hauber, my second supervisor. I have also been most fortunate to be able to work with him, and I have greatly appreciated the countless hours of discussions, all his advice regarding scientific issues, his feedbacks on my manuscripts, and everything. Thank you, Ernst!

I am grateful to Prof. Dr. Michael Schneider, Freie Universität Berlin, Institut für Geologische Wissenschaften, who kindly accepted to be examiner of this dissertation.

A special merci beaucoup for Laetitia Le Deit, who has been my best friend since the very first moment that I met her. She helped me through my Ph.D. as well as integration into Berlin and DLR.

A warm thank you goes to Frank Trauthan, with whom I shared each and every moment of my time at DLR, building 103, office 323. Vielen Dank, Frank!

I have appreciated the fruitful collaboration with Maarten Kleinhans at the Faculty of Geosciences, Universiteit Utrecht. Thanks Maarten for all your comments, and feedbacks, and also Thomas Platz at Max Planck Institute for Solar System Research.

I wish to thank all DLR colleagues, with whom I shared unforgettable moments, especially Karin Eichentopf, who is my inspiration. A danke schön to Katrin Stephan, Ekkehard Kührt, Claudia Hauschid, and Irene Vogt! To my dear friends who were there for me in all moments: Christian Althaus, Line Drube, Jérémy Brossier, and Mickael Baqué.

I would like to acknowledge the valuable discussions with Nicolas Mangold during my Ph.D. as well as my Master's internship which he supervised at the Laboratoire de Planétologie et Géodynamique de Nantes. And a warm merci to all the colleagues and friends at LPGN!

Thanks to Stephan van Gasselt and Greg Michael at the Freie Universitaet zu Berlin for their advice and help, also to all the colleagues at the FUB.

My acknowledgement list would not be finished without thinking about the professors, colleagues and dear friends at the Université Joseph Fourier, Observatoire des Sciences de l'Université de Grenoble and particularly at Institut de Planetologie et d'Astrophysique de

Grenoble where I first touched upon the planetary science. A very special thank you to Pierre Beck, Cyril Grima, Wlodeck Kofman, Thomas Appéré, and Eric Lewin.

I would like to mention my professors from the Azad University of Ashtian in Iran, particularly Maziar Nazari, and also my comrades: Elham Rahbar, Arash, and Kaveh Mehrkian, who have had a strong influence on my way from Tehran to Grenoble and later to Berlin.

My best friends, Kelly Antonini, Joana Oliveira, Katrin and Rainer Thürling: all I can say is a big big thank you. Thanks for being my friends. Thanks for all the wonderful moments that we have spent together and for the ones to come.

I was lucky to have Marc Kunstmann by my side in the hard moments of the last months of my Ph.D. Merci pour tout, Marc, surtout pour ta patience!

The last word is to my lovely mother. Mom, I am dedicating this thesis to you and to grandma, *Maman-Riahi*. I would have never ever been here without your unconditional love, endless support, and faith in me. *Azat kheili kheili manoonam, Mani joonam, baraye hamechi!* And of course my beloved dad … whose thoughts will always live in my heart … *Babai, kash boodi o in rooz o mididi!*

ABSTRACT

The history of water on Mars, after more than four decades of remote sensing investigation, has still some ambiguities. This work focuses on the major geological aspects of presence of water on the Martian surface in a regional scale, with the aim of reconstructing the evolution of aqueous activities in the Terra Sirenum–Terra Cimmeria region from the late Noachian epoch to the late Amazonian and current conditions. The research presented here is based on geomorphological observation, geological mapping, spectroscopical investigation, hydraulic analysis, and age determination by using imagery, topographic, and spectroscopic data. The study area is thought to have played host to one of the largest paleolakes on Mars, known as the Eridania lake which is believed to have existed during middle-late Noachian. This work provides new insights into the depositional, erosional, alteration mechanisms, and development of liquid water existence from the early Mars large bodies of water (e.g., Eridania lake), into local Amazonian fluvial and ice-related features.

The large Eridania lake drained into the Ma'adim Valles and transformed into isolated closed lakes after the late Noachian-early Hesperian boundary. The closed lakes may have lasted over a long geological time, believed to be during the Hesperian period, which is evidenced mainly by the thickness of the sediments and various alteration products. The presence of materials rich in Fe/Mg-phyllosilicates, Al-phyllosilicates, and chloride salts, in addition to their stratigraphical relation, suggests chemical environment change(s) at the last stages of the lakes existence and/or after their desiccation. The produced geologic map combined with the age determination results show that the bodies of water, related alteration and erosional processes, took place before the early Amazonian epoch. The presence of a ~340 km long fluvial valley system located southwest of the Eridania lake hypothesised shoreline, dated as early to middle Amazonian, indicates that the liquid water presence on the surface of the Terra Sirenum–Terra Cimmeria region has not completely ceased after the isolated lakes disappearance. At the downstream section of the fluvial system a unique braided alluvial fan has been observed in the Kārūn Valles, which has not been previously reported. The morphological observations and hydraulic analysis point to geologically short-term event(s) which may have taken a few days up to a few tens of thousands of days to form the Kārūn Valles alluvial fan, and consequently the correspondent upstream fluvial features. The source of water is assessed as surface run-off due to ice/snow melt. This observation reveals that liquid water was present on the Martian surface during early-middle Amazonian. Under the current climatic conditions, which do not sustain the accumulation of ice/snow on the surface, several ice-rich and glacial-related features have been observed on the floor of the mentioned valley system. The morphology and stratigraphy of these valley fill deposits (VFD) infer to a formation prior to the latitude dependent mantle (LDM) emplacement. The VFD presence supports the previously hypothesised Amazonian climate change phases, at mid-latitudes, due to obliquity oscillations. These deposits, their host fluvial valley, and the rich past aqueous history of Terra Sirenum-Terra Cimmeria, show that the water re-appeared on the Martian surface repeatedly over time, although its abundance decreased from the late Noachian to the current late Amazonian epoch.

KURZFASSUNG

Selbst nach vier Jahrzehnten der fernerkundlichen Erforschung, ist die Entwicklung der Wasservorkommen auf dem Mars nicht vollständig verstanden. Diese Arbeit legt ihr Augenmerk auf die wichtigsten geologischen Aspekte von Wasservorkommen auf der Marsoberfläche in regionalem Maßstab. Das Ziel ist die aquatische Entwicklung in den Regionen Terra Cimmeria und Terra Sirenum seit der späten Noachischen bis zur späten Amazonischen Periode und bis hin zu den heutigen Bedingungen zu rekonstruieren. Die hier präsentierte Forschung wurde auf Grundlage von geomorphologischen Beobachtungen, geologischen Kartierungen, spektroskopischen und hydraulischen Untersuchungen, sowie Altersbestimmungen mithilfe von Bilddaten, topografischen und spektroskopischen Daten gemacht. Es wird davon ausgegangen, dass die untersuchte Region einen der größten Paläoseen des Mars, den Eridania See, beinhaltete. Dieser existierte während der mittleren bis späten Noachiaschen Periode. Neue Erkenntnisse über die Ablagerungs-, Erosions- und Verwitterungsprozesse werden ebenso dargestellt, wie die Entwicklung der großen flüssigen Wasservorkommen der frühen Marszeit (z.B. Eridania See) zu den fluvialen und glaziären Formen der Amazonischen Periode.

Nach dem Übergang der späten Noachischen zur frühen Hesperianischen Periode floss der große Eridania See in das Ma`adim Valles ab und formte einzelne geschlossene Seen. Diese isolierten Seen können während der Hesperianischen Periode über eine geologisch lange Zeit vorhanden gewesen sein, was hauptsächlich durch die Mächtigkeit der Sedimente und verschiedene Alterationsprodukte bekräftigt wird. Die Anwesenheit von Material, das reich an Fe/Mg-Schichtsilikaten, Al-Schichtsilikaten und Chloridsalzen ist, sowie dessen stratigrafischer Vergleich, suggerieren eine chemische Umgebungsänderung während der letzten Phase der Seen und/oder nach dessen Austrocknung. Die geologische Karte und die Ergebnisse der Altersbestimmung deuten darauf hin, dass die Wasservorkommen und die dazugehörigen Verwitterungs- und Erosionsprozesse vor der frühen Amazonischen Periode stattgefunden haben. Die Anwesenheit eines ~340 km langen Flusssystems, welches sich auf die frühe bis mittlere Amazonische Periode datieren lässt und sich im Südwesten der hypothetischen Uferlinie des Eridania Sees befindet, deutet weiter darauf hin, dass das flüssige Oberflächenwasser nach Verschwinden der isolierten Seen auf Terra Sirenum-Terra Cimmeria nicht vollständig verschwand. Ein einzigartiger, verflochtener alluvialer Fächer, über welchen bisher keine Berichte existieren, befindet sich im Bereich flussabwärts des Flusssystems. Die morphologischen Beobachtungen, sowie die hydraulische Analyse, deuten auf ein geologisch kurzes Ereignis, das wenige bis zu einigen zehntausend Tagen für den Formationsprozess des alluvialen Fächers im Kārūn Valles brauchte und folglich für die dazugehörigen fluvialen Formen flussaufwärts sorgte. Die Wasserquelle ist vermutlich ein Oberflächenausfluss, der durch die Schmelze von Eis/Schnee entstand. Diese Erkenntnis impliziert, dass flüssiges Wasser auf der Marsoberfläche während der frühen bis mittleren Amazonischen Periode vorhanden war. Unter den aktuellen Klimabedingungen, welche keine dauerhafte Ansammlung von Eis/Schnee an der Oberfläche erlauben, wurden verschiedene eisreiche Strukturen und glaziale Strukturen auf dem Grund des beschriebenen Flusssystems beobachtet. Die Morphologie und Stratigraphie dieser sogenannten „valley fill deposits“ (VFD) lassen auf deren Formation vor der Ablagerung des sogenannten „latitude dependent mantle (LDM)“ schließen. Die Anwesenheit der VFD stützt die Annahme der durch Oszillation der Planetenrotationsachse entstehenden Klimaänderungen in den mittleren Breiten während der Amazonischen Periode. Diese Ablagerungen, ihr Herkunftsgebiet (das Flusssystem) und die üppige fluviale Vergangenheit der Terra Sirenum-Terra Cimmeria Region deuten darauf hin, dass

Wasser wiederholt auf der Marsoberfläche vorkam. Seine Menge nahm jedoch seit der späten Noachischen bis zu der heutigen späten Amazonischen Epoche ab.

TABLE OF CONTENTS

LIST OF FIGURES

LIST OF TABLES

1. INTRODUCTION

Mars, after Earth, is the only planet known to have geological history involving a water cycle on the planet's surface in the forms of ice, liquid, and vapour. Although Mars under its current condition is a frozen hyperarid desert, but there is extensive evidence of liquid water and ice presence on the planet's surface over its geologic history [e.g., *Carr*, 1995; *Cabrol and Grin*, 1999; *Baker*, 2001; *Craddock and Howard*, 2002; *Christensen et al.*, 2004a; *Bibring et al.*, 2006]. It is now more than four decades that the role of water in the Martian surface evolution is being investigated. Currently active orbital and rover missions are listed in Table 1.1. The first images revealing liquid water-worn valleys on the Martian surface were taken by Mariner 9 in late 1971 and completely changed our view about Mars from a geologically inactive and cratered planet to a planet with polar caps, volcanoes, tectonics, and fluvial valleys. Today we know that Mars has had a long and complex history of geologic activity, including volcanism, tectonic, impact, erosion, sedimentation, and weathering [e.g., *Carr and Head*, 2010; *Jaumann et al.*, 2014]. The highest volcano in the solar system, Olympus Mons, is located in Tharsis region of Mars (Figure 1.1). Volcanism probably started very early in the planet's history, and it may still occur today. Most of the large volcanoes on Mars are similar to terrestrial shield volcanoes, which form mostly by eruption of relatively fluid and basaltic lava [e.g., *Scott*, 1985; *Greeley et al.*, 2005]. Tectonic activity on Mars is partly linked to the rise of the Tharsis region which occurred during the Noachian period [*Carr*, 2007]. Formation of Tharsis appears to have mainly affected the planet's surface. In addition, the global north-south dichotomy is one of the main features corresponds to tectonic on the planet. The dichotomy between the heavily craters southern highlands and the sparsely cratered northern lowlands is one of the most remarkable features on the plant's surface [*Scott*, 1978]. Another distinctive landform on Mars is impact craters. Craters form as a result of high-velocity collision between planets and comets and asteroids orbiting the Sun [*Melosh and Vickery*, 1989]. The Lunar record shows that prior to 3.5 Gyr ago the crater formation rate was dramatically higher. This is known as heavy bombardment, which is believed to have roughly ended around 3.8 Gyr ago [*Hartmann and Neukum*, 2001].

Table 1.1: List of currently active missions around Mars. The data, which are used in this dissertation, are specified in the remarks column.

Spacecraft	Operator	Launch	Remarks
Mars Odyssey orbiter	NASA	2001	Data used in this dissertation
Mars Express orbiter	ESA	2003	Data used in this dissertation
Mars Exploration Rover (Opportunity rover)	NASA	2003	—
Mars Reconnaissance Orbiter	NASA	2005	Data used in this dissertation
Mars Science Laboratory (Curiosity rover)	NASA	2011	Some results used in this dissertation
Mars Orbiter Mission (MOM)	ISRO	2013	—
Mars Atmosphere and Volatile EvolutioN (MAVEN) orbiter	NASA	2013	—

Erosion by liquid water and aeolian activities are the two most known erosive mechanisms on Mars. Outflow channels and valley networks up to tens of kilometres across and lengths of a few hundreds to thousands of kilometres, incised the surface of the red planet. Numerous upland craters reveal evidence of standing bodies of water or lakes with flat floors due to the deposition of sediments [e.g., *Fassett and Head*, 2008; *Hauber et al.*, 2009; *Cabrol and Grin*, 2010]. Aqueous alteration products due to interaction with water have been observed widespread, including Fe/Mg- and Al-phyllosilicates, carbonates, sulfates, halides, gypsum [e.g., *Bishop et al.*, 2008b; *Mustard et al.*, 2008a; *Le Deit et al.*, 2012; *Loizeau et al.*, 2012; *Ruesch et al.*, 2012]. Dust devils, yardangs, and dunes are clear evidence of pervasive wind activity and have been observed both from orbit and on the ground [e.g., *Greeley et al.*, 1982; *Edgett and Malin*, 2000; *Malin and Edgett*, 2001; *Tirsch et al.*, 2011]. Erosion, sedimentation, and weathering as main surface shaping mechanisms are discussed in more detail in the following chapters (Figure 1.2).

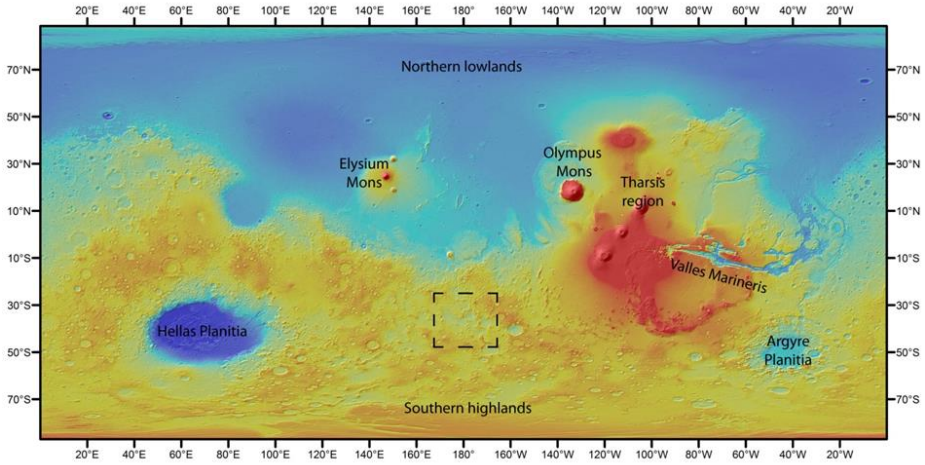

Figure 1.1: Global map of Mars with main surface features pointed out. The dashed box represents the study area. Data is from MOLA elevation colour map overlaying a MOLA hillshade map [Smith et al., 2001] to emphasize the topography.

From beginnings of telescopic observations of Mars, the question of "whether life could have started on that planet" has raised and stayed open and under debate ever since. The search for traces of life is one of the principal objectives of space exploration and particularly Mars exploration. Conditions at the surface today are very hostile for life, but orbital and *in-situ* rover data have shown and it is now widely accepted in the scientific community that the past conditions on Mars were very different from present-day, and that it may have been more favourable for life to develop. The most essential issue, while discussing the habitable conditions, is the longevity of the water presence on the surface of Mars in liquid and/or ice form, as well as the possibility of subsurface reservoir of liquid water or shallow ice deposits. These matters are, however, still open questions. In this manuscript, the goal is to tackle the puzzle of history of liquid water on the Martian surface by reconstructing a regional geologic history and particularly aqueous activity, from late Noachian to late Amazonian, in an area where one of the largest paleolakes was located early in the history of Mars.

a. THE SURFACE OF MARS

In this section, a brief geologic history of Mars and its main surface processes are presented (Figure 1.2). The section is divided into the three Martian periods; Noachian, Hesperian, and Amazonian. The focus of this section, as well as, this manuscript is on the cratered southern highlands of Mars, where most of the fluvial activities, degraded craters, tectonic features, and altered minerals have been observed. Period and epoch boundaries throughout this manuscript are based on Neukum system [*Hartmann and Neukum*, 2001] from *Michael* [2013].

i. NOACHIAN PERIOD

The Noachian Period is named after heavily cratered Noachis Terra (means "Land of Noah"), which is the type area of the Noachian period and is located west of the Hellas basin in the Noachis map quadrangle (MC-27). The base of the Noachian is not well defined, as very ancient terrains of that age tend to be poorly preserved due to later resurfacing. The pre-Noachian extends from the planet formation time at around 4.5 Ga [*Nyquist et al.*, 2001] to the development of northern lowlands estimated as ~4.1 Ga [*Frey*, 2006]. The end of the Noachian period is defined approximately at 3.7 Ga ago by *Hartmann and Neukum* [2001], roughly coincident with the upper Hadean on Earth. The oldest observed crust and geologic activities on Mars are dated as early Noachian epoch, when the dichotomy and consequently the northern lowlands are formed likely either by impact or tectonic origin [*Nimmo and Tanaka*, 2005]. The most distinguishing features of Noachian period are a high cratering record, the accumulation of most of Tharsis, valley formation, and surface conditions that enabled the widespread hydrous weathering products such as phyllosilicates.

The volcanism has probably started during pre-Noachian time and Tharsis may already have started to accumulate. Tharsis and Elysium were particularly active during Noachian and volcanism was widespread on the planet's surface at that time [see *Carr and Head*, 2010]. The main impacts, resulting in formation of huge impact basins e.g., Hellas, Argyre, and Isidis, took place at this period. Phyllosilicate-bearing materials are exposed extensively in ancient Noachian terrains and indicate a long-term interaction of liquid water with the Martian crust early in its history [e.g., *Poulet et al.*, 2005; *Bibring et al.*, 2006; *Mustard et al.*, 2008a]. The broad distribution of valley networks [*Craddock and Howard*, 2002] and crater lakes [*Fassett and Head*, 2008] in the southern highlands reveals that former climatic conditions on Mars could most probably sustain flow of liquid water on the surface. Nonetheless, whether the Martian climate was warm and wet [*Craddock and Howard*, 2002] or cold and wet [*Fairén*, 2010] is still uncertain and under debate. At the end of the Noachian period the impact rate, valley formation, weathering, and erosion significantly decreased. This time is known as the boundary of late Noachian-early Hesperian, after which the aqueous activities were suppressed but did not completely cease.

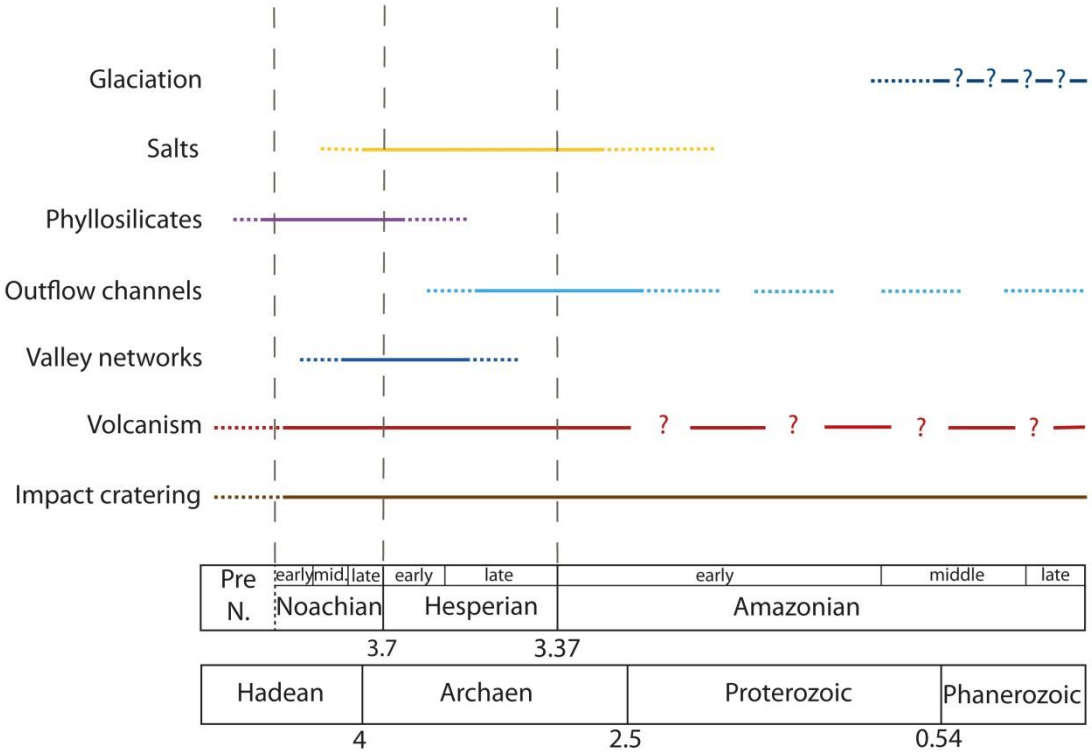

Figure 1.2: Major geological activities as a function of time on Mars, based on [Carr and Head, 2010; Ehlmann et al., 2011; Tanaka and Hartmann, 2012; Jaumann et al., 2014]. The period boundaries of Mars [Hartmann and Neukum, 2001] are compared with similar time subdivisions of Earth [Gradstein, 2012].

ii. HESPERIAN PERIOD

The Hesperian is named after Hesperia Planum, a moderately cratered highland region, which is the type area of the Hesperian period located in the Mare Tyrrhenum map quadrangle (MC-22). This period extends from the end of the heavy bombardment around 3.7 Gyr ago to ~3.37 Gyr ago [*Hartmann and Neukum*, 2001], roughly coinciding with the lower Archean on Earth. During the Hesperian period, the extensive volcanism has continued in the Tharsis and Elysium regions, as well as tectonism, chaotic terrain, and outflow channel development, northern plains and polar accumulations, and impact events which resulted in formation of large craters such as Gale, Holden, and Lowell. Hesperian volcanism is mainly evident in ridge plains [e.g., *Carr and Head*, 2010]. Tectonism during early Hesperian was dominated over most of Mars' surface [see *Tanaka et al.*, 2014 and references within] and formation of the chasmata of Valles Marineris continued. Catastrophic outflow flooding related to Tharsis and north of Valles Marineris and collapses which formed "chaotic terrain", led to a broad resurfacing of the Noachian terrain during Hesperian. Most of the large outflow channels on Mars are reported to be Hesperian-aged [*Tanaka*, 2005]. Some of them show features similar to lunar and venusian rilles, including streamlined islands, terraces, and anastomosing reaches [*Leverington*, 2004], and lava flows are clearly observable in some outflow channels. However, the outflow channels reveal more complex erosional features and are much larger

than the lunar and venusian rilles. They are more similar to large terrestrial outflow channels [*Baker et al.*, 1992]. A liquid water-related activity is also supported by sulfate-bearing deposits detected at source areas of some of these outflow channels, caused by chemical weathering in acidic environment [*Bibring et al.*, 2006; *Le Deit et al.*, 2008; *Jaumann et al.*, 2014]. The lack of clear morphologic evidence of source of water in some of these outflow channels indicates that they are formed by rapid release of large volumes such as an aquifer or a lake [see *Baker*, 2001; *Carr and Head*, 2010 and references within].

iii. AMAZONIAN PERIOD

Amazonis Planitia located in the Amazonis quadrangle (MC-8) is the type area for the Amazonian period and is characterized by low impact rates. The Amazonian period is the longest geologic period on Mars and extends from ~3.37 Ga until today [*Hartmann and Neukum*, 2001], roughly from the middle of the terrestrial Archean to the present. The erosion rates during the Amazonian were extremely low compare to the two previous periods, the global impact flux is reduced [*Hartmann and Neukum*, 2001], and the environment is oxidized [*Bibring et al.*, 2006]. Volcanism continued in the Amazonian but confined largely to the large shield volcanoes in the Tharsis and Elysium regions [*Greeley and Schneid*, 1991; *Jaumann et al.*, 2014]. Impact craters of Galle and Lyot are two examples of large impact events during this time. Amazonian climate is mainly characterised as cold and hyperarid. During the early Amazonian epoch (~3.37–~1.23 Ga [*Hartmann and Neukum*, 2001]) traces of fluvial activities have been observed in the highlands, such as channels [*Hynek et al.*, 2010] and fan-shaped deposits [*Hauber et al.*, 2013].

Under the current climatic conditions, water ice and glacier-related features have been observed on the surface of Mars in two different latitude ranges: in high latitudes (> 60°) and in mid latitudes (30°–60°). The high latitudes and pole areas show 3 km thick mounds of finely layered deposits [see *Carr*, 2007]. They are among the youngest deposits observed on the Martian surface. At each pole a ~1 m thick CO_2 ice is seasonally emplaced [*Malin et al.*, 2001]. In the mid latitude areas in both hemispheres, there is a 10 thick ice–dust mixture drape known as latitude dependent mantle (LDM) [*Mustard et al.*, 2001]. The LDM formation time is dated as a few million years [*Mustard et al.*, 2001; *Willmes et al.*, 2012], and its formative mechanism assumed to be caused by obliquity variations [*Kreslavsky and Head*, 2002; *Head et al.*, 2003; *Laskar et al.*, 2004; *Kostama et al.*, 2006]. Another very young and very likely water-related feature on the surface of Mars are gullies [*Malin and Edgett*, 2000b] and recurring slope lineae (RSL) [*McEwen et al.*, 2011a; *Ojha et al.*, 2014]. Gullies and RSLs are widely assumed as indicatives of near surface groundwater sources [*Malin and Edgett*, 2000b], although the possibility of dry ice origin, even though partly, cannot be completely ruled out [*Balme et al.*, 2006; *Dundas et al.*, 2015].

b. TERRA SIRENUM–TERRA CIMMERIA

Terra Sirenum and Terra Cimmeria are two regions of the southern highlands, located in the Memnonia, Phaethontis, and Eridania map quadrangles. A low-laying area in these two regions is believed to have once hosted one of the largest lakes on Mars, called Eridania lake, that drained through Ma'adim Vallis [*Irwin et al.*, 2002] toward the northern lowlands. The Eridania lake is hypothesized to have existed during the middle to late Noachian, and is a prime candidate for investigating and better understanding the early Mars climatic conditions, as lakes basins record the geological and environmental oscillations over a wide range of time and space. In addition to a rich aqueous past and early Mars presence of a large lake, this area has one of the largest chloride salts deposits [*Osterloo et al.*, 2008]. Phyllosilicate-rich material has, as well, been widely detected in the Eridania lake region [e.g., *Ruesch et al.*, 2012]. This broad diversity of minerals in the Eridania paleolake region reveals variation in chemical weathering resulting in alteration of minerals and on the other hand evaporates. Tectonism in Terra Sirenum and Terra Cimmeria has also played an important role. Sirenum Fossae extends from Tharsis region to Terra Cimmeria, and shows ancient activities during the early Hesperian as well as activities as young as middle Amazonian [*Kneissl et al.*, 2015]. Volcanism has also been reported in this area, such as middle Amazonian viscous lava flows [*Brož et al.*, 2015]. As this region is located in the mid latitudes of Mars, there has been several reports of the presence of ice-related features and glacial landforms which were most likely formed during middle to late Amazonian climate change phase [e.g., *Souness et al.*, 2012; *Levy et al.*, 2014].

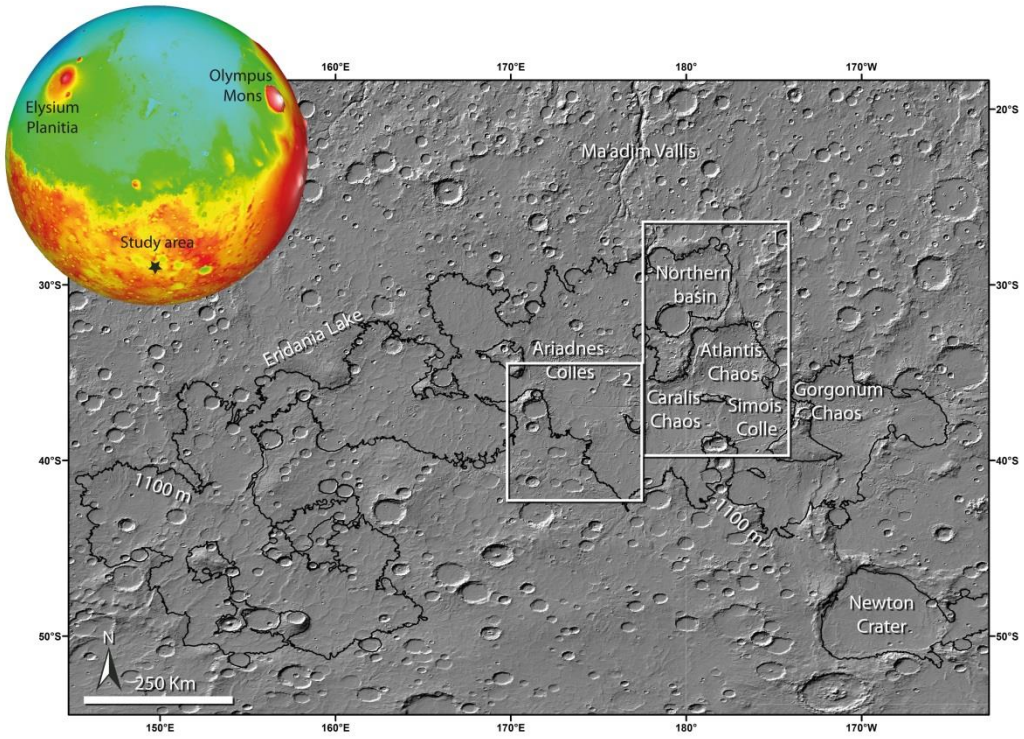

Figure 1.3: The study area with main physiographic elements, shown on a MOLA hillshade map. The two white boxes show the study areas discussed in Chapter 3 (box 1 at right) and Chapter 4 and 5 (box 2 at left). Black solid line corresponds to the contour line of 1100 m of Eridania paleolake upper limit. The top left hand map represents the study area location on Mars.

The Terra Sirenum and Terra Cimmeria region is geologically diverse, and this diversity offers a broad insight into the past and recent regional geological processes which shaped the Martian surface. Our main goal, in this work, is to understand the evolution of liquid water presence on the surface from the late Noachian/early Hesperian paleolakes-bearing environments to the cold and hyperarid current Amazonian conditions. It is essential for understanding the habitability possibilities to know whether the amount of surface liquid water, from the Noachian to Amazonian decreased gradually, or it was rather an episodic reappearance of liquid water on the surface. Investigating high-resolution images permit the observation of geomorphological evidence for erosional and depositional mechanisms. Analysing topographic data allows revealing the geometry of the area during their formation/deposition state as well as its development into the current morphology. Characterising the mineralogical composition of the sediments provides information about the chemical condition during the material deposition state. Hydraulic analysis leads to understanding the formative mechanism of valleys and the source of water. Crater size–frequency distribution (CSFD) would permit us to infer the timing of events. These approaches were used in order to assess the regional early Mars climatic condition, the transit between early Mars to Hesperian, and then to the Amazonian, in order to reconstruct the regional history of liquid water from late Noachian to present.

c. THESIS ORGANIZATION AND AUTHOR CONTRIBUTION

This cumulative dissertation consists of an introductory chapter (Chapter 1) including scientific background, aims, objectives, and motivations of this work as well as an introduction into the study area, followed by the Chapter 2, which describes the data and methods employed in this thesis in order to meet the objectives. The following three chapters (Chapter 3-5) include the original research papers published and/or submitted in peer-reviewed journals (as described below). They are stand-alone articles, and therefore contain individual introduction and conclusion sections. The last chapter (Chapter 6) summarize these three papers and discuss their conclusions. As first author of all three papers, I selected the study area, reviewed the relevant literature, processed the relevant data, chose the methods and approaches, analysed the data, interpreted the results, and concluded the work. The co-authors participated in discussion and draft manuscript reviews. Ralf Jaumann and Ernst Hauber were consulted during drafts preparation of all three papers, as they supervised this doctoral work. In the paper of Chapter 3, Laetitia Le Deit guided me for spectroscopical analysis. In the paper of Chapter 4, Maarten Kleinhans contributed in hydraulic modelling, Thomas Platz was partly consulted in crater size–frequency distribution, and Peter Fawdon produced the CTX DTM used for the hydraulic modelling.

Chapter 3 contains a paper published as **S. Adeli,** E. Hauber, L. Le Deit, and R. Jaumann (2015), Geologic evolution of the eastern Eridania basin: Implications for aqueous processes in the southern highlands of Mars (2015), *Journal of Geophysical Research-Planets*, 120, 1774-1799, doi: http://dx.doi.org/10.1002/2015JE004898. It describes the investigation of the geologic history of the eastern part of the Eridania paleolake located in

Terra Sirenum, in order to understand the role of water in observed mineralogical setting and reconstructing the timing of events from the late Noachian to the early Amazonian. This paper has been featured on the ESA Science & Technology web site on 10 May 2016, in an article titled as "The rise and fall of Martian lakes" and could be found in http://sci.esa.int/mars-express/57796-the-rise-and-fall-of-martian-lakes/.

Chapter 4 includes a paper published as **S. Adeli,** E. Hauber, M. Kleinhans, L. Le Deit, T. Platz, P. Fawdon, and R. Jaumann (2016). Amazonian-aged fluvial system and associated ice-related features in Terra Cimmeria, Mars (2016), *Icarus*, 277, 286-299, doi: http://dx.doi.org/10.1016/j.icarus.2016.05.020. The paper deals with the fluvial activity and presence of ice-rich deposits in Terra Cimmeria from the early to middle Amazonian with the aim of better understanding the Amazonian climate and climate change(s), and transit between early Mars to the Amazonian period.

Chapter 5 represents a paper submitted as **S. Adeli,** E. Hauber, and R. Jaumann. Geomorphology of ice-rich valley fill deposits in Terra Cimmeria, Mars: Implications for Amazonian climate changes, submitted to *Geophysical Research Letters (GRL)*. This paper is focusing on the present existence of ice-rich and glacial-like deposits on the surface of Terra Cimmeria. This paper reports a new class of ice-rich features, which have not been reported previously, and offers insight into the current climatic conditions on Mars.

2. DATA AND METHODS

Data from various data sets, instruments, and spacecrafts have been used in this work with the aim of combining imagery, topographic, and spectroscopic data in addition to applying several methods including geologic and geomorphologic mapping, spectroscopic analysis, hydraulic modelling, and crater size–frequency distribution. This multi-dataset approach permitted to reach the objectives of this study. The data used in this work are presented in Table 2.1. There is also a detail explanation related to each data set, related instruments, and methods in the "data and methods" or "introduction" section of each paper (chapters 3, 4, and 5). A brief description about the data processing as well as applied methods is offered in this section.

a. DATASETS AND DATA PROCESSING

In remote sensing, data processing is one of the basic and major steps toward geologic investigation and interpretation. On Mars, although data acquisition is limited to current active missions (Table 1.1); we still have large different datasets with various data type and resolutions to work with. Table 2.1 summarizes the data used in this work with relevant citations to the technical information for each instrument. A detailed description of dataset resolution and processing (if applicable) is presented in each corresponding section (i.e., section 3-b; 4-b, and 5-a), however, the two next parts summarize the implied datasets.

i. IMAGERY DATA AND TOPOGRAPHIC DATA

The Imagery and topographic data used in this work are from High Resolution Stereo Camera (HRSC) [*Neukum et al.*, 2004; *Jaumann et al.*, 2007] on board Mars Express (MEX), Context Camera (CTX) [*Malin et al.*, 2007], High Resolution Imaging Science Experiment (HiRISE) [*McEwen et al.*, 2007] on board Mars Reconnaissance Orbiter (MRO), and Mars Orbiter Laser Altimeter (MOLA) [*Smith et al.*, 2001] on board Mars Global Surveyor (MGS). The HRSC data used in this work are available via the HRSC team website. Besides HRSC data, all other datasets were downloaded from PDS Geosciences Node archive (http://pds-geosciences.wustl.edu/). The HRSC imagery and topographic data have been prepared for insertion into the mapping software, ArcGIS, using VICAR (Video Image Communication And Retrieval) routines developed and provided by DLR Berlin. For this work, no special data processing has been done on HRSC data, besides preparing ArcGIS compatible files. Data processing methods and issues are described in *Scholten et al.* [2005] and *Gwinner et al.* [2010]. The CTX imagery data have been processed and converted to ArcGIS compatible data via ISIS (Integrated Software for Imaging Spectrometers). In order to process HiRISE images, Perl programming language has been used. The Perl scripts are available in USGS website (http://webgis.wr.usgs.gov/pigwad/tutorials/scripts/perl.htm). The MOLA data were directly downloaded from the PDS Geosciences Node archive. The resolution of each imagery data used in this work, is described in the relevant "data" part of the each paper (Chapters 3, 4, and 5).

The topographic data in this work are from the Mars Orbiter Laser Altimeter (MOLA), High Resolution Stereo Camera (HRSC), and Context Camera (CTX). The MOLA pulsed laser obtained altimetry measurements every 300 m along-track with footprint coverage of about 120 m across. The absolute vertical precision is in the range of 30 m with a horizontal precision of about 400 m [*Smith et al.*, 2001]. The MOLA data used in this work are gridded data with 128 pixel per degree in mid-latitudes, which were calculated by the MOLA science team based on all ground–measurements [*Smith et al.*, 2003]. The HRSC represents a multi-sensor push broom instrument composing of nine CCD line sensors permitting a simultaneous stereo, multicolour, and multi-phase imaging [*Jaumann et al.*, 2007]. The HRSC instrument permits to illustrate the Martian surface in three–dimension. The driven DTM has a spatial resolution of around 200 m and vertical accuracy of around 23 m. The CTX topographic data were produced using ISIS and SocetSet®, a commercially available photogrammetry suite (http://www.socetset.com). Its preparation phase has been mostly done by Peter Fawdon (co-author in the Chapter 4) and is described in detail in the Chapter 4b.

Table 2.1: Data sets used in this manuscript.

Imagery and topographic data [a]	**On board**	**Data type** [b]	**References**
Mars Orbiter Laser Altimeter (MOLA)	Mars Global Surveyor [c]	Topographic	[*Smith et al.*, 2001]
High Resolution Stereo Camera (HRSC)	Mars Express	Imagery Topographic Stereo	[*Neukum et al.*, 2004]; [*Jaumann et al.*, 2007]
Context Camera (CTX)	Mars Reconnaissance Orbiter	Imagery Topographic Stereo	[*Malin et al.*, 2007]
High Resolution Imaging Science Experiment (HiRISE)	Mars Reconnaissance Orbiter	Imagery	[*McEwen et al.*, 2007]
Spectroscopic data			
Thermal Emission Imaging System (Themis)	Mars Odyssey	Imagery Thermal inertia Spectroscopic	[*Fergason et al.*, 2006]
Compact Reconnaissance Imaging Spectrometer for Mars (CRISM)	Mars Reconnaissance Orbiter	Imagery Spectroscopic	[*Murchie et al.*, 2007]

a) Used data resolution is mentioned in the corresponding section.
b) Data type column represents the type of data used in this manuscript and not all of the data type available from the mentioned instrument.
c) The NASA's Mars Global Surveyor mission was ended in 2007.

ii. SPECTROSCOPY DATA

The spectroscopic data are mainly from Compact Reconnaissance Imaging Spectrometer for Mars (CRISM) [*Murchie et al.*, 2007] on board Mars Reconnaissance Orbiter (MRO) and partly from Thermal Emission Imaging System (THEMIS) [*Christensen et al.*, 2004b] on board Mars Odyssey. Both datasets have also been partly used as imagery data. CRISM data have been processed using ENVI (ENvironment for Visualizong Images) and THEMIS DCS data were available via the JMars [*Christensen et al.*, 2009] open source software (see Chapter 3.b.ii for more detail).

Spectroscopy is the study of the absorption and emission of light and other radiation by matter, and it allows the investigation of the chemical composition of the material. The electromagnetic spectrum extends from below the low–frequency radio waves (few kilometers wavelength) to the high–frequency gamma radiation (less than 1 nm). Visible light has a wavelength from 400 to 700 nm. All surfaces (except for black body) reflect partly the light that they receive. If a light source (sun in the case of this work) with a continuous spectrum is shining upon an atom, the wavelengths corresponding to possible energy transitions within that atom will be absorbed and therefore an observer will not see them. In this case, the detector captures the electromagnetic waves of the sun light reflected by the Martian surface, and therefore in a spectrum, one can see the absorbed wavelengths by the surface material.

THEMIS is a multispectral imaging instrument. Multispectral imaging combines two complementary techniques: spectrometry and imaging. Spectrometry characterizes the mineralogical composition of surface. Imaging provides the spatial distribution of different spectral units. Data from a spectral imager are in the form of a spectral cube. Each image pixel is associated with a reflectance spectrum. Thus, obtaining several hundred images of each of the pixels, each image corresponds to a wavelength in the visible and near infrared. The THEMIS instrument includes visible/near infrared and thermal infrared cameras (TIR instrument) [*Christensen et al.*, 2004b]. The TIR camera acquires images at a spatial resolution of ~100 m/pixel and operates at both daytime and nighttime at nine wavelengths between ~6.8 and 14.9 μm.

CRISM is a hyperspectral imaging instrument which functions in both multi and hyperspectral [*Murchie et al.*, 2007]. In multispectral mode, CRISM collects images of the surface in a resolution of 100 m/pixel or 200 m/pixel in a range of 72 spectral channels. In hyperspectral mode, CRISM acquire data on the target regions (10 km x10 km) at full spatial resolution (15-19 m/pixel) and spectral resolution (6.55 nm/channel). It acquires 544 images between 0.362 μm and 3.920 μm.

b. METHODS AND APPROACHES

i. GEOLOGIC MAPPING

Photogeologic mapping on Earth as well as on planetary bodies is an effective method to investigate regional- and global-scale mechanisms which shaped the surface of a given area. Using imagery data for this purpose, on Mars, began by the Mariner 6 and 7 spacecrafts followed by Viking 1, 2, and missions shown in Table 2.1. About 90 geologic maps of Mars have been published so far [*Tanaka et al.*, 2009]. The most recent global geologic map of Mars is been published by *Tanaka et al.* [2014] at a general scale of 1:1,000,000. Mapping the Martian surface is mainly based on geomorphic characteristics recognition mapped and interpreted in image and topographic data. Those maps are being supplemented by multi- and hyperspectral data that provide insight into the mineralogical composition of the material and timing of events estimated via crater counting methods (see Part iv of this chapter).

In this work, the geologic analyse techniques have been used to map the study area 1, and a part of the study area 2 (Figure 1.3), and is described extensively in Chapter 3 and 4. In order to generate the maps, ArcGIS [*ESRI*, 2013] software was used. ArcGIS is a powerful software including tools to manage, store, and present spatial data, and to work with large amount of datasets. ArcGIS permits the user to deal with various map projections and coordinate systems, and to project the data in the preferred projection system. This software is used by a large community in Earth science as well as in planetary science.

In the geologic map of Chapter 3 (Figure 3.3), map units were identified based on the unit's surface morphology, spatial distribution, IR brightness, albedo characteristics in visual images, relative ages, stratigraphical relation, absolute model age (for certain units only; method described in Part ii), and spectroscopical parameters of the material (also for certain units; method described in Part iv). Unit labels consist of chronostratigraphic age, unit group, and subtype [*Tanaka et al.*, 2010]. In Chapter 4, a geomorphologic map (Figure 4.8) has been generated for a valley located in study area 2 (see Figure 1.3). The geomorphologic map is mainly based on the relief observed in visible imagery, and topographic data and the unit names are descriptive morphologic names.

Three features have been named officially via International Astronomical Union (IAU) upon the request of the first author in order to facilitate the understanding of the location of outcrops and features of interest. Two of these features are Caralis Chaos and Simois Colles located in Terra Sirenum. They are extensively discussed in the Chapter 3. The third feature is Kārūn Valles, discussed in detail in Chapter 4. The name suggestion is based on the Kārūn River located at the southwest of Iran.

ii. SPECTROSCOPIC ANALYSIS

In order to understand the composition of surface material, the spectroscopical data of Compact Reconnaissance Imaging Spectrometer of Mars (CRISM) [*Murchie et al.*, 2007] and Thermal Emission Imaging Spectrometer (THEMIS) [*Fergason et al.*, 2006] have been used. These data and method was used and is extensively described in Chapter 3. The CRISM data allowed detection the presence of phyllosilicate-bearing material in a location, where a paleo-lacustrine environment was expected. Our result permitted to distinguish between two various phyllosilicates, which then were used for the interpretation of the aqueous regional history of the study area. The THEMIS data set was also used with the aim of detecting and confirming the presence of chloride salts, which as well permitted to interpret the development of aqueous alterations in the area.

iii. HYDRAULIC ANALYSIS

Hydraulic modelling is widely used on Earth in order to understand the physics of water and sediment discharge which is in turn crucial for reconstructing the surface morphology caused by erosion and sedimentation. On Mars, channel beds morphology provide insight into the past climate due to liquid water abundance. The resolution of remote sensing data, however, sets a constraint on the accuracy of hydraulic calculations due to the dimension of hydraulic systems. In chapter 4 the hydraulic modelling performed in this study is extensively described. The method described by *Kleinhans* [2005] has been used for this thesis, because (1) the author adopted the terrestrial methods with Martian condition and (2) this method has been widely used in literatures [e.g., *Jaumann et al.*, 2010; *Kleinhans et al.*, 2010; *Hauber et al.*, 2013; *Mangold and Howard*, 2013; *Salese et al.*, 2016]. The flow discharge and sediment transport computation on Mars had not been, previously, discussed so broadly.

iv. CRATER SIZE–FREQUENCY DISTRIBUTION (CSFD)

Estimating the age of planetary surface units is essential for understating the chronology of geological processes shaping those surfaces. The measurement of crater size–frequency distribution (CSFD) is a commonly used method to estimate the age of surfaces of terrestrial planets based on the density of impact craters in a given area. This method assumes that when a unit is formed, it has no superposed impact craters on its surface and the craters accumulation starts after the unit's formation [*Hartmann and Neukum*, 2001; *Michael et al.*, 2012]. The projectiles in solar system accumulate on a planetary surface through time, in other words, older surfaces have higher density of impact craters than younger ones. Therefore estimation of the surface age would be possible by investigating the number of craters per area of interest [*Neukum and Dietzel*, 1971]. This method is dependent to the impact flux. Absolute ages were driven by correlating crater size–frequency measurements to radiometric ages measured from the Apollo lunar samples. Therefore an accurate knowledge of the lunar cratering chronology is necessary for estimating the absolute model ages of planets surfaces in the inner solar system [*Neukum et al.*, 1975]. Resurfacing processes (lava

flows, aeolian deposits, liquid water/ice activities, and etc) affect craters size as well as their density on a surface [*Hartmann*, 1971; *Neukum et al.*, 1975]. The secondary craters are another issue which manipulates the model age results. The user has to keep these issues in mind while selecting the area, and mapping the craters within.

In Chapters 3 and 4 the absolute model ages of several geological units have been estimated and described, in detail. Crater counting was performed in an ArcGIS environment. Craters were mapped using the CraterTools extension for ArcGIS software [*Kneissl et al.*, 2011]. The Craterstats 2 software [*Michael and Neukum*, 2010] was used to produce the partial crater size–frequency distribution, based on the chronology function of *Hartmann and Neukum* [2001] and the production function of *Ivanov* [2001]. The epoch boundaries, throughout this thesis, are based on Neukum system [*Hartmann and Neukum*, 2001] as explained in *Michael* [2013].

3. GEOLOGIC EVOLUTION OF THE EASTERN ERIDANIA BASIN: IMPLICATIONS FOR AQUEOUS PROCESSES IN THE SOUTHERN HIGHLANDS OF MARS

The following section has been published as: **Adeli, S.**, E. Hauber, L. Le Deit, and R. Jaumann (2015), Geologic evolution of the eastern Eridania basin: Implications for aqueous processes in the southern highlands of Mars, *Journal of Geophysical Research-Planets*, 120, 1774-1799, doi: http://dx.doi.org/10.1002/2015JE004898. The author contribution is explained in the Section 1.c.

Abstract: The Terra Sirenum region of Mars is thought to have hosted the Eridania paleolake during the Late Noachian/Early Hesperian, and it offers an insight into the regional aqueous history of Mars. We focus on four basins, including Atlantis, Simois, Caralis, and an unnamed basin. They are hypothesized to have hosted isolated lakes after the drainage of the Eridania Lake. We produced a geologic map and derived model absolute ages of our main mapped units. The map and model ages enable us to interpret the geologic history of the region. The basin floors are covered by light-toned materials containing Fe/Mg-phyllosilicates. Across most of the region, the Electris unit covers the highlands and is eroded into mesas. The deposition of this unit corresponds to air fall and/or fluvial mechanisms that transported the material into the basins and accumulated it on the plateaus and basin floors and rims. The deposits on the basin floors were later degraded into light-toned knobs that are rich in Fe/Mg-phyllosilicates. On the rim of the Simois and the unnamed basins, a sequence of Al-phyllosilicates on top of Fe/Mg-phyllosilicates has been observed. These Al-phyllosilicate-rich materials may have been formed by pedogenic leaching. The presence of chloride in the area suggests that a playa environment prevailed during the last stage of water presence or after desiccation of the lakes. In the Early Amazonian, the last aqueous activity cemented the post lacustrine air fall deposits in the basins and shows that liquid water was present in Terra Sirenum long after the Noachian.

Key Points:

Reconstructing the Noachian-Amazonian geological history of the Eridania basin.
Investigating the mineralogical composition of light-toned materials.
Understanding the aqueous activity after the Noachian period.

a. INTRODUCTION

Morphological and mineralogical evidence supports the hypothesis that liquid water was abundant early in Martian history [e.g., *Carr*, 1995; *Cabrol and Grin*, 1999; *Baker*, 2001; *Craddock and Howard*, 2002; *Christensen et al.*, 2004a; *Poulet et al.*, 2005; *Bibring et al.*, 2006]. The existence of ancient lakes on Mars is suggested by both mineralogical and sedimentological evidence. However, the duration and extent of standing bodies of water on the surface are still debated. Impact craters hosted such lakes [e.g., *Fassett and Head*, 2008; *Cabrol and Grin*, 2010] (e.g., Eberswalde crater [e.g., *Malin and Edgett*, 2003; *Moore et al.*, 2003a], Holden crater [e.g., *Grant et al.*, 2008] and Gusev crater [*Carter and Poulet*, 2012]). Former crater lakes are widely distributed in the Noachian highlands, where more than two hundred paleolakes in the form of closed, open and lake chain systems have been reported [*Cabrol and Grin*, 1999; 2001; *Fassett and Head*, 2008; *Hauber et al.*, 2009; *Goudge et al.*, 2012]. Surface runoff and groundwater aquifers are the likely water sources, and both have been important in the Martian hydrology system [e.g., *Cabrol and Grin*, 2010]. Lake basins capture a record of geological and environmental conditions over their lifetime of activity and a wide range of spatial scales. Hence, they are prime candidates for exploration.

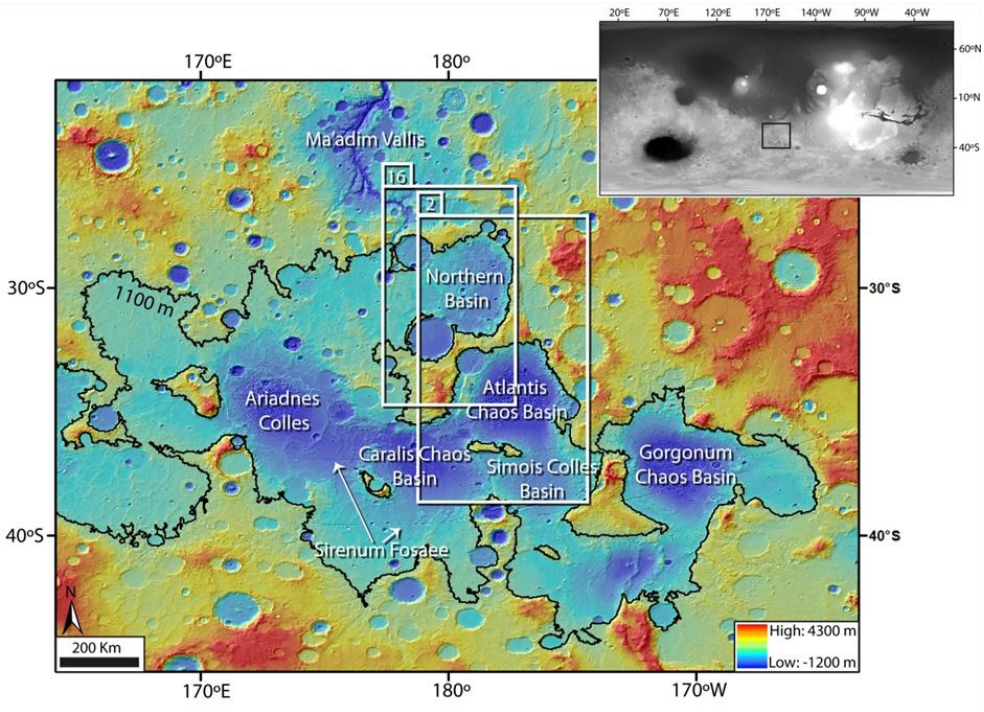

Figure 3.1: Color-coded MOLA digital elevation model at 128 pixels/degree merged with a MOLA hillshade map showing the location of the Eridania paleolake, the studied basins, and major geological features. the black solid line indicates the 1100 m contour line corresponding to the approximate shoreline as proposed by Irwin et al. [2004]. The white boxes marked the study area shown in figure 3.2 and 3.16. The location on mars is shown in the top right inset.

The Terra Sirenum region of Mars (Figure 3.1), located in the cratered southern highlands, is geologically diverse. It displays large degraded basins that appear to have contained isolated paleolakes [*Irwin and Howard*, 2002; *Howard and Moore*, 2004; *Irwin et al.*, 2004; *Wray et al.*, 2011], relatively young extensional tectonic grabens (Sirenum Fossae), and one of the largest outflow channels on Mars (Ma'adim Vallis). The formation of Ma'adim Vallis has been the subject of several studies since it was identified in Mariner 9 images [*Milton*, 1973]. Gusev crater, situated at the terminus of Ma'adim Vallis, was selected as the landing site for the Mars Exploration Rover Spirit [*Cabrol et al.*, 1994; 2003; *Squyres et al.*, 2004]. Based on the morphology of the valley and the head basin, *Irwin et al.* [2002] proposed that Ma'adim Vallis may have been carved by the drainage of a large paleolake. This paleolake, informally named Eridania, was one of the largest paleolakes on Mars, covered an area of 1.1×10^6 km^2 [*Irwin et al.*, 2004], and was composed of multiple subbasins (Figure 3.1).

The large degraded basins, which are probably of impact origin [*de Pablo and Fairén*, 2004; *Irwin et al.*, 2004], were once part of the larger Eridania paleolake that existed during the Late Noachian, Early Hesperian Epochs [*Irwin et al.*, 2004]. At the end of its existence, the Eridania lake was subdivided into smaller, isolated lakes. The floors of these lake basins, including Gorgonum Chaos, Atlantis Chaos, Ariadnes Colles, Simois Colles, Caralis Chaos, and one unnamed site situated north of the Atlantis basin, informally termed the northern basin, (see Table 1 and Figure 3.1 for locations) display unusual features [*Irwin et al.*, 2004] compared to other degraded craters that are usually flat-floored in the Martian highlands [*Mangold et al.*, 2012a]. The floors of the above basins are partly occupied by so-called chaotic material, which locally consists of knobs or hills of relatively high relief. These hills are composed of light-toned materials that contain phyllosilicates in Gorgonum Chaos [*Howard and Moore*, 2004], Ariadnes Colles [*Annex and Howard*, 2011; *Molina et al.*, 2012], and Terra Sirenum in general [*Glotch et al.*, 2010; *Grant et al.*, 2010; *Davila et al.*, 2011; *Ruesch et al.*, 2012; *Wendt et al.*, 2012].

Table 3.1: Basins location, diameter, and topographic information[a].

Basin name	**Location**		**Diameter (km)**	**Topographic information**	
	Latitude (°N)	Longitude (°E)		Lowest point (m)	Highest point (m)
Atlantis Chaos basin	-34	177	~240	-600	1400
Simois Colles basin	-37	-176	~160	-400	1400
Caralis Chaos basin	-37	178	~190	-200	1300
Northern basin	-29	-178	~200	300	1500

[a] Topographic data are derived from a gridded MOLA DEM.

In this study, we focus on the geologic events that occurred in the Atlantis, Simois, Caralis, and northern basins (Figure 3.2) after the transformation of the large Eridania lake into the hypothesized smaller lakes. These four basins have been mainly selected in our study because of the morphological variety of light-toned materials on their rims and floors. We analyzed the morphological and mineralogical characteristics of the mapped units, reconstructed the stratigraphic relations between individual units on the basis of our geologic map of the area, and performed crater counts on the main geologic units. Our goal was to better understand past environmental conditions in the eastern Eridania paleolake from Noachian to Amazonian.

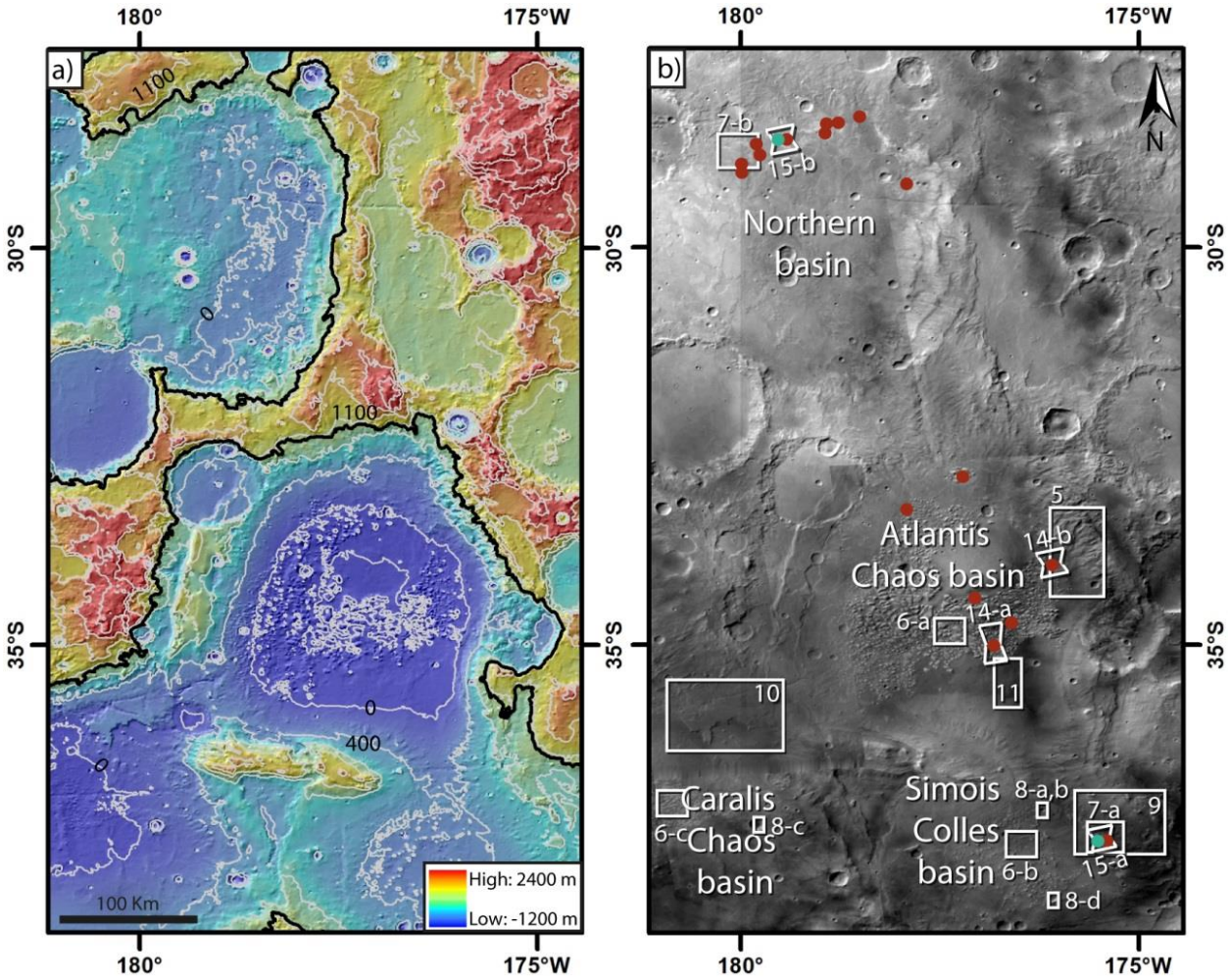

Figure 3.2: Study area. (a) Topographic details (color-coded MOLA DEM on MOLA hillshade map). Contour interval is 400 m. The contour line in black corresponds to the Eridania shoreline at 1100 m [Irwin et al., 2004]. (b) Mosaic of HRSC nadir images. The locations of almost all figures in this paper are indicated as white boxes. The red circles represent the location of CRISM datasets where we detected Fe/Mg-phyllosilicates and the green circles represent the location of CRISM datasets where we detected Al-phyllosilicates. The list of CRISM datasets is presented in Table 3.2.

b. DATA SETS AND METHODS

i. IMAGERY AND TOPOGRAPHY DATA SETS

Geological mapping was performed on the basis of High Resolution Stereo Camera (HRSC) data [*Neukum et al.*, 2004; *Jaumann et al.*, 2007] from the Mars Express (MEX) orbiter and Context Camera images (CTX) [*Malin et al.*, 2007] from the Mars Reconnaissance Orbiter (MRO), which have typical ground pixel sizes of 10 to 40 m and ~6 m, respectively. Several images acquired through the High Resolution Imaging Science Experiment (HiRISE, 25 cm/pixel [*McEwen et al.*, 2007]) were used to study the detailed surface texture of geologic units. Topographic information was derived from HRSC gridded Digital Elevation Models (DEMs) with a cell size of 50 m and a height accuracy of 12 m [*Scholten et al.*, 2005; *Gwinner et al.*, 2010] as well as the gridded Mars Orbiter Laser Altimeter (MOLA) global DEM with a resolution of 128 pixels/degree (grid cell size ~461 m) [*Smith et al.*, 2001]. We defined the geologic units based on several morphological characteristics including their observable albedo, color, and texture differences. Topographic data was also used to study the stratigraphic relations between the units.

ii. SPECTROSCOPIC DATA

Hyperspectral data acquired by the Compact Reconnaissance Imaging Spectrometer for Mars (CRISM) [*Murchie et al.*, 2007] from the Mars Reconnaissance Orbiter (MRO) were used to analyze the location and nature of phyllosilicate-rich materials (Figure 3.2). CRISM is a visible/near-infrared imaging spectrometer that acquires 10 km × 10 km images. Each image covers the wavelength range between 0.362 μm and 3.92 μm in 544 spectral channels at a spectral resolution of 6.5 nm/channel [*Murchie et al.*, 2007]. We used Full Resolution Targeted (FRT) data products and Half Resolution Long Targeted (HRL) data products, with 18 m/pixel and 36 m/pixel resolutions respectively [*Murchie et al.*, 2007]. The CRISM data have been atmospherically [*McGuire et al.*, 2009] and photometrically [*Murchie et al.*, 2007] corrected via the CAT tool v6.7 in the ENVI software. We compared our results with the USGS Digital Spectral Library [*Clark et al.*, 2007] and spectra published by *Bishop et al.* [2008a]. In order to reduce the effects of dust and atmospheric residuals, the selected spectra have been ratioed against spectra of neutral and dusty regions extracted from the same data cubes. This method highlights spectral variability and provides spectra with reduced atmospheric effects so that they can be compared to the spectral library.

We used Thermal Emission Imaging System (THEMIS) daytime and nighttime data from the Mars Odyssey orbiter to analyze the relative thermal radiance of surface materials (as a proxy for thermal inertia [*Fergason et al.*, 2006]) and to identify chloride-bearing materials. The THEMIS instrument is a multispectral imager that includes visible/near infrared and thermal infrared cameras (TIR instrument) [*Christensen et al.*, 2004b]. The TIR camera acquires images at a spatial resolution of ~100 m/pixel and operates at both daytime and nighttime at nine wavelengths between ~6.8 and 14.9 μm. In order to identify chloride-

rich material, we used decorrelation stretch (DCS) images. The DCS is an image enhancement technique that strengthens contrast in multispectral information [*Gillespie et al.*, 1986]. In this study, we used DCS images which display bands of 8/7/5 in red, green, and blue respectively. The chloride-rich materials appear blue in the 8/7/5 stretch [*Osterloo et al.*, 2008; *Osterloo et al.*, 2010].

iii. AGE DETERMINATION

We performed crater size–frequency distribution analysis on CTX images [*Malin et al.*, 2007], in order to estimate the model absolute age of the four main geological units. Crater counting was performed at a scale of 1:24,000 in a GIS environment. Craters were mapped using the CraterTools extension for ArcGIS software [*Kneissl et al.*, 2011]. The Craterstats 2 software [*Michael and Neukum*, 2010] was used to produce the partial crater size–frequency distribution, based on the chronology function of *Hartmann and Neukum* [2001] and the production function of *Ivanov* [2001]. The results have been corrected for crater clustering [*Michael et al.*, 2012], a procedure that reveals possible secondary crater populations. Estimating the model absolute age of the knobby fields is not possible without very large uncertainties due to their highly eroded surface. Hence, to constrain the age of the knob formation, we dated the basement as well as those units that are stratigraphically on top of the knobs.

Table 3.2: List of CRISM observations with phyllosilicate detections

CRISM Observation ID[a]	Latitude (°N)	Longitude (°E)	Geologic Unit	Mineralogical Composition[b]	Location[c]
FRT CB5C (13b)	-28.60	-179.62	NHlts	Al- & Fe/Mg-rich phyllosilicates	NB
FRT 11EBF	-28.90	-179.86	NHlts	Fe/Mg-rich phyllosilicates	NB
FRT 1382E	-28.59	-179.38	NHlts	Fe/Mg-rich phyllosilicates	NB
FRT 98D1	-28.79	-179.86	NHlts	Fe/Mg-rich phyllosilicates	NB
FRT 232F3	-28.72	-179.46	NHlts	Fe/Mg-rich phyllosilicates	NB
FRT 9E4C	-28.36	-178.73	NHlts	Fe/Mg-rich phyllosilicates	NB
FRT 9BBC	-28.57	-178.88	NHlts	Fe/Mg-rich phyllosilicates	NB
FRT 92F7	-28.43	-178.84	NHlts	Fe/Mg-rich phyllosilicates	NB
FRT 96FE	-28.34	-178.44	NHlts	Fe/Mg-rich phyllosilicates	NB
FRT 13039	-29.21	-178.02	NHlts	Fe/Mg-rich phyllosilicates	NB
FRT 865F	-32.88	-177.23	NHltk	Fe/Mg-rich phyllosilicates	AB
HRL 8D2D (12a)	-35.08	-176.77	NHltk	Fe/Mg-rich phyllosilicates	AB
FRT 913A (12b)	-34.01	-176.01	NHltk	Fe/Mg-rich phyllosilicates	AB
FRT 12636	-34.64	-176.48	NHltk	Fe/Mg-rich phyllosilicates	AB
HRL 7E3A	-33.29	-177.87	NHltk	Fe/Mg-rich phyllosilicates	AB
FRT 8175	-34.34	-176.94	NHltk	Fe/Mg-rich phyllosilicates	AB
FRT 951C (13a)	-37.58	-175.31	NHlts	Al- & Fe/Mg-rich phyllosilicates	SB

[a] Numbers in parentheses refer to figure numbers in this paper.

[b] Locations of the detection of Fe/Mg-phyllosilicates and Al-phyllosilicates are shown in Figure 2-b as red and green circles, respectively.

[c] NB, AB and SB are referring to the northern, Atlantis and Simois basins, respectively.

c. REGIONAL SETTING

The study area, located in the southern Noachian highlands, is composed of four large basins (Table 1). At the south of this area the large Sirenum Fossae graben system extends from east to west over at least 3700 km across Terra Sirenum [*Wilson and Head*, 2002] (Figure 3.1). The Atlantis Chaos basin, the largest and deepest among the four, has a diameter of ~240 km. (Figures 3.2a, and Table 3.1). The roughly circular (plan view) morphology of this basin suggests a probable impact origin [*de Pablo et al.*, 2004; *Irwin et al.*, 2004]. The floor of this basin is mostly covered by high-relief knobs that are composed of light-toned materials interpreted as clay-bearing materials in other basins of Terra Sirenum [*Glotch et al.*, 2010; *Annex and Howard*, 2011; *Davila et al.*, 2011; *Adeli et al.*, 2012; *Molina et al.*, 2012; *Ruesch et al.*, 2012; *Wendt et al.*, 2013].

Simois Colles and Caralis Chaos basins are located south and southwest of Atlantis basin (Figure 3.2) and have circular shapes in plan view. The Simois basin has a diameter of ~166 km, and the Caralis basin has a diameter of ~200 km (Table 1). The floors of the Simois and Caralis basins are partly covered by knobby materials, which are smaller in size (height and width) than to those covering the Atlantis basin floor. The divide between the Atlantis and Caralis basins has its lowest point at ~350 m. The two basins are connected by a small channel that feeds an ~50 m thick, 12 km wide depositional fan where it debouches into a ~25 km diameter impact crater, located at the west side of the Atlantis basin.

To the north of Atlantis Chaos, an unnamed basin is located at the head of Ma'adim Vallis with a diameter of ~200 km (Table 1). In this study, we refer to this basin as the northern basin. Contrary to the other basins discussed above, this one does not display knobs that are as prominent. However, outcrops of light-toned materials are widespread on the basin's floor. *Osterloo et al.* [2010] reported the local presence of chloride salts where light-toned outcrops are exposed.

d. GEOLOGICAL MAPPING

Few geological and geomorphological maps have previously been produced for this area. *de Pablo et al.* [2005] used Viking images to produce a geological map, whereas *Wendt et al.* [2013] and *Molina et al.* [2012] mapped the geomorphology of individual basins on the basis of imaging and spectral data from the MEX, Odyssey, and MRO missions. We produced a more detailed geological map of the entire area of the Atlantis, Simois, Caralis, and northern basins (Figure 3.3a) based on all currently available imaging and topographical data sets. Moreover, it covers a larger area and, therefore, provides a synoptic view on the geologic history of the eastern Eridania basin. In addition, model absolute age assignments for the units are derived.

Table 3.3: Crater densities of the map units for which the model absolute ages has been produced.

Unit name	Unit label	N(1)[a]	Model Absolute Age	Epoch[b]
Noachian cratered plateau[c]	Nplc	3,877.3 (±15.9)	3.99 Ga (+0.04/-0.05)	Early Noachian
Noachian-Hesperian Electris deposit[d]	NHlte	1.13×10^{-3} ($\pm1.86\times10^{-4}$)	2.31 Ga (+0.37/-0.38)	Early Amazonian
Early Amazonian basin unit I	eAbI	1.36×10^{-3} ($\pm1.47\times10^{-4}$)	2.77 Ga (+0.24/-0.29)	Early Amazonian
Early Amazonian basin unit II	eAbII	7.52×10^{-4} ($\pm5.29\times10^{-5}$)	1.54 Ga (+0.05/-0.09)	Early Amazonian
Early Amazonian plains unit	eAp	1.35×10^{-3} ($\pm4.22\times10^{-4}$)	2.75 Ga (+0.49/-0.85)	Early Amazonian

[a] N(1) shows the number of craters > 1 km in diameter/counting area.
[b] Epoch assignments are based on Michael [2013].
[c] For the Nplc unit, crater density, model absolute age, and epoch assignment are derived from *Tanaka et al.* [2014].
[d] The model absolute age of the NHlte unit represents the mantling layer's age that widely covers the mesas of NHlte and therefore represents the last stage of the airfall deposition in the area (see Section 3.f).

i. NOACHIAN PLATEAU

1) CRATERED PLATEAU (NPLC)

Surfaces of Noachian age are highly modified by large impact craters and include the oldest surfaces on Mars. *Scott* [1985] defined the "Noachian cratered plateau" as the elevated topographic massifs constituting the rims of large basins. In our geological map, highly degraded upland surfaces have been mapped as Noachian cratered plateau (Nplc) (Figure 3.3a). This unit has been mapped as Early Noachian highland unit (eNh) by *Tanaka et al.* [2014] and is characterized by a dense crater population (density number: N(1): 3,877.3 (Table 3.3)) and rough, low-relief inter-crater plains. The Nplc unit is observed at elevations between 1100 m and 3100 m. The crater size–frequency distributions derived for three units in the area show a maximum age of around 3.95 (+0.08/-0.20) Ga, 3.79 (+0.05/-0.09) Ga, and 3.55 (+0.13/-1.50) Ga (Figure 4b, c, and d), which corresponds to the Middle Noachian to Early Hesperian Epochs [*Hartmann*, 2005; *Michael*, 2013]. The craters that are used to derive these ages clearly predate the surface on which we mapped them. They have no observable ejecta and are partly covered by the upper unit material. Therefore, the basement mapped as the Nplc unit in our geological map in interpreted to be aged between 3.95 (+0.08/-0.20) Ga to 3.55 (+0.13/-1.50) Ga.

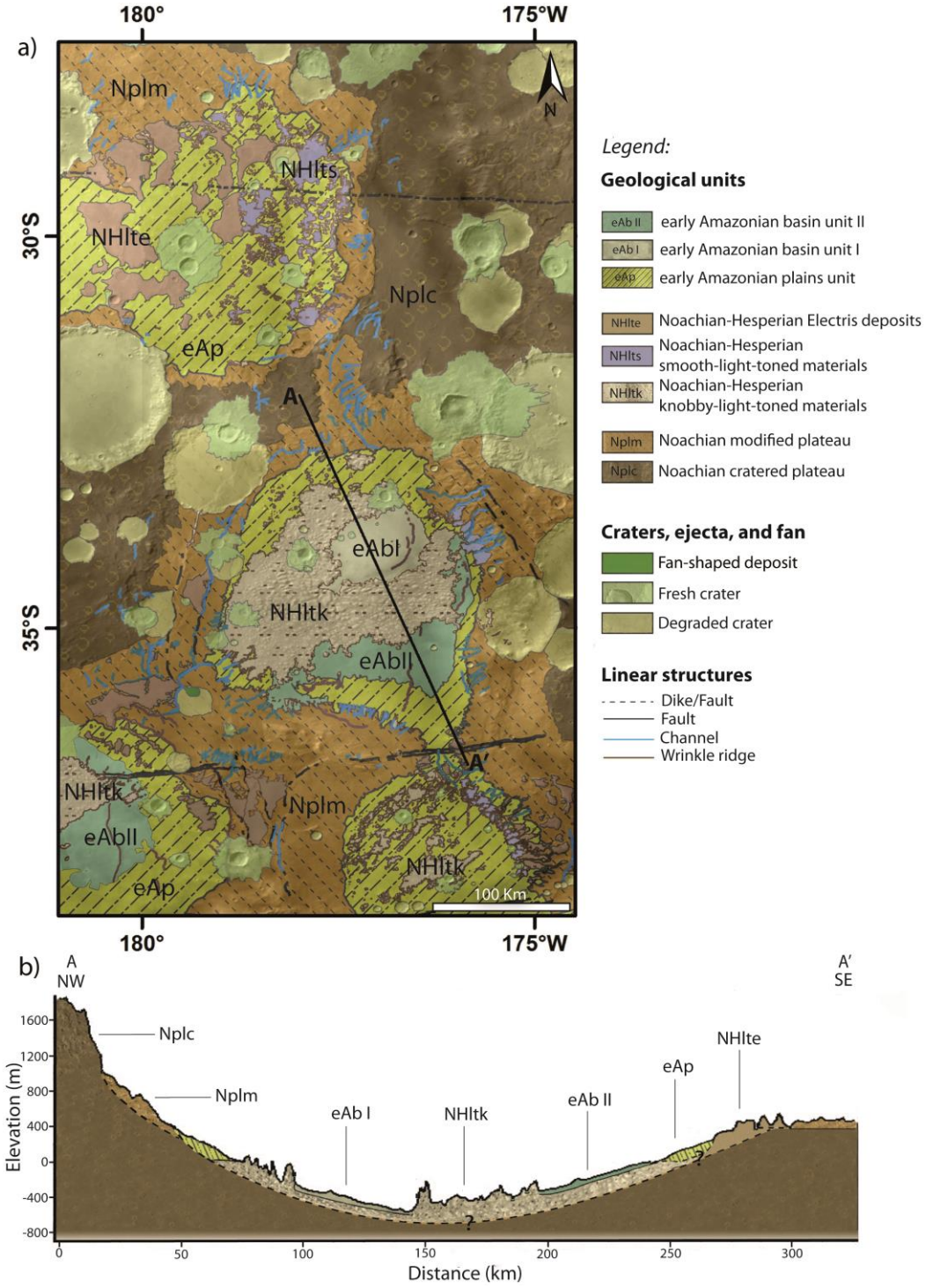

Figure 3.3: (a) Geologic map of the eastern Eridania basin shown on a MOLA hillshade map. Eight main geological units have been mapped. (b) Interpretive cross-section based on MOLA topographic profile (AA' in Figure 3.3a), showing the stratigraphic relations between the geological units. Vertical exaggeration is 36x.

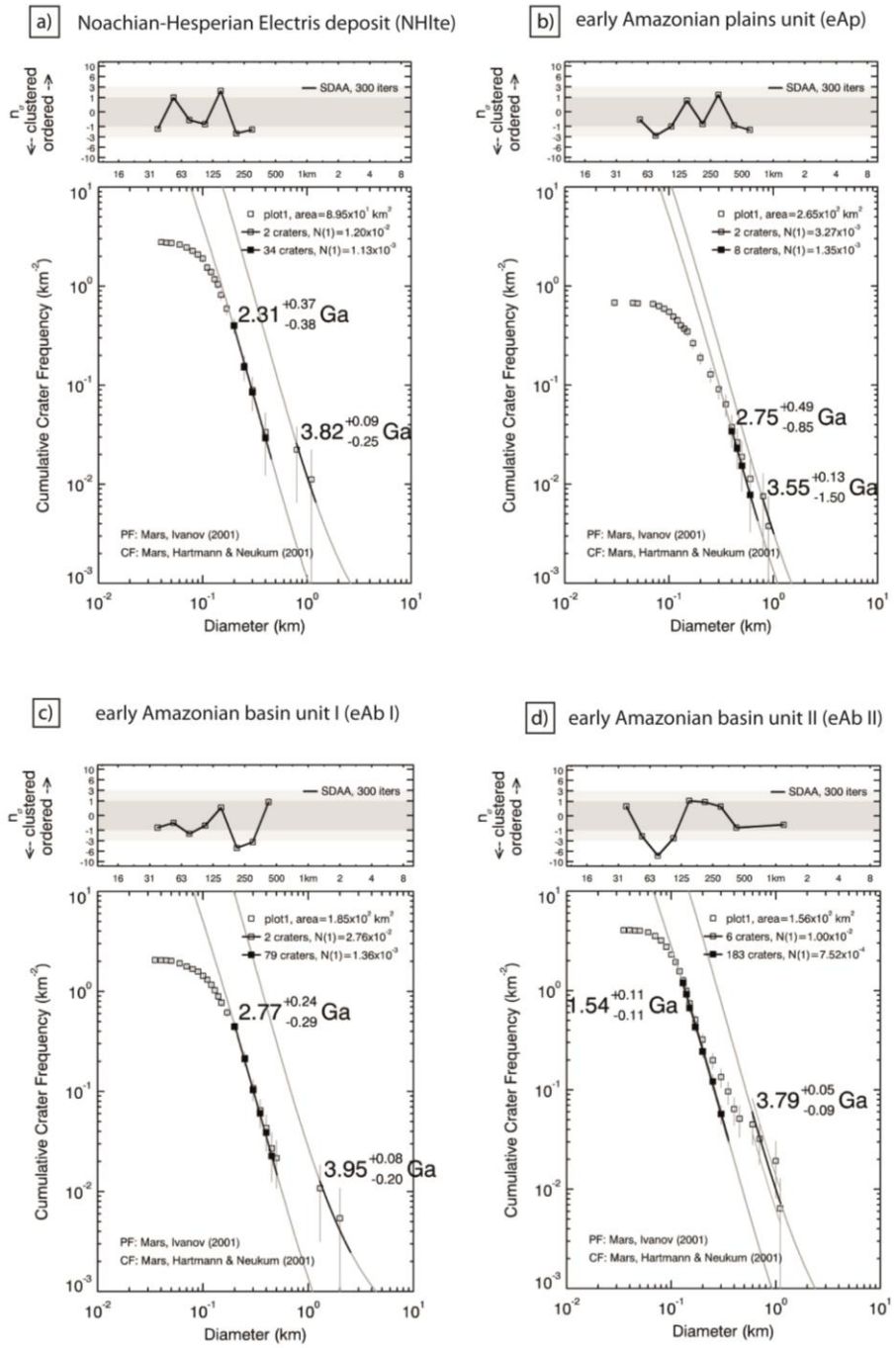

Figure 3.4: The model absolute ages of the four main geological units. (a) The NHlte unit. The 2.31 Ga age corresponds to the mantling layer that covers the surface of the NHlte unit. (b) The eAp unit. (c) The eAbI unit. (d) The eAbII unit. Crater size distributions, randomness analyses, and isochrons are shown. The plot shown above each crater size–frequency distribution represents the randomness analysis for a given range of crater diameters versus a given area.

2) MODIFIED BASEMENT (NPLM)

The modified basement unit (Nplm, Figure 3.3a) is located along the rim of each basin (elevation range: 400 to 1200 m). It has been mapped as Early Noachian Highland unit (eNh) by *Tanaka et al.* [2014]. However, in our geologic map, it represents the part of the Nplc unit, which has been modified by aqueous and tectonic processes (Figure 3.5). Fluvial valleys are observed within Nplm on the eastern slopes of the basin walls. In the Caralis basin, a few valleys have been observed within the Nplm unit located on the eastern basin wall, sourced likely at a high elevation on the south margin of the Atlantis basin and also in highlands located to the north of this basin. The Nplm unit is partly covered by a thin mantling layer of young airfall deposits that are widespread in the study area.

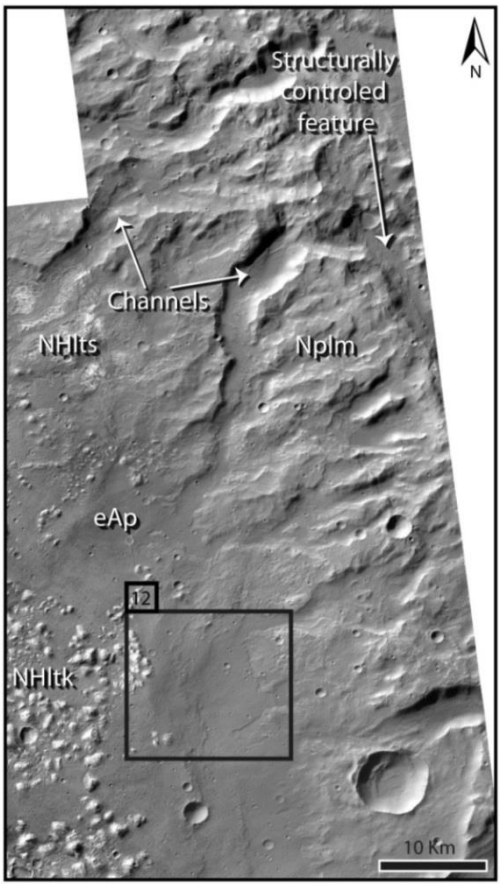

Figure 3.5: The Noachian modified basement (Nplm) unit located on the eastern wall of the Atlantis Chaos basin. Channels and a structurally controlled feature that modified this unit are shown by arrows. Mosaic of three CTX images (P15_007038_1437; B05_01160_1452; P17_007684_1461). The location of Figure 3.5 is indicated in Figure 3.2b. The black box shows the location of Figure 3.12.

ii. NOACHIAN-HESPERIAN UNIT

The Noachian-Hesperian units represent the light-toned materials, located on the basin floors, rims, and plateaus, in three sub-units (Figure 3.3) that are distinguishable by different morphologies and elevations. Knobby light-toned (NHltk) material (Figure 3.6) is observed on the basin floors, smooth light-toned material (NHlts) (Figure 3.7 and 3.8) is observed on the rims of the basins, and Electris deposits (NHlte) (Figure 3.9) are located on plateaus around the basins at higher elevations. We discuss each of these units in the following sections.

1) KNOBBY LIGHT-TONED MATERIALS (NHLTK)

The chaotic terrain in Terra Sirenum consists of isolated hills that cover a large fraction of the Atlantis (Figure 3.6a), Simois (Figure 3.6b), and Caralis (Figure 3.6c) basin floors (Figures 3a) and are composed of light-toned materials (Figure 3.6). The knobby light-toned material (NHltk) appears to be the thickest depositional unit in the study area (Figure 3b). The minimum thickness of NHltk (i.e. knob height) varies from ~600 m at the center of the Atlantis basin to a few meters on the rims of all three basins. The bowl-shaped topography of the floor of the Atlantis basin demonstrates the change in knob size from the center (~600 m

in height and a few hundred meters in width) to the rim (a few meters in height and a few tens of meters in width).

At the southern part of the NHltk in the Atlantis basin, and locally in other basins, thin linear features of different orientation are visible within the knobs (Figure 3.6c and d). At HiRISE resolution we observed that they have positive relief and cross-cut each other in a random orientation (Figure 3.6d). Such ridges, however, are not observed in the valleys between the knobs. On top of the NHltk unit, a thin dark cap with a smooth, flat surface is locally observed. Figure 3.6b shows an example of a few knobs covered by such a cap in the Simois basin, where this dark cap is best preserved. In most cases, the knobs have an irregular surface, except those that are covered by the dark cap. This thin dark cap may correspond to the dark-toned and thin mesa unit mapped by *Malin and Edgett* [2000a] that overlie lighter-toned units.

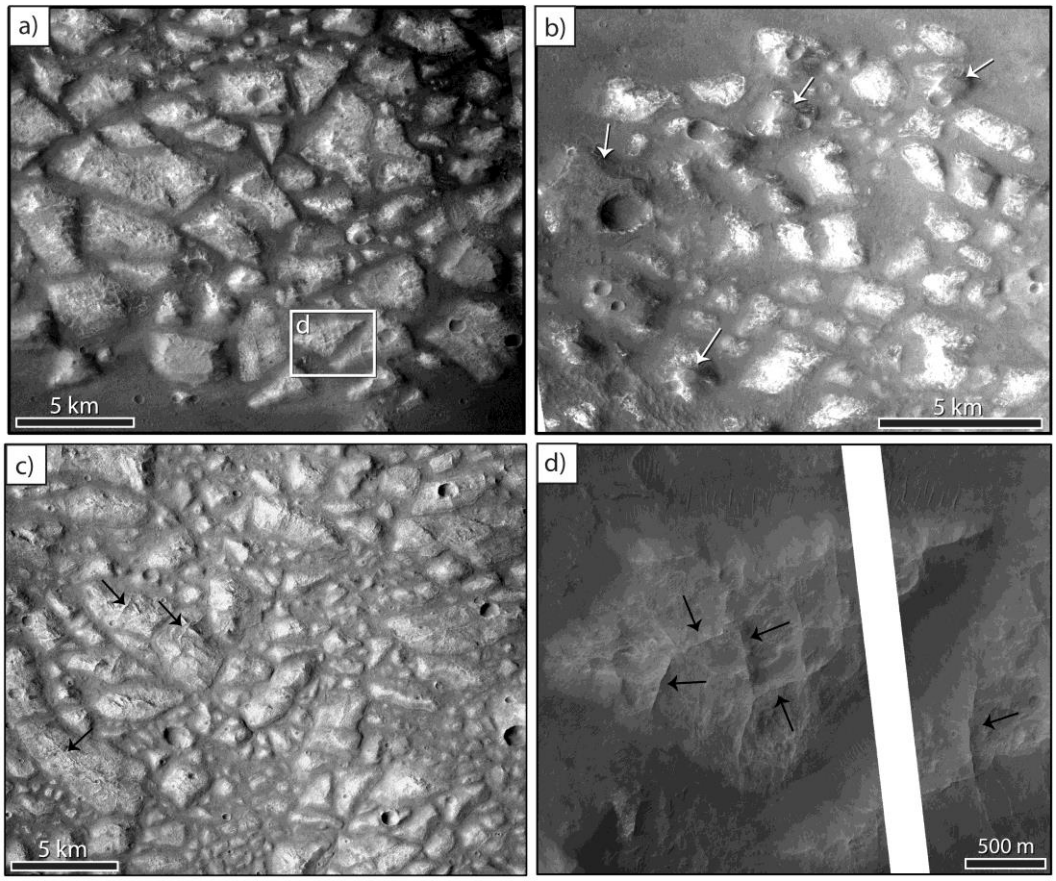

Figure 3.6: The Noachian-Hesperian Knobby light-toned materials (NHltk) unit in the eastern Eridania basin. (a) The NHltk unit in the Atlantis basin (CTX image P12_005614_1455). (b) The NHltk unit in the Simois basin. White arrows represent the knobs where the remnant of a dark cap is observable (CTX image B09_013156_1424). (c) The NHltk unit in the Caralis basin (CTX image P05_002911_1418). Black arrows represent the linear features within the knobs. (d) HiRISE image (PSP_006181_1445) showing the linear features within the knobs in the Atlantis basin. The location of this image is shown in the panel (a). The locations of Figure 3.6a, b, c are marked in Figure 3.2b.

2) SMOOTH LIGHT-TONED MATERIALS (NHLTS)

Outcrops of the smooth-light-toned materials (NHlts) can also be observed along the eastern rims of the basins (Figure 3.3a). These materials are topographically flat, in contrast to the knob-shape of the NHltk unit's morphology. The outcrops are defined as a sub-unit of the Noachian-Hesperian light-toned materials (Figure 3.3a). NHlts is deposited on the basement and is covered by thin, dark material that has been locally eroded, leading to exposure of the NHlts (Figures 3.7a). Outcrops of the NHlts unit are observed on the eastern walls of the Simois (Figure 3.7a) and Atlantis basins. Moreover, clear outcrops of these materials are found at the floor of the northern basin, where no knobs are observed (Figure 3.7b). Figure 3.8 represents the craters wall that reveals the presence of the NHlts unit under a thin and dark layer, in Simois and Caralis basins. It suggests that a contiguous layer of light-tones material is deposited on the floor and rims of theses basins (Figure 3.3b). In THEMIS nighttime data, the outcrops of the NHlts unit appears higher in radiance, and in THEMIS daytime data it is lower in radiance. The inspection of HiRISE images of the NHlts unit reveals fracture patterns characterized by polygonal shapes that are 1 to 2 meters wide (Figure 3.7c and d).

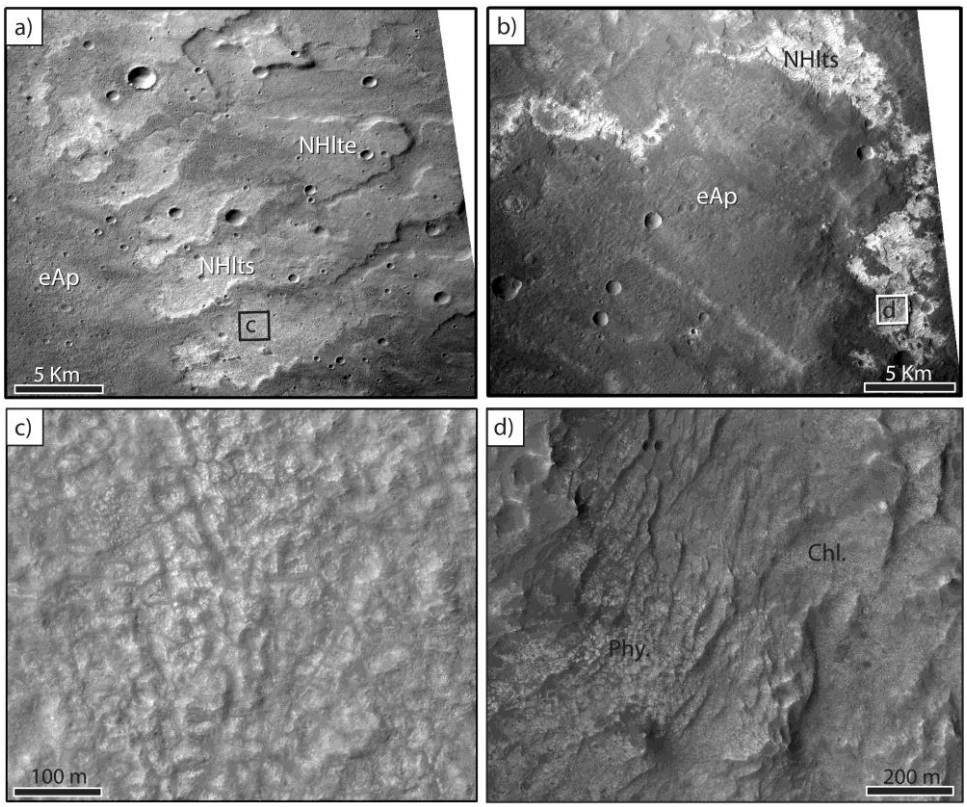

Figure 3.7: The Noachian-Hesperian Smooth light-toned materials (NHlts) unit in the eastern Eridania basin. (a) The NHlts outcrops in the Simois basin (CTX image P15_006827_1422). (b) The NHlts outcrop in the northern basin (CTX image P12_005680_1522). In (a) and (b), we can observe that the NHlts is partly covered by the eAp. (c) Polygonal features observed within the NHlts unit in the Simois basin (HiRISE image PSP_005970_1420). (d) Polygonal features observed within the NHlts unit in the northern basin (HiRISE image ESP_012655_1510). "Phy." shows the location of phyllosilicate-bearing materials that are partly covered by a thin dark cap, whereas "Chl." shows the location of chloride-bearing materials that are on top of the dark cap. The locations of Figure 3.7a, b, are marked in Figure 3.2b.

3) ELECTRIS DEPOSITS (NHLTE)

The Electris deposit (NHlte) (Figure 3.9, and Table 3.3) is broadly distributed between 30°S to 45°S and 160°E to 200°E [*Grant and Schultz*, 1990; *Grant et al.*, 2010]. It lies unconformably on cratered upland surfaces (Figure 3.3b). In our study area, NHlte is characterized by mesas with steep flanks that are located at high elevations around the basins (Figure 3.9). Such mesas are not observed on the basin floors of our study area. The surface of the NHlte is covered by a mantling layer of airfall deposits. This mantling layer also partly covers the plains of Nplm and has a model absolute age of around 2.31 (+0.37/-0.38) Ga, corresponding to the Early Amazonian (Figure 3.4a), whereas the bulk of the mesas covered by the mantling layer are composed of Noachian-Hesperian material, as shown by the un-resurfaced age of 3.82 (+0.09/-0.25) Ga in the Figure 3.4a. The local erosional windows on the NHlte unit expose light-toned materials under the mantling layer as shown in Figure 3.10. On the eastern wall of the Simois basin, moreover, we observed that the NHlte mesas and the NHlts outcrops are connected (Figure 3.9), suggesting that they consist of the same materials. We mapped them separately, however, due to the morphological differences of NHlte as mesas, and NHlts as smooth outcrops.

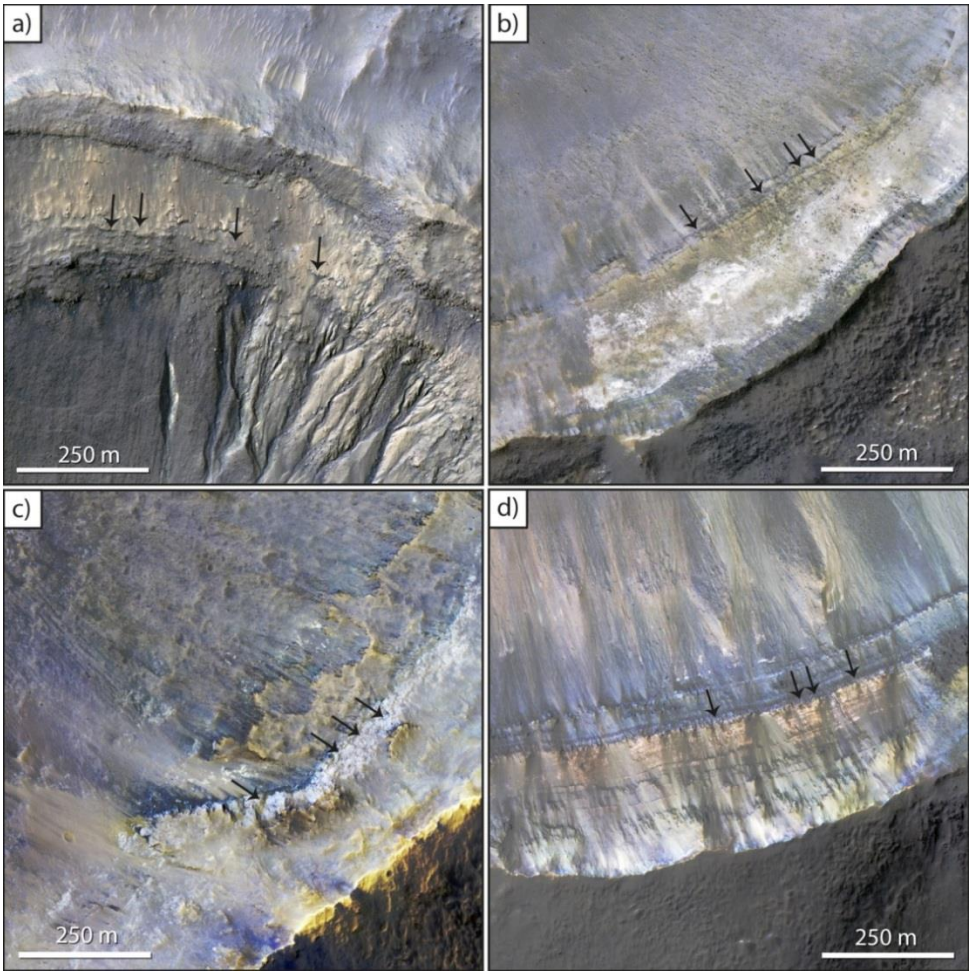

Figure 3.8: HiRISE images showing the walls of three craters located on the basin rims and revealing the light-toned material outcrops (pointed out by black arrows) under the eAp dark material. a) and b) Located in Simois basin, image number: ESP_032408_1425. c) Located in Caralis basin, image number: ESP_031762_1415. d) Located in Simois basin, image number: ESP_032975_1415.

The NHlte material appears as higher radiance in THEMIS daytime and lower radiance in THEMIS nighttime data which is consistent with fine-grained particles (i.e. smaller than sand-sized [*Grant et al.*, 2010]) and/or relatively high porosities [*Kieffer et al.*, 1973; *Osterloo et al.*, 2010], as encountered in loess-like, unconsolidated, thin and fine-grained deposits.

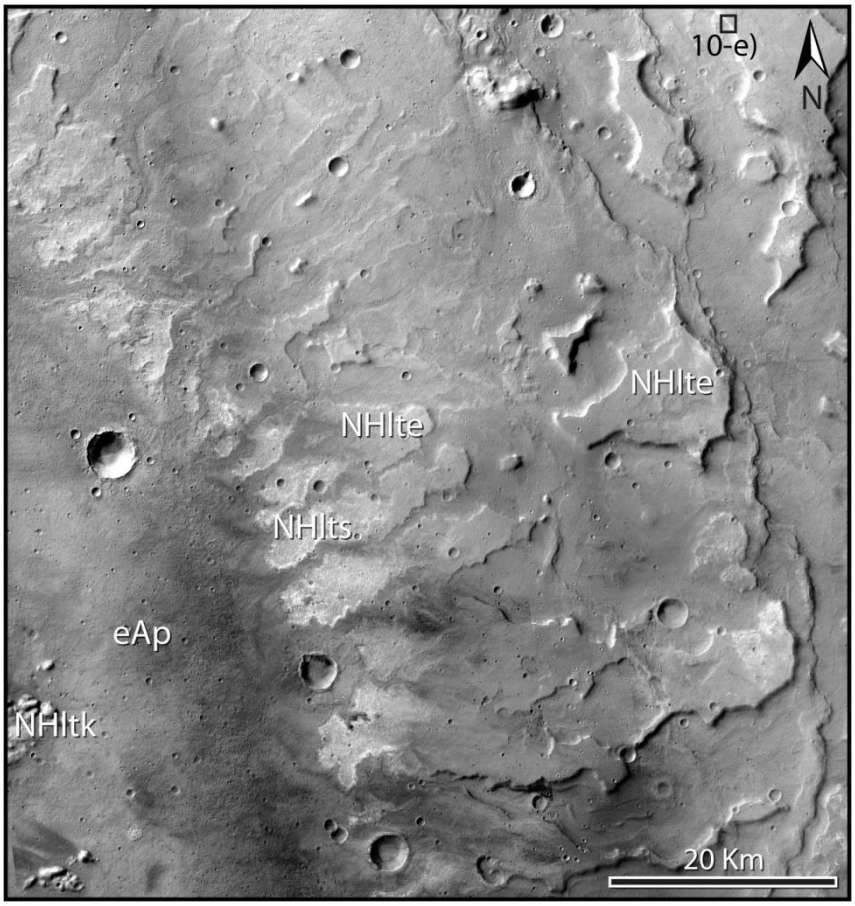

Figure 3.9: The Nochian-Hesperian Electris deposit (NHlte) unit located on the eastern wall of the Simois basin (mosaic of CTX images: P12_005759_1421; B02_010466_1417; P13_005970_1418; P15_007038_1437; B09_013156_1424). The stratigraphical relations between the units are clearly observable. The location of Figure 3.9 is marked in Figure 3.2b.

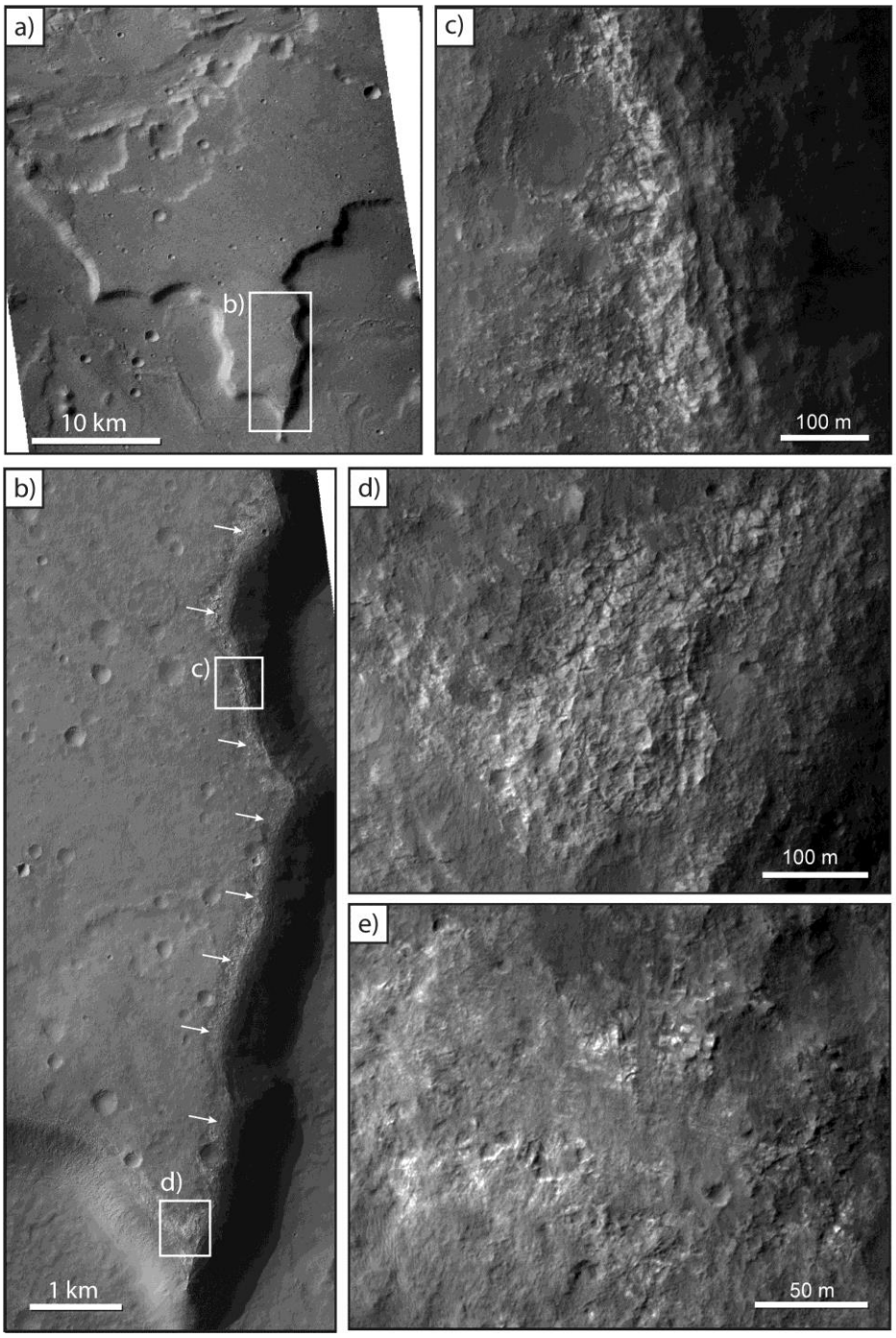

Figure 3.10: Outcrops revealing the presence of the light-toned material within the NHlte mesas. a) CTX image (P02_001922_1442) showing an NHlte mesa, located north of the Caralis basin (the exact location of (a) is marked in Figure 3.2b). b) HiRISE image (ESP_019446_1435) showing the edges of the mesas where light-toned material outcrops (pointed out by arrows). c) and d) Blow-ups of the mesa's edge, showing the light-toned material with similar albedo, texture, and fractures as observed in NHltk and NHlts (same HiRISE image as in Figure 3.10b. e) HiRISE image (PSP_001724_1425) revealing the edge of another mesa located east of the Simois basin. The light-toned material is clearly observable. Location of Figure 3.10e is marked in Figure 3.9.

iii. EARLY AMAZONIAN UNIT

1) BASIN UNIT I/II (EABI/EABII)

The basin units I/II are located at the northeastern and southern parts of the NHltk unit in the Atlantis basin and the eastern part of NHltk in the Caralis basin. They appear as thin and smooth materials that partly cover the NHltk unit (Figure 3.11). We mapped them as two sub-units according to their location in the basin and their model absolute ages (Table 3.3), i.e., the basin unit I (eAbI) located in the northeastern part of the Atlantis basin, with an age of 2.77 (+0.24/-0.29) Ga (Figure 3.4c), and the basin unit II (eAbII) located in the southern part of the Atlantis basin (Figure 3.11) and eastern part of the Caralis basin, with a model absolute age of 1.54 (±0.11) Ga (Figure 3.4d). Both model ages correspond to the Early Amazonian, however, these two sub-units outcrop in distinct locations.

The eAbI/eAbII units fill the depressions between the knobs in Atlantis and partly in Caralis basins (Figure 3.3a), indicating that they were emplaced after the deposition of the light-toned material and its degradation into knobs. In the southern part of the Atlantis basin, within the eAbII unit, a network of fractures has been observed. They may either be desiccation cracks of a mud flow or cooling fractures related to lava flow. The eAbII unit has a lobate margin (Figure 3.11), which enables identifying the contact between eAbI/eAbII and the eAp unit (see Section 3.d.iii.2).

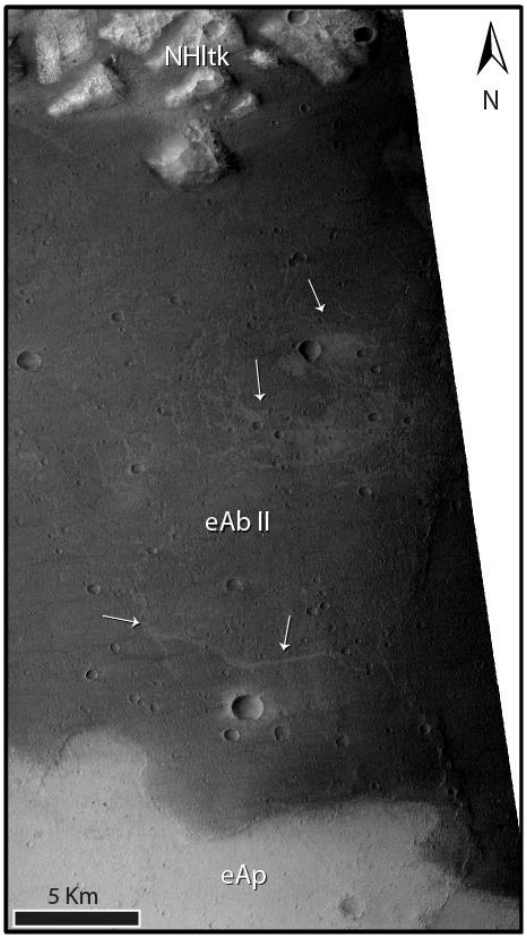

Figure 3.11: The Early Amazonian basin unit II (eAbII) in the Atlantis basin. White arrows point to fractures in the potential lava flow. The lobe shape of the eAbII and its contact with the Early Amazonian plains (eAp) unit are clearly observable (CTX image P12_005614_1455). The location of Figure 3.11 is marked in Figure 3.2b.

2) PLAIN UNIT (EAP)

The plains unit (eAp) (Table 3.3 and Figure 3.12) is a thin, dark layer covering broad parts of the floors of the four basins (Figures 3.9, 3.11, and 3.12). It has a smooth texture at CTX resolution and partly covers the light-toned materials. It has a model absolute age of ~2.75 (+0.49/-0.85) Ga, corresponding to the Early Amazonian (Figure 3.4). The eAp unit

partly covers the light-toned material in the northern basin (Figure 3.7b) and fills the depressions between the knobs in the Atlantis (Figure 3.5 and 3.12), Simois (Figure 3.9), and Caralis basins showing later emplacement than the knob formation. On the eastern wall of the Simois and northern basins, where the NHlts unit is best exposed, we observed that the eAp unit is stratigraphically on top of the NHlts unit, and that the eAp unit has also filled the channels that appear to be related to the erosion of NHlte (Figure 3.12).

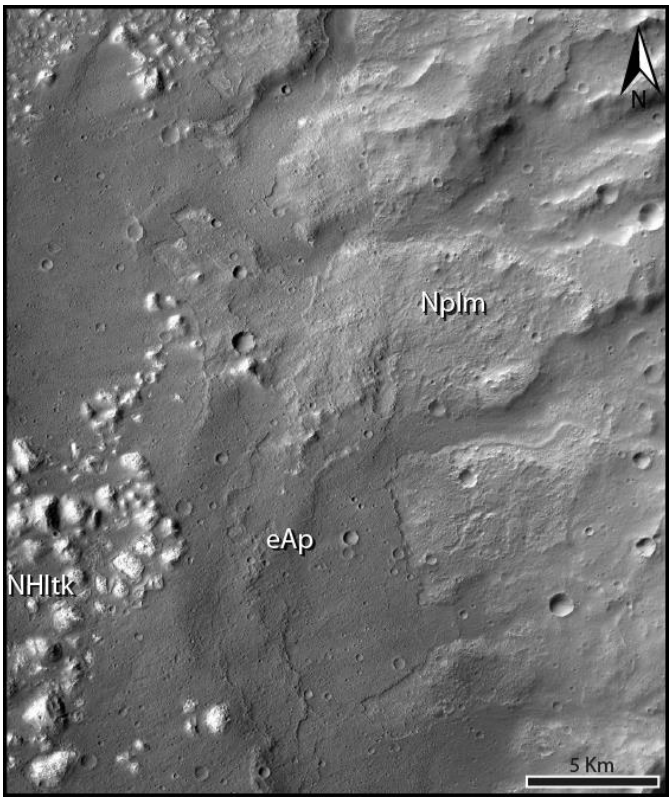

Figure 3.12: The Early Amazonian plains unit (eAp) in the Atlantis basin, covering the channel floors. The contacts between the eAp unit with the Nplm and NHltk units are visibly observable (CTX images B05_011600_1452 and P17_007684_1461). The location of Figure 3.12 is marked in Figure 3.5.

iv. STRATIGRAPHY

The Noachian cratered plateau (Nplc) and modified basement (Nplm) units represent the oldest surface units in the study area (Figure 3.13). Directly on top of Nplm lies the light-toned material (Figure 3.3b), which has been observed in all four studied basins of the eastern Eridania region. As discussed above, light-toned materials are found in three different morphological varieties: knobby light-toned (NHltk), smooth light-toned (NHlts), and Electris deposit (NHlte). They are partly covered by the Early Amazonian plains unit (eAp) and basin units (eAbI/eAbII) (Figure 3.3b and Figure 3.13). The NHltk is located on the floors of the basins, and it is the first observable depositional unit in the study area. The valley between the knobs is partly covered by eAp and partly by eAbI/eAbII. These two units may also cover any light-toned materials between the knobs as well as on the basin rim. The extent to which light-toned materials are present under the surface is unknown, and therefore the total thickness of the NHltk unit is not clear. The outcrops of NHlts observed at the basin rims are also partly covered by the eAp unit.

The NHlte is the third sub-unit of light-toned material. It has not been observed on the floors of the basins, but it is found at higher elevations in the form of mesas on the plateaus around the basin rims (Figure 3.3b, and Figure 3.9). At the Atlantis and Simois basins, these deposits are exposed close to the NHlts outcrops, and they appear to be stratigraphically lower than eAp (Figure 3.9). Furthermore, the local outcrops on the surface of NHlte reveal that materials under the thin mantling layer covering this deposit are light-toned (Figure 3.10). The light-toned albedo of the NHlte suggests that they are composed of similar material as in

NHltk and NHlts. They also have similar stratigraphical relations, i.e., being overlaid by eAp, which suggests that they were deposited close to the same period of time.

The basin units of eAbI and eAbII are mainly observed in the Atlantis and Caralis basins. The eAbI unit is located in the center of the Atlantis basin floor, and eAbII is on the southern part of the Atlantis and Caralis basin floors. These two units cover the gaps between the knobs, and in high-resolution images we can clearly observe that eAbI and eAbII are located stratigraphically above NHltk (Figure 3.11). We infer, therefore, that the emplacement of eAbI and eAbII occurred after the formation of the knobby terrain.

The eAp unit is stratigraphically on top of the light-toned materials (NHltk, NHlts, and NHlte) (Figure 3.5, 3.9, 3.12). It is abundant in these four basins, and its distribution does not seem to be related to elevation. On the eastern wall of the Atlantis and Simois basins, the eAp unit is observed in close association with the channels and locally covers their floors (Figure 3.9 and 3.12). The eAp may correspond to the mantling layer that partly covers the Nplm and NHlte units, suggesting its late emplacement, and the airfall-related deposition. The model absolute age of the mantling layer is around 2.31 (+0.37/-0.38) Ga (Figure 3.4a) corresponding to the Early Amazonian, which is comparable with the Early Amazonian age of the eAp unit.

Our crater count shows that the eAp unit and the earliest volcanic activity (eAbI) have an age of ~2.75 (+0.49/-0.85) Ga and ~2.77 (+0.24/-0.29) Ga, respectively, which corresponds to the Early Amazonian (Figure 4b, and c). The fact that eAp and eAbI are stratigraphically on top of NHltk indicates that the knob fields (NHltk) were emplaced before the Early Amazonian epoch. The model absolute age of the eAbII unit, which is around 1.54 (±0.11) Ga (Figure 3.4d), indicates that the potential volcanic activity occurred in this area between 2.77 (+0.24/-0.29) Ga and 1.54 (±0.11) Ga (Early Amazonian) (Figure 3.13).

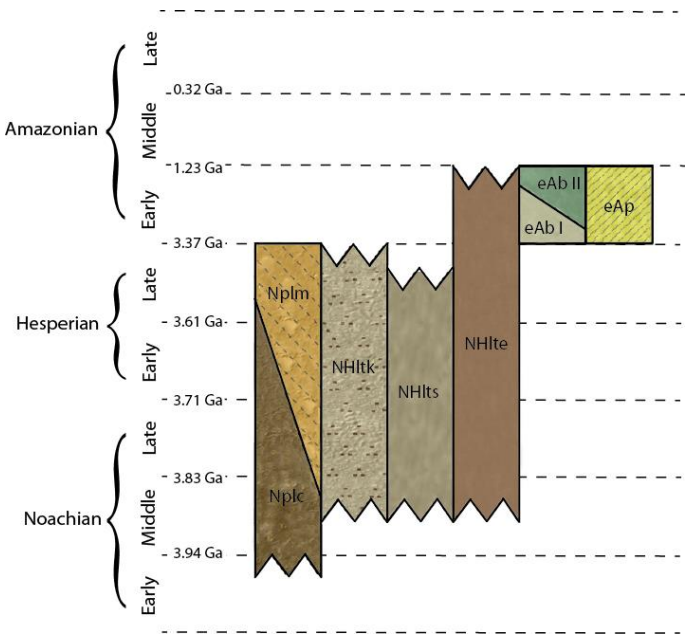

Figure 3.13: Stratigraphic column of the mapped units. Unit labels and colours correspond to the Geologic map shown in Figure 3.3-a. The epoch boundaries are from Michael [2013].

e. MINERALOGICAL COMPOSITION OF THE LIGHT-TONED MATERIALS

Fe/Mg-phyllosilicates are the most common alteration products detected from orbit in most regions on Mars [e.g., *Bibring et al.*, 2006; *Mustard et al.*, 2008b; *Ehlmann et al.*, 2011; *Wray et al.*, 2011; *Carter et al.*, 2013]. Minerals in geologic context yield strong constraints on their paleo-environmental conditions, and they, therefore, provide a unique insight into the past Martian climate and geologic history. The composition of light-toned materials in Terra Sirenum has been the subject of several recent studies [*Glotch et al.*, 2010; *Annex and Howard*, 2011; *Davila et al.*, 2011; *Ruesch et al.*, 2012; *Adeli et al.*, 2013; *Wendt et al.*, 2013], which all agreed that these materials are at least partly composed of Fe/Mg-phyllosilicate-rich material. Additionally *Osterloo et al.* [2010], using THEMIS data, reported the presence of chlorides in the northern basin. The Al-rich phyllosilicate outcrops [*Adeli et al.*, 2013] in direct contact with Fe/Mg-phyllosilicates and the location of chloride-bearing materials nearby suggest a more complex history of alteration and erosion than has been previously recognized in the studied basins in Terra Sirenum.

We analyzed 45 CRISM TRDR (Targeted Reduced Data Record) observations that were available in our study area. The 17 datasets, in which we detected Fe/Mg- and/or Al-phyllosilicates, are reported in Table 2 and their locations are shown in Figure 3.2b. The frequency of the phyllosilicates detected may be underestimated due to the spatial resolution of the data and the poor quality of some of them due to surface dust.

i. FE/MG-PHYLLOSILICATES

The Fe/Mg-phyllosilicate-rich material has been widely detected in Terra Sirenum [e.g., *Glotch et al.*, 2010; *Ruesch et al.*, 2012; *Wendt et al.*, 2013]. It appears as light-toned and polygonally fractured deposits. Fe/Mg-phyllosilicates rest on top of materials of Noachian age (the Nplc unit), and they have been detected in knobs on the floors of all four basins (the NHltk unit), as well as in the smooth light-toned material (NHlts).

We identified Fe/Mg-phyllosilicates in 17 observations (Table 3.2 and Figure 3.2b). Three CRISM observations showing characteristic spectra of Fe/Mg-phyllosilicates are shown in Figures 3.14 and 3.15. These spectra have a small absorption band at 1.4 μm, a larger band at 1.9 μm, and an additional band at 2.31 μm. The band at 2.3 μm is due to vibrations of Mg^{2+}-OH and $Fe^{2+/3+}$-OH in the mineral structure. The CRISM ratio spectra suggests that the Fe/Mg-phyllosilicates detected in this area may correspond to Fe/Mg-smectites (e.g., nontronite [*Bishop et al.*, 2008a] and saponite [*Clark et al.*, 2007]). The Fe/Mg-rich phyllosilicate minerals were detected in both types of light-toned deposits: the Knobby-light-toned on the floor of all basins (NHltk, Figure 3.14) and the smooth-light-toned materials along the basins rim (NHlts, Figure 3.15).

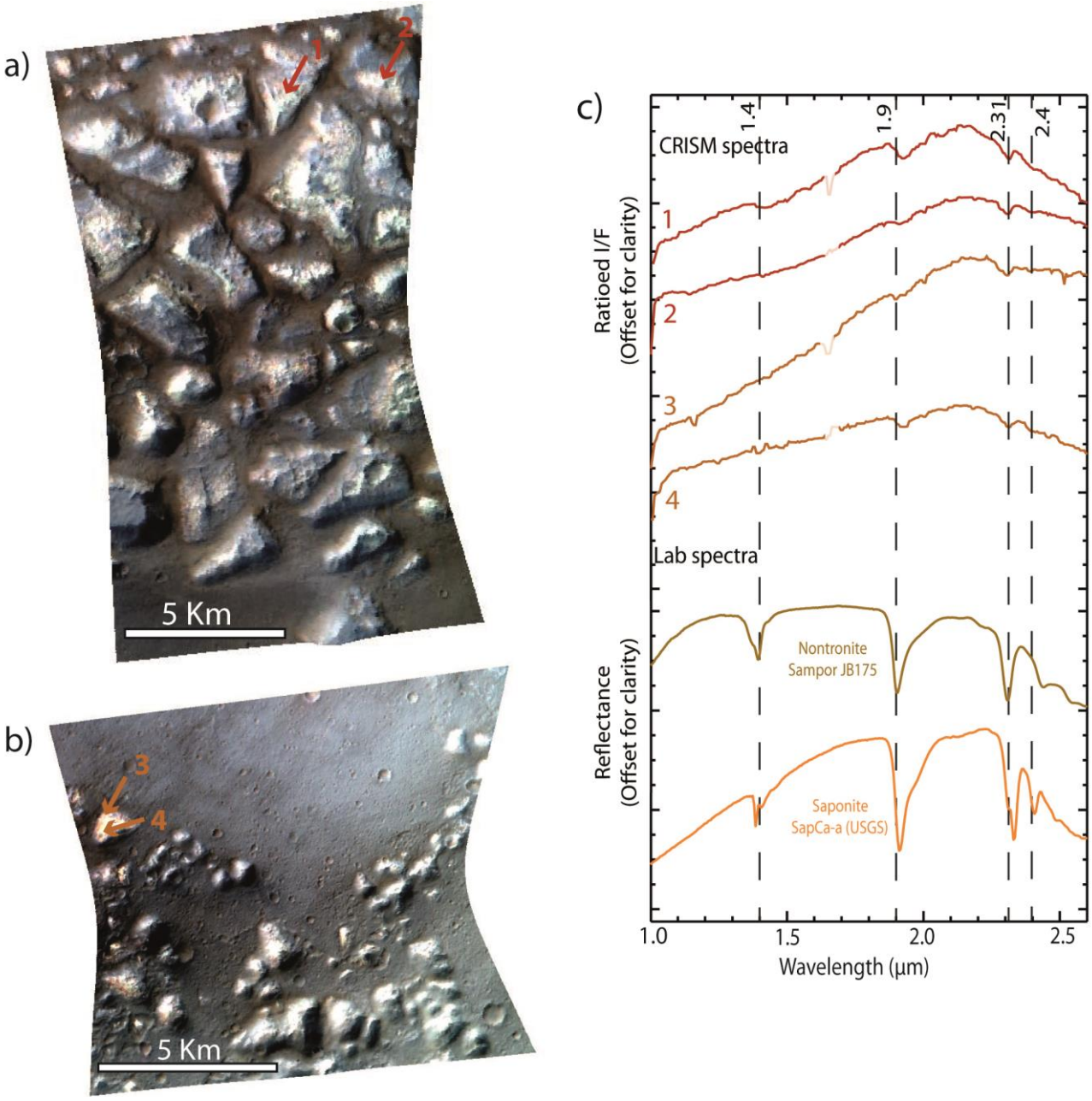

Figure 3.14: Fe/Mg-phyllosilicates in the NHltk unit located on the floor of the Atlantis basin. (a) False color image of the CRISM observation HRL 8d28 (red: 2.5μm; green: 1.5μm; blue: 1.08μm). (b) False color image of the CRISM observation FRT 913a (same RGB parameters as in (a)). (c) CRISM spectra (ratioed I/F) averaged for a 3×3 pixel area of Fe/Mg-phyllosilicates compared to spectral laboratory (see Section b.ii). Locations of the averaged pixels are indicated by color-coded and numbered arrows in (a) and (b). High-frequency noise at ~1.65μm correspond to spurious features formed at the boundary of detector zones [Murchie et al., 2009] and are partially masked. Locations of Figure 3.14 (a and b) are marked in Figure 3.2b and Table 3.2.

ii. AL-PHYLLOSILICATES

Al-phyllosilicate spectra were observed in two CRISM observations (Table 3.2 and Figure 3.15). Al-phyllosilicate-bearing materials are identified by their absorption bands at ~1.4 μm, ~1.9 μm, and ~2.2 μm. The band at 2.2 μm is due to the presence of the Al^{2+}-OH bond. Fe/Mg and Al-phyllosilicate spectra are also characterized by an absorption band at ~1.4 μm due to the first overtone of the OH stretch and at ~1.9 μm due to the combination of molecular H_2O with OH stretches [*Clark et al.*, 1990]. Most of the analyzed spectra have a band at 2.2 μm that is likely due to an Al-OH bond indicative of Al-phyllosilicates. The exact nature of Al-phyllosilicates is unclear, but the 2.2 μm-band has a rather narrow and symmetric shape suggestive of Al-smectites (e.g., montmorillonite [*Bishop et al.*, 2008a]) (Figure 3.15). Some spectra display an asymmetric doublet that is more consistent with kaolinite [*Clark et al.*, 1990; *Bishop et al.*, 2008a] (Figure 3.15).

The Al-phyllosilicates are located on the rim of the Simois basin (Figure 3.15a) and the floor of the northern basin (Figure 3.15b). In contrast to the Fe/Mg-phyllosilicates, the Al-phyllosilicates are only detected on the smooth light-toned materials (the NHlts unit). Exposed below a dark cap, the Al-phyllosilicate-rich material appears as light blue to green outcrops in CRISM false-color images (Figure 3.15a and b). The Al-phyllosilicate-rich outcrops are on top of Fe/Mg-phyllosilicate-rich outcrops that appear in red tones on the false-color image of Figure 3.15a. The phyllosilicate-rich outcrops were exposed where the Early Amazonian plains (eAp) unit has been removed by erosion.

iii. CHLORIDE SALTS

Analyses of orbital data, mostly THEMIS and partly OMEGA and CRISM, have indicated the presence of chloride salts in Terra Sirenum [*Glotch et al.*, 2010; *Osterloo et al.*, 2010; *Davila et al.*, 2011; *Ruesch et al.*, 2012; *Nazarian and Rogers*, 2013]. Using THEMIS DCS data, we confirm the detection of chloride-bearing materials in shallow depressions in the northern basin by *Osterloo et al.* [2010] (Figure 3.16). These materials appear as light-toned deposits with polygonal fractures that are a few tens of meters wide with an irregular shape that does not follow a geometrical pattern (Figure 3.16d). They are located at five sites within the smooth light-toned material (NHlts unit), ranging from a few tens of meters to a few kilometers wide (Figure 3.16b, and c). The chloride-bearing materials have a thickness of about 5 meters in Terra Sirenum [*Osterloo et al.*, 2010] and are found in proximity to phyllosilicate-rich deposits (Figure 3.7d and 3.16c). The HiRISE images reveal that the chloride-bearing deposits are stratigraphically on top of phyllosilicate-bearing materials (Figure 3.16c). Thus, the chloride-bearing deposits likely formed after the deposition of the phyllosilicate-bearing material. This relation between chloride-bearing and phyllosilicate-rich materials has also been observed in other areas in Terra Sirenum [e.g., *Glotch et al.*, 2010; *Osterloo et al.*, 2010; *Ruesch et al.*, 2012] and interpreted as resulting from water accumulation in ponds, brine concentration by water evaporation, and precipitation [*Osterloo et al.*, 2010].

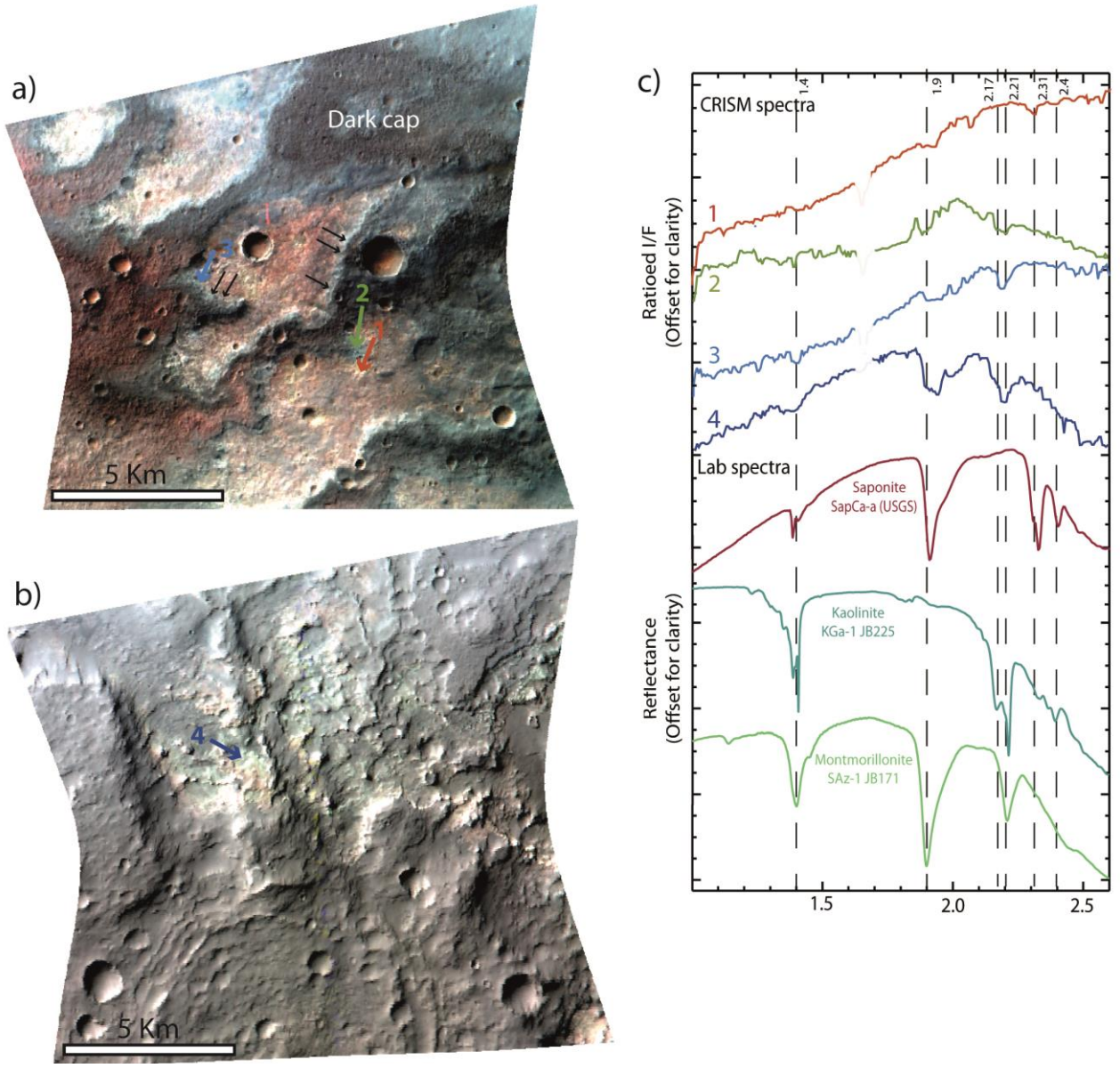

Figure 3.15: The sequence of the Al-phyllosilicate-rich materials on top of the Fe/Mg-phyllosilicate-rich material in NHlts unit. (a) False color image of the CRISM observation FRT 951c (red: 2.5μm; green: 1.5μm; blue: 1.08μm), located on the rim of the Simois basin. The Al-phyllosilicate-rich material appears in green/blue color and been pointed out by black arrows. The green arrow numbered as 2 and the blue one numbered as 3 show the location of the correspond spectra in c). The Fe/Mg-phyllosilicate-rich material appears as red/orange and the red arrow numbered as 1) shows the location of the correspond spectrum in c). (b) False color image of the CRISM observation FRT cb5c (red: 2.5μm; green: 1.5μm; blue: 1.01μm), located in the northern basin. (c) CRISM spectra (ratioed I/F) averaged for a 3×3 pixels area compared to spectral laboratory (see Section 2-2). Locations of the averaged pixels are indicated by color-coded and numbered arrows in (a) and (b). Ratioed spectra display a band at ~1.65 μm corresponding to a spurious band formed at the boundary of detector zones [Murchie et al., 2009] and are partially masked. Locations of the Figure 3.15 (a and b) are marked in Figure 3.2b.

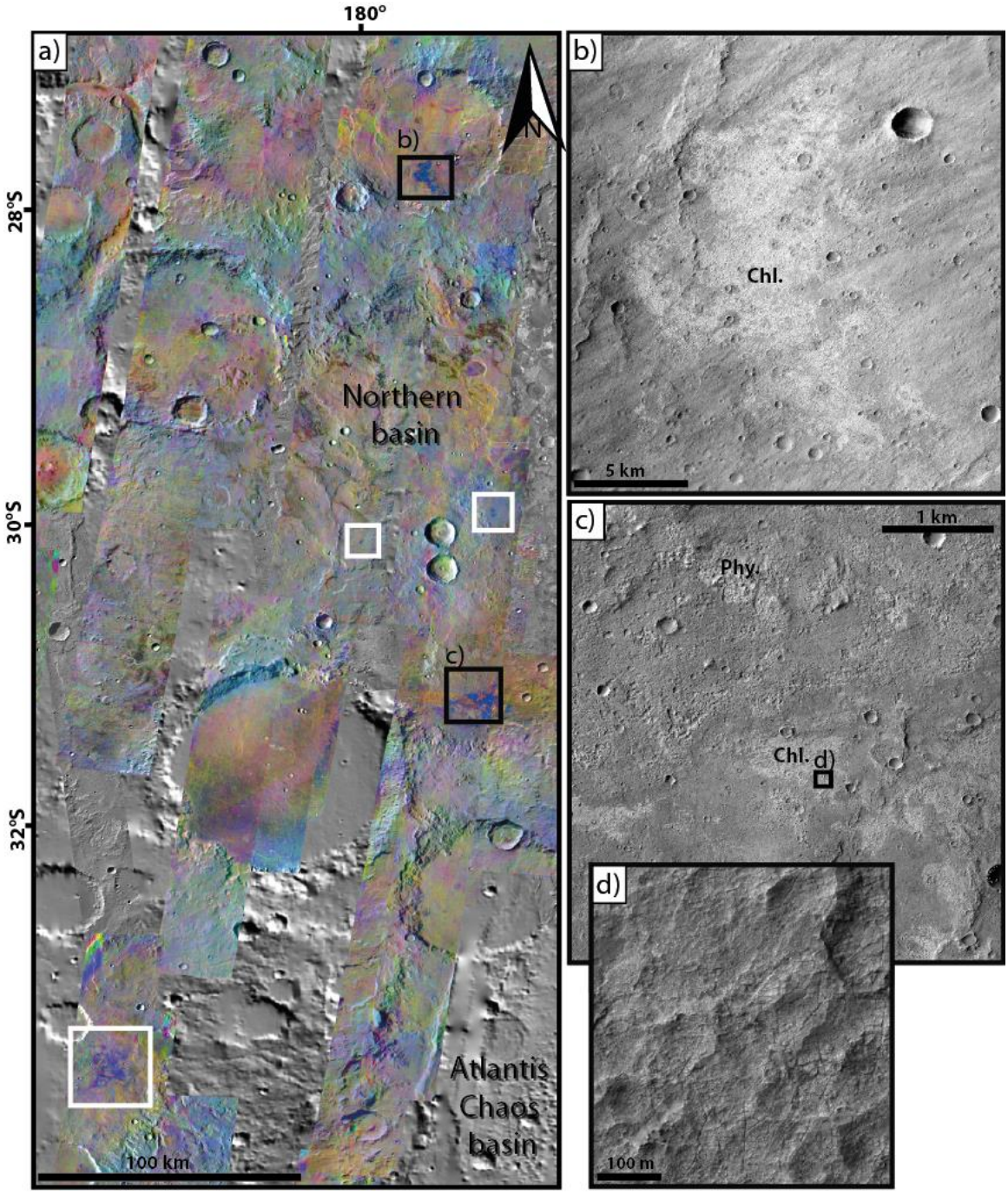

Figure 3.16: (a) Mosaic of false-color THEMIS TIR radiance data that are displayed in 8/7/5 DCS bands as red/green/blue overlying a MOLA hillshade map. Chloride salts appear in blue (white and black boxes). Black boxes represent location of (b) and (c). (b) Chloride-rich materials deposited on the floor of a crater in the northern basin (CTX image P12_005680_1522). (c) Chloride-bearing deposits in the northern basin (HiRISE image B02_010387_1483). (d) Blow-up of portion of panel (c) showing the texture of the chloride-bearing materials. Location of the Figure 3.16 is marked in Figure 1.

f. DISCUSSION

i. ERIDANIA PALEOLAKE

The Eridania lake is hypothesized to have existed, perhaps intermittently, sometimes during the Middle to Late Noachian Epochs [*Irwin et al.*, 2002; 2004; *de Pablo et al.*, 2004], and it may have drained through Ma'adim Vallis [*Cabrol et al.*, 1996; 1998; *Irwin et al.*, 2002; 2004] which is one of the largest valleys on Mars. The highest possible level of this paleolake would have been about 1100 m [*de Pablo*, 2003; *Irwin et al.*, 2004]. Only a few types of landforms may be indicative of a potential shoreline, e.g., a common break in slope below 1100–1200 m [*Irwin et al.*, 2004]. The lack of clear indicators of shorelines does not constrain the duration of the Eridania lake. The water level may have been variable, and most morphological evidence for shorelines may have been eroded. In general, ancient shorelines are not likely to be well preserved due to impact gardening and aeolian erosion [*Irwin and Zimbelman*, 2012], especially in an area like Terra Sirenum, where a significant amount of post-lacustrine resurfacing has occurred. Moreover, the lake may have been seasonally or perennially ice-covered, and the formation of typical shoreline landforms may have been impeded. The extent of the paleolake is indicated by the elevation of the overspill into Ma'adim Vallis, which may have been formed by one or a few catastrophic overflows of the Eridania lake near the Noachian/Hesperian boundary [*Irwin et al.*, 2004].

Our geologic map (Figure 3.3a) and stratigraphic results (Figure 3.3b, and 3.13) show that the thick unit of phyllosilicate-bearing material is the first observable unit that was deposited on top of the Noachian basement (Nplc unit). Other units were deposited on top of the phyllosilicate-bearing materials and post-date the formation of the knobs, i.e., they must have formed after the decline of the lake. By comparing the age of the upper units (Early Amazonian) with the basement (Middle-Late Noachian), we can conclude that deposition, alteration and erosion of the knobby materials took place between the Late Noachian and Early Amazonian, and accordingly, the age of the Eridania lake and later smaller lakes is bracketed by these upper and lower limits.

When the water level decreased, each basin would have hosted an individual lake. *Irwin et al.* [2004] interpreted the elevation-controlled fluvial incision around the Eridania basin as an indication of the presence of standing bodies of water in these depressions. Their interpretation is consistent with our observation that the channels on the basin rims terminate at a certain elevation (Figure 3.2-a). The source of water could have been surface runoff or groundwater. Evidence for fluvial erosion (Figure 3.5) and degraded impact craters suggest an active role for surface hydrological processes. However, the relatively sparse valley networks in our study area do not support surface runoff as the dominant water source for the Eridania lake. Another possibility is rise of groundwater aquifer. The model of *Andrews-Hanna et al.* [2008] suggests that in the Terra Sirenum region, groundwater would have reached the surface [see Figure 7 in *Fassett and Head*, 2008]. A subsurface aquifer may have been partly recharged by precipitation, surface runoff, and/or melting of seasonal ice/snow

cover. A regional aquifer has also been proposed as source of water for the Columbus crater lake [*Wray et al.*, 2011], located at the northeast of our study area.

ii. FORMATION OF ALTERATION AND EVAPORATION MINERALS

1) FE/MG-CLAY MEMBER OF THE LIGHT-TONED MATERIALS

Fe/Mg-phyllosilicates have been widely detected in the light-toned material located on the floor (the NHltk unit) and on the rims (the NHlts units) of the basins (Figure 3.14, 3.15, and Table 3.2). The widespread deposition of this light-toned material and the lack of large inlet channels and alluvial fans in the basins suggest that the light-toned materials of the NHltk and NHlts units are primarily airfall, rather than fluvio-lacustrine deposits. Airfall deposits such as volcanic ash and other sources such as tuff or dust may have covered a wide region, including both the subaqueous and subaerial domains. Airfall deposits are thought to be major landform-building materials in this area [*Grant and Schultz*, 1990; *Irwin et al.*, 2004; *Grant et al.*, 2010; *Wendt et al.*, 2013]. A continuous layer of airfall materials may have covered the surface, including NHlte in higher elevations, NHlts on the basin rims, and NHltk on the basin floors. The inner wall of several impact craters located in the Early Amazonian plains (eAp) unit reveals the presence of light-toned material under eAp (Figure 3.8), suggesting that this unit is widespread and contiguous between the NHltk and NHlts units. HiRISE images of the surface and margins of the Electris deposits (NHlte) mesas also show outcrops of light-toned material that display similar albedo and polygonal fractures as NHltk and NHlts (Figure 3.10). These outcrops suggest that phyllosilicate-rich material may be present on the NHlte mesas, although the lack of CRISM observations and a thin mantling layer inhibit their detection. The NHlte deposit was later eroded by either fluvial (Figure 3.9) or aeolian activity and transported into the basins. The remnants of the NHlte are now observable as mesas, located on plateaus around the basins.

The Fe/Mg-phyllosilicates generally form in neutral to alkaline environments [e.g., *McKeown et al.*, 2009], and they are major products of chemical weathering of mafic silicate minerals [*Poulet et al.*, 2005]. The most essential factors influencing the formation of clay minerals are salinity and pH-value. Low salinity and near-neutral pH are suitable for the formation of fibrous clay minerals like sepiolite, whereas higher salinity or pH are more suitable for layered phyllosilicates (silicate sheets) [*Weaver*, 1989] like saponite and smectite. The change in salinity and pH is generally controlled by sediment concentration and evaporation. The Fe/Mg-phyllosilicates in our study area are saponite and/or nontronite (Figures 3.14 and 3.15), suggesting a formation in alkaline environment.

It is unclear whether the detected phyllosilicates are authigenic or detrital, and distinguishing between detrital/fluvial and authigenic/lacustrine clay minerals using orbital data is difficult. The basins were sediment sinks, and therefore, in the case that transported sediments were originally unaltered, the environment may have been suitable for post-depositional alteration to phyllosilicates. Yet the wide distribution of a thick layer of phyllosilicate-rich material on the floor, rim and on the plateaus around the basins would

argue that the phyllosilicates or some fraction of them may have been detrital, and were transported into the basins by aeolian and/or fluvial activity. In this case, they must have been a result of the Noachian crust alteration, which is very likely considering the abundance of liquid water on the Martian surface at ~3.96 to 3.56 Ga. Alternatively, the Fe/Mg-phyllosilicates may have also formed in a hydrothermal environment, either magmatic or impact-related. Secondary minerals expected in hydrothermal alteration are mostly montmorillonite, kaolinite, beidellite, nontronite, vermiculite, chlorite, and prehnite [*Ehlmann et al.*, 2011; *Le Deit et al.*, 2012], most of which have been detected in the study area (Figure 3.14, 3.15, 3.16), except prehnite, which is expected in case of impact-related hydrothermal systems. However, these minerals can also form in other alteration environments and thus do not provide conclusive evidence for hydrothermal activity. Both impact-related and magmatic hydrothermal systems would tend to produce spatially restricted outcrops. However, the widespread lateral (Figure 3.3a) and vertical distribution (Figure 3.3b) of Fe/Mg-phyllosilicates does not support an origin by localized processes.

The raised ridges observed within the phyllosilicate-bearing material (Figure 3.6d) have similar characteristics to ridges exposed in other phyllosilicate-rich outcrops on Mars, including the Nili Fossae region [*Mangold et al.*, 2007] and Gale Crater [*Léveillé et al.*, 2014]. Their positive relief implies that they are more resistant to erosion than surrounding materials, suggesting that they represent fractures that had been filled and cemented after the deposition of the host material. They are mostly interpreted as mineralized fracture fillings resulting from fluid circulation [*Mangold et al.*, 2007; *Saper and Mustard*, 2013; *Léveillé et al.*, 2014]. *Léveillé et al.* [2014] analyzed these fractures in the Sheepbed mudstone, Yellowknife Bay formation in Gale Crater, and they reported the presence of Fe/Mg-rich smectite, or saponite in the filled fractures, which may also be the main clay mineral constituent of the host mudstone.

2) Al- and Fe/Mg-clay member of the light-toned materials

Al-rich phyllosilicates as well as Fe/Mg-rich phyllosilicates are detected in the smooth-light-toned materials (the NHlts unit) located on the rims of the Atlantis, Simois, Caralis and northern basins. The spectra of the Al-phyllosilicates are consistent with kaolinite and Al smectites (e.g., montmorillonite) (Figure 3.15). Pedogenic alteration, hydrothermal activity, and burial metamorphism are common terrestrial processes for Al-phyllosilicate formation. Kaolinite formation on Earth occurs mainly in tropical areas with extensive leaching by a substantial amount of water [*Curtis and Spears*, 1971]. However, acidic water containing carbonic acid (H_2CO_3) can potentially increase the kaolinite formation rate [*Noe Dobrea and Swayze*, 2010]. Pedogenic leaching through preexisting phyllosilicates in a slightly acidic condition [*Poulet et al.*, 2005] would convert superficial deposits into kaolinite [*McKeown et al.*, 2009]. Both montmorillonite and kaolinite have been observed on the eastern rim of the Simois basin and in the northern basin, but no stratigraphic relation between these Al-phyllosilicate-bearing materials has been observed. The stratigraphic sequence of Al-rich phyllosilicates on top of Fe/Mg-rich phyllosilicate minerals has also been observed in other places on Mars (e.g., Mawrth Vallis [*Loizeau et al.*, 2012], Valles Marineris [*Le Deit et*

al., 2012], and Nili Fossae [*Ehlmann et al.*, 2009]). In all of these cases it has been interpreted as the result of a pedogenic alteration.

After the decrease of the water level in the lakes, the basin rims were exposed to a limited amount of liquid water feeding the smaller lakes (precipitation and/or ice/snow melt). It produced a widespread pedogenic leaching process in the superficial Fe/Mg-phyllosilicate-rich soil. This process led to a preferential top-down transport of more soluble ions such as Na, K, Ca, Fe, and Mg, whereas the less mobile Al^{3+} has remained in the upper part of the altered unit [*Le Deit et al.*, 2012], resulting in a sequence of Al-phyllosilicates above Fe/Mg-phyllosilicates [*McKeown et al.*, 2009; *Le Deit et al.*, 2012]. As the leaching process continued and more water washed the Fe away, montmorillonite (Al smectite) formed [*McKeown et al.*, 2009]. As long as this subsequent alteration mechanism continued, kaolinite group minerals were formed near the surface, and the formation of montmorillonite continued at a greater depth [*McKeown et al.*, 2009].

Late erosional mechanisms have opened geological windows into the smooth light-toned material (NHlts unit) by locally eroding the plains unit (eAp) cap rock (Figure 3.9), revealing the light-toned material of the NHlts unit and presence of the sequence of Al-phyllosilicates and Fe/Mg-phyllosilicates. The exposed outcrops of Al-phyllosilicate-rich material are only a few tens of meters wide in CRISM images (Figure 3.15) and, therefore, opportunities for observation and detection are limited. The Al-phyllosilicates are mainly observed along the rim of these outcrops (Figure 3.15a), suggesting that the erosional processes have removed them from the surface of the outcrops, where we can observe only Fe/Mg-rich phyllosilicates (Figure 3.15a).

Hydrothermal alteration [*Marzo et al.*, 2010] and burial metamorphism [*Weaver*, 1989] are other formation mechanisms that could explain the observation of Al-phyllosilicates above Fe/Mg-phyllosilicates. These mechanisms, however, are not consistent with our morphological observations. The NHlts unit is currently buried not under a thick layer of deposits but under a thin layer of cap rock (the eAp unit), and neither does it show morphological evidence of an earlier thick covering layer nor of exhumation. Hence we consider burial metamorphism to be unlikely in this area. In addition, we have not observed any clear mineralogical and morphological evidence of hydrothermal activity in our study area as discussed in the previous Section (3.f.ii.1). The presence of fluvial channels along the basin rims suggests precipitation as the major source of water for the pedogenic alteration, and not hydrothermal fluids, which would be more localized.

3) CHLORIDE MEMBER OF THE LIGHT-TONED MATERIALS

On the smooth light-toned material (NHlts unit) observed in the northern basin, we detected chloride salts in small depressions (Figure 3.16). The chloride salts have been observed on top of a thin and dark layer covering the phyllosilicate-bearing deposits (Figure 3.7d) and, therefore, it can be inferred that chloride-rich sediments are located stratigraphically on top of Fe/Mg-phyllosilicates, which suggests that they formed after the

deposition of phyllosilicates. The formation age of chlorides cannot be constrained by crater counting, however, their distribution and stratigraphic relations suggest that they formed after the last stage of small lakes, and before the emplacement of the Early Amazonian plains unit (eAp). The lack of chloride observations in other basins may indicate that the northern basin hosted a different environment, in which evaporite minerals formed at the end of or after the lake desiccation. Chloride salts may also have existed in other basins but were eroded [*Osterloo et al.*, 2010] or covered by the eAp unit.

Two main hypotheses for the formation of chloride salts on Mars have been suggested by *Osterloo et al.* [2010]. The first is ponding of surface runoff or groundwater upwelling, which has been proposed as the dominant salt formation mechanism in Meridiani Planum [e.g., *McLennan et al.*, 2005]. The main expected observations in this case are location in topographic lows, polygonal desiccation fractures [*El-Maarry et al.*, 2014], and a close proximity to valleys and phyllosilicate-bearing deposits. The second hypothesis is hydrothermal activity through impact cratering or volcanism, in which case a location of the chlorides in topographic depressions or close to a crater center would be expected. We favor precipitation in ponds fed by surface runoff or ground water discharge, because all expected features have been observed, such as polygonal patterns (Figure 3.16d), location of the chloride-rich material in depressions, and a close proximity to phyllosilicate-rich deposits (Figure 3.7d).

The formation of evaporite minerals indicates the characteristics of aqueous fluids and the chemical environment where they formed. Depending on the relative amount of the acidic fluids of HCO_3/SO_4 that are the result of basaltic weathering, as compared to the concentration percentage of evaporative elements, different minerals could precipitate [*Tosca and McLennan*, 2006]. The composition of the aqueous fluids would change as new minerals are being formed. On Earth, carbonates, sulfates, and chloride salts are common evaporite minerals formed as part of an evaporate sequence and occur in characteristic mineral assemblages, depending on the chemical characteristics of the fluid. In our study area, however, neither carbonates nor sulfates have been observed. This lack of detectable outcrops may suggest either an enigmatic chemical composition of the fluid that did not lead to the formation of carbonates and/or sulfates, or later removal of these minerals by erosion. It is, however, unclear which of the above options is more likely in our study area.

iii. POST-LAKE GEOLOGICAL EVENTS

1) DESICCATION OF ISOLATED LAKES

We do not observe outlets through which surface water could have escaped from the sub-basins, so the water likely infiltrated into the ground, evaporated, or sublimated (if the lake was ice-covered). These loss mechanisms imply either that the water input rate decreased (e.g., less precipitation) or that the evaporation or sublimation rate increased (e.g., by climate change). However, it is unclear which mechanism was responsible for the loss of the isolated lakes. Although the duration of these lakes is poorly constrained, they are hypothesized to

have existed sometimes during the Late Noachian and Early Hesperian [*Irwin et al.*, 2004]. However, the possibility of a complete desiccation of the Eridania lake and a later refilling of the small depressions cannot be ruled out.

In the light-toned materials of NHltk and NHlts, polygonal fractures are visible in HiRISE images (Figure 3.7c, d, and Figure 3.16d). They are observed in the phyllosilicate-rich and chloride-rich deposits. This kind of fracture pattern on Mars is typically interpreted as resulting from either desiccation [*Osterloo et al.*, 2010; *El-Maarry et al.*, 2014] or thermal contraction in a permafrost environment [*Levy et al.*, 2009]. Thermal contraction polygons are found mostly on young geological surfaces, particularly Amazonian in age [*Levy et al.*, 2009], whereas desiccation fractures are found on Hesperian and Noachian surfaces [*Ehlmann et al.*, 2008; *Osterloo et al.*, 2008]. Polygons related to desiccation in a playa-like environment are commonly observed in basins hypothesized to be paleolakes [*Osterloo et al.*, 2008]. Thermal contraction cracks occur in environments lacking fluvial features [*Levy et al.*, 2008]. Desiccation cracks appear in high-albedo and light-toned deposits containing phyllosilicates and/or salts [*Osterloo et al.*, 2008; *Le Deit et al.*, 2012; *El-Maarry et al.*, 2014], whereas in moderate to low albedo materials [*Christensen et al.*, 2001], thermal contraction cracks have been observed. The observed polygons in Terra Sirenum show characteristics (i.e., size, substrate age, and distribution in phyllosilicate-bearing material) similar to the polygons observed in Mawrth Vallis [e.g., *Bishop et al.*, 2008b; *Loizeau et al.*, 2010; *McKeown et al.*, 2013] and in former lacustrine settings [*El-Maarry et al.*, 2013]. The ubiquitous presence in the study area of these crack patterns in the Noachian–Hesperian-aged light-toned deposits is consistent with the rich aqueous history of these terrains.

During and/or after the desiccation of the residual lakes, erosional processes started to shape the basin floors into their current morphology. The most likely mechanisms to shape the knobs may have been wind abrasion, dissolution weathering, and dewatering [*Moore et al.*, 2003b], although the possibility of a late aqueous activity cannot be ruled out in this area, as suggested by the deposition of the Early Amazonian plains unit (eAp). Aeolian erosion may be the mechanism that mobilized materials in structurally weak zones. On the other hand, dissolution weathering [*Moore et al.*, 2003b] and seepage may have partly weakened the sediments. Those weakened parts could have been later removed by both wind and/or water. Similar mechanisms would be expected in the case of dewatering, with desiccation cracks locally weakening materials and thus permitting their subsequent mobilization. Alternatively, the floor material may have been initially fractured by an igneous intrusion and uplift that could have formed a largely structural set of floor fractures. The susceptible material along the fractures was later removed by aeolian degradation. The fractures between the knobs, however, do not reveal a preferential direction, geometric distribution, or extensional but nonsystematic joints that would be expected in the case of an igneous uplift.

In the knob fields, we sometimes observe a dark cap on top of several knobs (Figure 3.6b). It may represent the remnant of a continuous layer that was eroded and removed by the erosional mechanisms, which led to the exposure of the knobby material. Alternatively, it may represent the deposition of a late airfall material on top of the flat-

surface knobs after their formation. This dark cap may have locally preserved the knobby materials of the NHltk unit from weathering and erosion.

2) LATE STAGE AQUEOUS EVENTS

The plains unit (eAp) has an age of ~2.75 (+0.49/-0.85) Ga and is distributed homogenously and widely over the four studied basin floors (Figure 3.3a). The dark eAp materials fill the channels located on the eastern walls of the Atlantis, Simois, Caralis, and northern basins (Figure 3.5, 3.9, and 3.12). The eAp unit may have a fluvial, volcanic, or airfall origin. In case of a fluvial origin, the dark eAp materials must have been transported through the valleys into the basins, which requires liquid water with enough transport capacity to carry the materials into all four basins and distribute them widely on the basin floors, which seems unlikely given the generally cold and dry Early Amazonian climate [e.g., *Fairén*, 2010; *Lammer et al.*, 2013] and the limited presence of liquid water. Additionally, we would expect to see evidence of alluvial fans or deltas, neither of which have been observed. The eAp unit may correspond to Amazonian volcanic lava flows, which have been reported in this area at approximately the same time (see Section 3.f.iii.3). Lava flows would also cover the valley floors, if the lava source were at a high elevation on the basin rims. However, no vent that may correspond to a lava flow source has been observed. The wide and homogenous distribution of the eAp material in all four basins would instead be inconsistent with a lava flow emplacement.

The other alternative mechanism for the eAp formation could be airfall deposition that would be consistent with the widespread and homogenous distribution of this material in all four studied basins. Volcanic ash from regional volcanic activity or local volcanos [*de Pablo et al.*, 2005; *Brož et al.*, 2015] may be a source for the airfall material (see the model of *Kerber et al.* [2013]) . In the case of airfall processes, we would expect to observe this dark material all over the study area, including on the plateau and rims of the basins. The material deposited on the plateau may have been eroded either by wind or liquid water and transported into the basins. On the basin rims, however, the eAp is preserved on the floors of the valleys. This occurrence may suggest that a limited amount of liquid water originated from rainfall or ice/snow melt, flowed through the valleys into the basin, and cemented the airfall deposits. Hence the airfall processes could still have been active during the Amazonian, and not only during earlier periods when the light-toned material forming the NHltk, NHlts, and NHlte units was deposited. Considering the emplacement of the eAp unit as an airfall deposit during the Early Amazonian, we infer that Early Amazonian is the time when airfall deposition ceased in the study area.

3) VOLCANIC EVENTS

The eAbI and eAbII units with an age of 2.77 (+0.24/-0.29) Ga and 1.54 (±0.11) Ga, respectively (Early Amazonian, Figure 3.4), have been observed in Atlantis and Caralis basins. The observation of the lobate margins of eAbII may point to an emplacement by flowing lava. In this case, the observed local fracture network (Figure 3.11) in the eAbII unit

in the Atlantis basin could be interpreted as lava cooling fractures [e.g., see Figure 1b in *Aydin and DeGraff*, 1988]. Alternatively, these deposits may represent mud flows [*de Pablo and Fairén*, 2004], in which case desiccation cracks and lobe-shaped fronts would also be expected. Given the transport direction indicated by the lobe-shaped flow front, the source of water/mud would have to be located in the knobby terrain. We have, however, not observed any evidence of a water/mud source within the knobby terrain. Volcanic resurfacing, however, is a common process in former open-basin lakes in the Martian highlands, and in most of these cases it appears to have a local origin [*Goudge et al.*, 2012]. If the lava had a low viscosity, it may have spread easily covering vents or feeder fractures, thereby rendering them invisible (e.g., as in Gusev crater [*Greeley et al.*, 2005]). Ash produced by this volcanic activity could be the source of airfall materials deposited in the study area (the eAp unit). This assumption is also consistent with eAbI/eAbII and eAp having a similar age range.

iv. INTERPRETED GEOLOGIC TIMELINE

We generated a geological map of topographic basins (Atlantis, Simois, Caralis, and northern basins) in the Terra Sirenum region and determined the model absolute age of essential units in this area. We were able to reconstruct a geologic history that spans a long time period from the Noachian to Early Amazonian. Here we summarize the sequence of events (Figure 3.17):

(1) During the Late Noachian-Early Hesperian, the large Eridania lake covered the area, and its drainage to the north carved Ma'adim Vallis [*Irwin et al.*, 2002; 2004]. Later, the water level decreased, and the Eridania lake split into smaller lakes that were confined to preexisting topographic depressions. Airfall deposits accumulated light-toned and altered material on the plateaus, floors, and rims of the lakes, forming the NHltk, NHlts, and NHlte units (Figure 3.17-step 1).

(2) As the water level decreased, the NHlte that had been deposited on the plateau was eroded and transported into the basins. Additionally, the environment on the basin rims changed from subaqueous to subaerial. Surficial sediments containing Fe/Mg-rich phyllosilicates on the basin rims were partly altered to Al-phyllosilicates by pedogenesis in the presence of a limited amount of water. In the northern basin, the detection of chloride salts, located stratigraphically on top of Al-phyllosilicates, suggests that evaporite minerals may have been precipitated in a playa environment after the formation of Al-phyllosilicates (Figure 3.17-step 2).

(3) After the desiccation of the lakes during the Hesperian, weakened and weathered materials on the lake bottom were removed by wind erosion and/or episodic aqueous activity and were re-shaped into the current knobby topography of the NHltk unit (Figure 3.17-step 3)

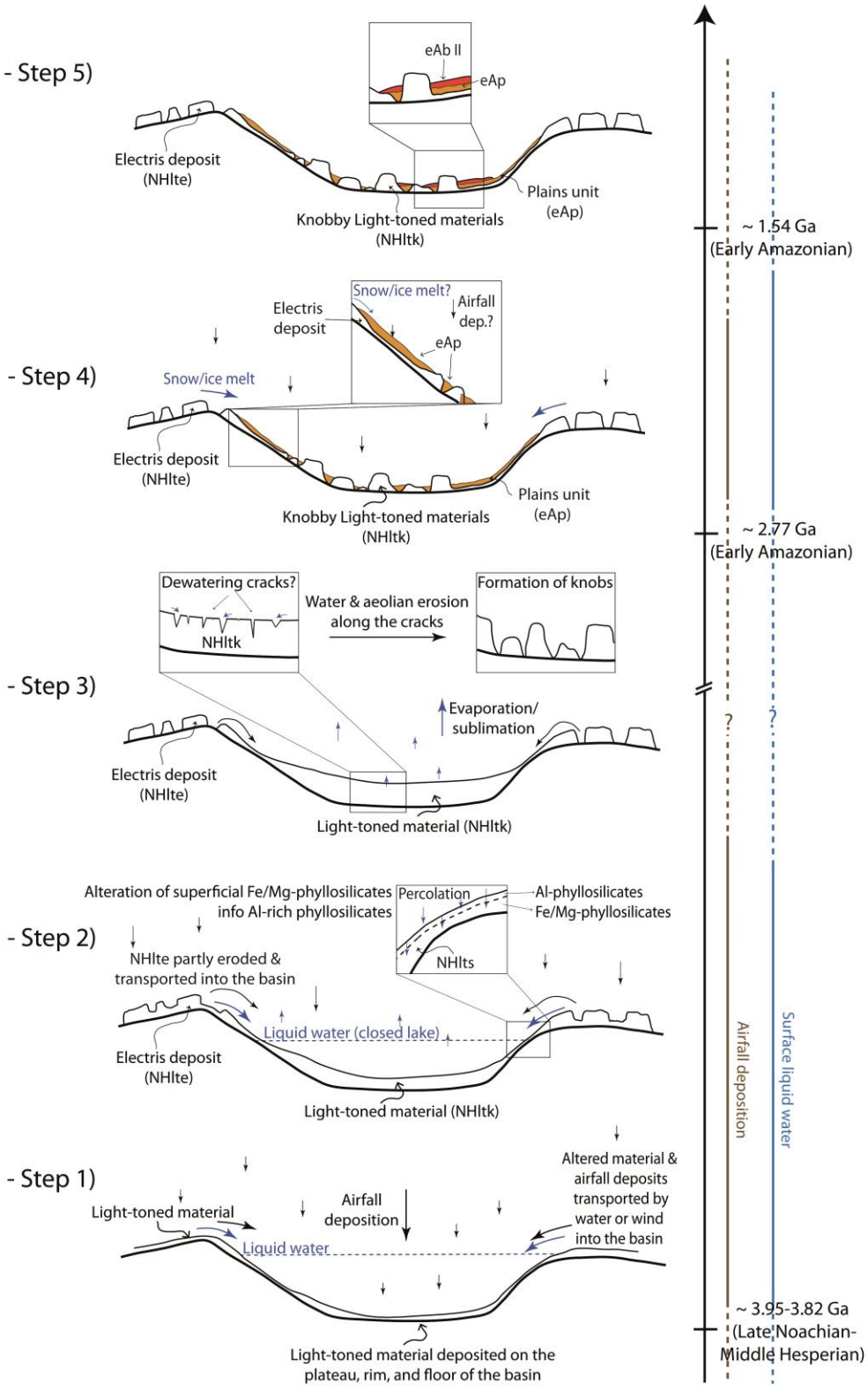

Figure 3.17: Interpreted geologic timeline deduced from the geological mapping, stratigraphic, mineralogical composition and age determination results. The Martian epochs are derived from Michael *[2013] and* Hartmann and Neukum *[2001]. [Continue in the next page]*

(4) Airfall deposition re-occurred in the Early Amazonian and covered the floors of all basins in our study area with a thin and dark material forming the eAp unit. This deposited material, especially at the basin rims, was partly indurated by late aqueous activity probably linked to rainfall and/or ice/snow melt (Figure 3.17-step 4).
(5) Thin lava flows partly covered the basin floors including the eAbI/eAbII units, suggesting that volcanism may have been episodically active during the Early Amazonian, in particular in the Atlantis and Caralis basins (Figure 3.17-step 5).

g. CONCLUSION

- We produced a geologic map of the eastern Eridania region, which includes four ancient depositional basins within the Noachian highland terrain. We mapped eight different geological units that range in age from the Late Noachian to the Early Amazonian. The map is complemented by a spectral analysis, which reveals the presence of phyllosilicates and chlorides.

- The deep basins of Atlantis, Caralis, northern, and Simois hosted lakes around the Late Noachian/Early Hesperian boundary, but their longevity is unknown. During the presence of liquid water, airfall sediments containing Fe/Mg-phyllosilicates were deposited on the plateau, rims, and floors of these basins. Outcrops of Al-phyllosilicates on the basin rims indicate a different alteration mechanism after Fe/Mg-phyllosilicate formation and deposition. Pedogenesis is most likely the process that formed Al-phyllosilicates on top of Fe/Mg-phyllosilicates by aqueous leaching. Chloride-bearing deposits that are stratigraphically above phyllosilicates suggest evaporation in a playa-type environment during the last stage of the lacustrine phase. After the eventual desiccation of the lakes, the knobby terrains were formed by dewatering, wind abrasion, and/or dissolution weathering.

[Continue from the previous page-Figure 3.17] Step 1) during the presence of a lake, potentially light-toned and altered material transported into the basin via airfall and/or fluvial mechanisms. Step 2) Decrease of level of water and erosion of light-toned material deposited on the plateau into the basin which leads to formation of mesas of NHlte. In addition, pedogenic alteration occurs through the light-toned Fe/Mg-phyllosilicate-rich material (NHlts) deposited on the basin rim, resulting to the formation of Al-phyllosilicate in the superficial soil. Step 3) Desiccation of the lake, and erosion of light-toned material deposited on the basin floor, into knobs (NHltk). Step 4) During the early Amazonian, the loess and dark airfall material deposits in the basin. Material deposited on the basin rim has been cemented by limited fluvial activity (eAp). Step 5) Potential volcanic activity (eAbI&II) took place and covered partly the eAp unit.

- The formation of the Fe/Mg-phyllosilicates, Al-phyllosilicates, and chloride salts requires conditions very different from those currently prevailing on Mars, and it suggests an active hydrologic system that has changed from enabling formation of clay minerals to evaporite minerals such as chloride salts.

- During the Early Amazonian, volcanic or other resurfacing episodes occurred in the Atlantis and Caralis basins. The Early Amazonian age of the plains unit and our assumption of its water-related deposition indicate that aqueous processes on Mars may have been episodically active from the Late Noachian/Early Hesperian to the Early Amazonian.

- Aqueous activity occurred over different periods of time in this area, as did the airfall deposition. Liquid water may have provided a habitable environment in the region, with energy and nutrition sources. Hence the eastern Eridania region is a candidate area to search for traces of past life on Mars.

Acknowledgements

This research was partly supported by the Helmholtz Association through the research alliance "Planetary Evolution and Life" and partly by the German Aerospace Center (DLR-Berlin), and the Centre National D'Études Spatiales (CNES). Data to support this paper are from the PDS Geosciences Node archive (http://pds-geosciences.wustl.edu/). We thank M.A. de Pablo, R. Irwin, T. Goudge, N.A. Cabrol, and M. Osterloo for their detailed and constructive reviews. We also appreciate the valuable discussions with T. Platz, N. Mangold, and J. Bishop during this project.

4. AMAZONIAN-AGED FLUVIAL SYSTEM AND ASSOCIATED ICE-RELATED FEATURES IN TERRA CIMMERIA, MARS

The following section has been published as: **Adeli, S.**, E. Hauber, M. Kleinhans, L. Le Deit, T. Platz, P. Fawdon, and R. Jaumann (2016). Amazonian-aged fluvial system and associated ice-related features in Terra Cimmeria, Mars. *Icarus*, 277, 286-299, doi: http://dx.doi.org/10.1016/j.icarus.2016.05.020. The author contribution is explained in the Section 1.c.

Abstract: The Martian climate throughout the Amazonian is widely believed to have been cold and hyper-arid, very similar to the current conditions. However, ubiquitous evidence of aqueous and glacial activity has been recently reported, including channels that can be tens to hundreds of kilometers long, alluvial and fluvial deposits, ice-rich mantles, and glacial and periglacial landforms. Here we study a ~340 km-long fluvial system located in the Terra Cimmeria region, in the southern mid-latitudes of Mars. The fluvial system is composed of an upstream catchment system with narrow glaciofluvial valleys and remnants of ice-rich deposits. We observe depositional features including fan-shaped deposits, and erosional features such as scour marks and streamlined islands. At the downstream section of this fluvial system is an outflow channel named Kārūn Valles, which displays a unique braided alluvial fan and terminates on the floor of the Ariadnes Colles basin. Our observations point to surface runoff of ice/snow melt as the water source for this fluvial activity. According to our crater size–frequency distribution analysis the entire fluvial system formed during early to middle Amazonian, between $\sim 1.8^{+0.2}_{-0.2}$ Ga to 510^{+40}_{-40} Ma. Hydraulic modelling indicates that the Kārūn Valles and consequently the alluvial fan formation took place in geologically short-term event(s). We conclude that liquid water was present in Terra Cimmeria during the early to middle Amazonian, and that Mars during that time may have undergone several episodic glacial-related events.

Keywords:

Mars, Surface, Climate, Ices

a. INTRODUCTION

There is extensive geomorphological and mineralogical evidence for the presence of liquid water on the Martian surface during the late Noachian and early Hesperian epochs. This includes widespread fluvial features [e.g., *Carr*, 1995; *Hynek et al.*, 2010], crater lakes [e.g., *Fassett and Head*, 2008], and abundant phyllosilicates in Noachian terrains [e.g., *Bibring et al.*, 2006; *Murchie et al.*, 2007]. These features point to a different climate, most probably to a warmer and wetter environment, during early Mars as compared to the current environmental conditions. It is debated, however, how much warmer and wetter early Mars really was, and whether it was characterized by "warm and wet" [e.g., *Craddock and Howard*, 2002] or "cold and icy" [e.g., *Wordsworth et al.*, 2015] conditions. The Amazonian climate, on the other hand, is globally considered as cold and hyperarid [e.g., *Marchant and Head*, 2007]. The nature and the time frame of the transitional phase(s) into the relatively cold and dry Amazonian period remain uncertain. Morphological evidence of Amazonian liquid water, however, has been recently identified in high-resolution images of the Martian surface returned by the Mars Odyssey (MO), Mars Express (MEX), and Mars Reconnaissance Orbiter (MRO) missions. These observations revealed the presence of Amazonian-aged fluvial channels [*Howard and Moore*, 2011; *Hobley et al.*, 2014; *Salese et al.*, 2016], alluvial fans and fan deltas [*Hauber et al.*, 2013], and very recent features including gullies [*Malin and Edgett*, 2000b], and recurring slope lineae (RSL) [*McEwen et al.*, 2011b; *Ojha et al.*, 2014]. The remnants of Amazonian-aged tropical mountain glaciers [*Head and Marchant*, 2003], mid-latitude glacial deposits [*Gallagher and Balme*, 2015], and latitude-dependent mantle [*Mustard et al.*, 2001; *Kreslavsky and Head*, 2002; *Head et al.*, 2003] point to potential recent ice ages [*Head et al.*, 2003]. Variation in spin-axis/orbital parameters [*Laskar et al.*, 2004] during the late Amazonian may have caused the mobilization of ice from high-latitudes and its re-deposition at mid-latitudes. Local melting of these ice-rich deposits may have led to the incision of the Martian surface with channels and fluvial valley systems which would offer unique insights into the Amazonian climate, which would increase our understanding of the climatic evolution of Mars and the transition from early Mars to the recent Amazonian period.

Here we study the morphology, context, likely formative processes and duration of activity of an Amazonian-aged fluvial system, including the Kārūn Valles located in the downstream section of this system. The fluvial system is located in the Terra Cimmeria region and terminates on the floor of the Ariadnes Colles basin. We conduct the first geomorphological analysis of this fluvial system based on the analysis of MO, MEx and MRO images. Our analyses revealed the existence of very well–preserved erosional features such as incised channel beds and streamlined islands, as well as depositional features including alluvial fans and fan deltas. In order to infer potential sources of water, and the formative time frame and mechanism, we investigated the geomorphology and calculated the hydraulic parameters of this fluvial system. This will help to understand the climate at the time of formation and thus the subsequent climate development towards the current conditions.

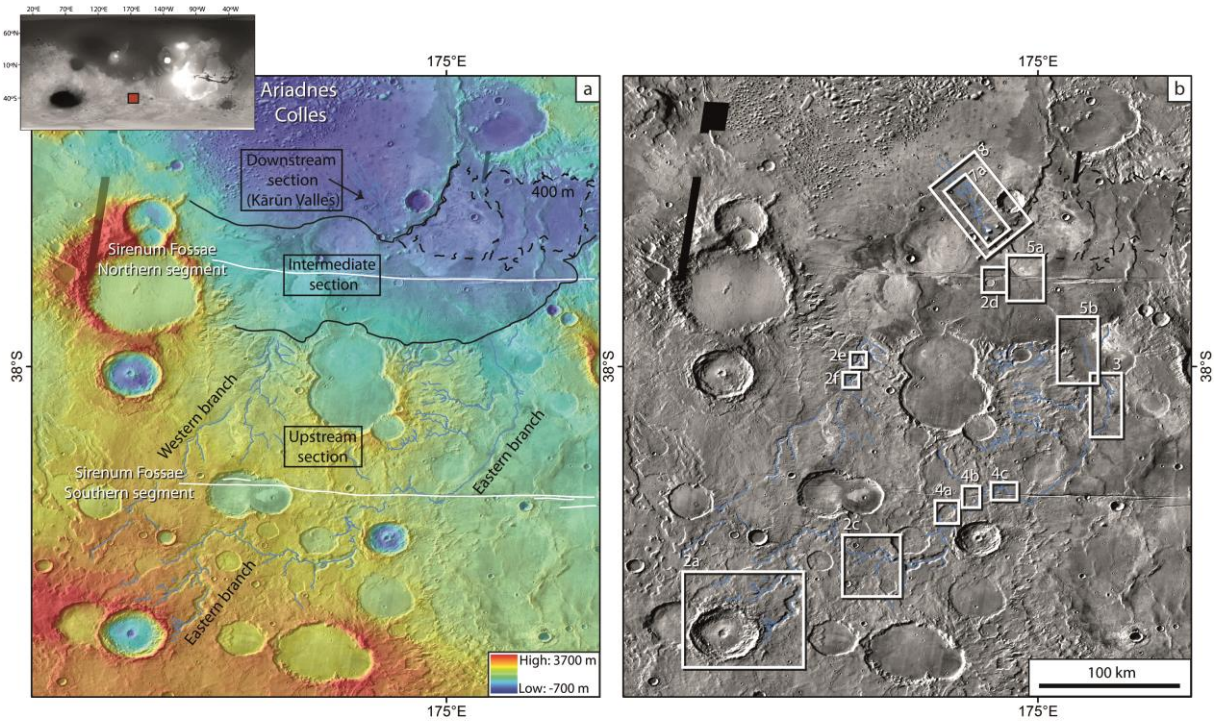

Figure 4.1: a) Study area with main physiographic elements. Colour-coded MOLA digital elevation model at 128 pixels/degree merged with a THEMIS daytime mosaic. The main geomorphologic features are mapped. The fluvial system is represented by solid blue lines, and the eastern and western branches are indicated. Solid black lines show the limit between the intermediate section and the upstream and downstream sections. The Sirenum Fossae are mapped with solid white lines. The location on Mars is shown in the top left inset. b) THEMIS daytime mosaic with white boxes indicating the locations of most figures in this paper.

b. DATA AND METHODS

For morphological investigations we used images acquired by the High Resolution Stereo Camera (HRSC) [*Neukum et al.*, 2004; *Jaumann et al.*, 2007] on board the Mars Express (MEX) orbiter and the Context Camera (CTX) [*Malin et al.*, 2007] on board the Mars Reconnaissance Orbiter (MRO), which have typical ground resolutions of 10 to 40 m and ~5 m, respectively. In order to analyse the hydraulic parameters, we generated a digital elevation model (DEM) from two CTX images (D10_031182_1435 and D09_030892_1435) using the method of *Kirk et al.* [2008]. This method uses public-domain Integrated Software for Images and Spectrometers (ISIS) software to pre-process the raw experimental data records (EDRs) before further processing using SocetSet®, a commercially available photogrammetry suite (http://www.socetset.com). During the processing in SocetSet®, we controlled the DTM using MOLA (Mars Orbital Laser Altimeter [*Smith et al.*, 2001]) track data, thus allowing us to correlate elevations between topographic datasets of different scales. The output from SocetSet® was an 18 meter per pixel (m/px) DTM resolving topography of

~50-60 m and an orthorectifed CTX image (from D09_030892_1435) at 6 m/px. The topographical information for the surrounding area of the outflow channel was derived from the gridded MOLA global DEM with a resolution of 128 pixels/degree (grid cell size ~463 m at equator) [*Smith et al.*, 2001].

Hydraulic modelling was performed on the high resolution stereo-based CTX DTM, using the method described in *Kleinhans* [2005], in order to calculate the discharge rate of the Kārūn Valles, its volumetric sediment transport rate, and other parameters described in Section 4.e aiding to better understand the formative mechanism of the outflow channel. In order to estimate the absolute model age of the fluvial activity, we analysed crater size–frequency distributions (CSFD) on CTX images at a scale of 1:24,000 in ESRI's ArcGIS. Craters were mapped using the CraterTools [*Kneissl et al.*, 2011] extension for the ArcGIS software. The Craterstats 2 software [*Michael and Neukum*, 2010] was used to model crater-based ages based on the chronology function of *Hartmann and Neukum* [2001] and the production function of *Ivanov* [2001]. Measured crater populations have been tested for randomness using the method of *Michael et al.* [2012]. The data are plotted as a cumulative presentation of the crater size–frequency distribution. As counting areas, we chose the largest possible zones, however none of the counting areas are large enough to meet the area size of larger than 1000-10,000 km^2 as suggested by *Warner et al.* [2015]. The epoch boundaries are based on Neukum system [*Hartmann and Neukum*, 2001] as explained in *Michael* [2013].

c. REGIONAL SETTING

The fluvial system is located in the mid-latitude highlands of the Terra Cimmeria region between 35° and 37° south. It terminates on the floor of the 200 km diameter Ariadnes Colles basin (Figure 4.1). This basin, as well as others in the region, presumably hosted a relative small lake during the Hesperian [*Adeli et al.*, 2015], which was a remnant of the late Noachian-early Hesperian large Eridania paleolake [*Irwin et al.*, 2002]. This area shows not only a rich aqueous history, but also Amazonian-aged water/ice-related features (as shown in this study). In fact, ice-related features have been widely reported in the mid-latitude regions of Mars [e.g., *Mustard et al.*, 2001; *Kreslavsky and Head*, 2002; *Head and Marchant*, 2003; *Hauber et al.*, 2011; *Conway and Balme*, 2014]. Latitude Dependent Mantle (LDM) is an example of these ice-related landscapes. LDM is a young (formation in the last tens of millions of years [*Kostama et al.*, 2006; *Willmes et al.*, 2012]) and ice-rich mantle located at ~30°-60°latitude in both hemispheres [*Mustard et al.*, 2001]. The mobilization of polar ice and its re-deposition due to spin-axis/orbital perturbations has been suggested as LDM formation mechanism at mid-latitudes [e.g., *Madeleine et al.*, 2009]. It has been suggested that the post-Noachian valleys in mid-latitudes may be related to the melting of snow and/or ice and subsequent runoff [*Fassett and Head*, 2007; *Howard and Moore*, 2011]. However, localized events such as melting of ground ice by emplacement of impact ejecta or a transient climate episode [*Mangold et al.*, 2012b] have also been proposed as potential source of water.

In the study area, the Sirenum Fossae graben system extends from east to west over a distance of approximately 2600 km [*Wilson and Head*, 2002]. We can clearly see two main segments of it (Figure 4. 1a) that are named "northern" and "southern" segments in this study. *Kneissl et al.* [2015] estimated the main formation time frame for Sirenum Fossae at around $3.44^{+0.1}_{-0.25}$ Ga to $3.46^{+0.046}_{-0.064}$ Ga, and a minimum activity age at 710^{+140}_{-140} Ma. The Sirenum Fossae start in the Tharsis region and terminate at ~200 km to the south of the Ariadnes Colles center. Its age shows that tectonism in Terra Cimmeria was still active during the middle Amazonian.

d. GEOMORPHOLOGICAL INVESTIGATION

We divided the fluvial system under study into three sections, i.e. the upstream, intermediate and downstream sections, based on their different morphological characteristics (Figure 4. 1a). The upstream section includes the catchment system, crater lakes, alluvial fans, and fan deltas and is composed of two main branches, i.e. an eastern and a western branch. The downstream section includes a valley system that is named Kārūn Valles, which displays a wide alluvial fan, and terminates on the floor of the Ariadnes Colles basin. These two sections are separated by the intermediate section, which is characterized by a flat surface which is cut by the northern segment of the Sirenum Fossae.

i. UPSTREAM SECTION

The upstream section of the fluvial system represents the catchment system and hosts two main unnamed channels, which form the eastern and the western branches of the fluvial system. The eastern branch is ~340 km long, has a sinuous plan-view pattern, and is located between impact craters. The western branch is ~220 km in length, appears straight and does not seem to be diverted by pre-existing impact craters. The first observable traces of the fluvial activity appear at an elevation of ~1700 m north and northeast of an impact crater (Figure 4.2a). The impact crater has a sharp rim and does not display traces of fluvial activity on its inner rim. The ejecta blanket of this crater is, however, partly eroded. Channels representing the head of the fluvial system appear on the outer wall and ejecta of this crater (Figure 4.2a), and therefore they postdate the impact event. A ~5 km-wide deposit is preserved adjacent to a high crater wall (~2000 m height) (Figure 4.2b). A narrow channel is most likely originated from this deposit. This channel is linked to the wider channel traceable to the visible heads of the fluvial system. Small channels originating at high elevations join the main eastern and western branches of the fluvial system (Figure 4.2c). They have a simple morphology and have no tributaries. They typically start at a local depression and end at the main channel. We have not observed any depositional features such as alluvial fans that are related to these narrow channels. The mentioned depressions are a few kilometres wide (Figure 4.2c) and have shallow and irregular shapes, and therefore do not represent old impact craters (Figure 4.2c).

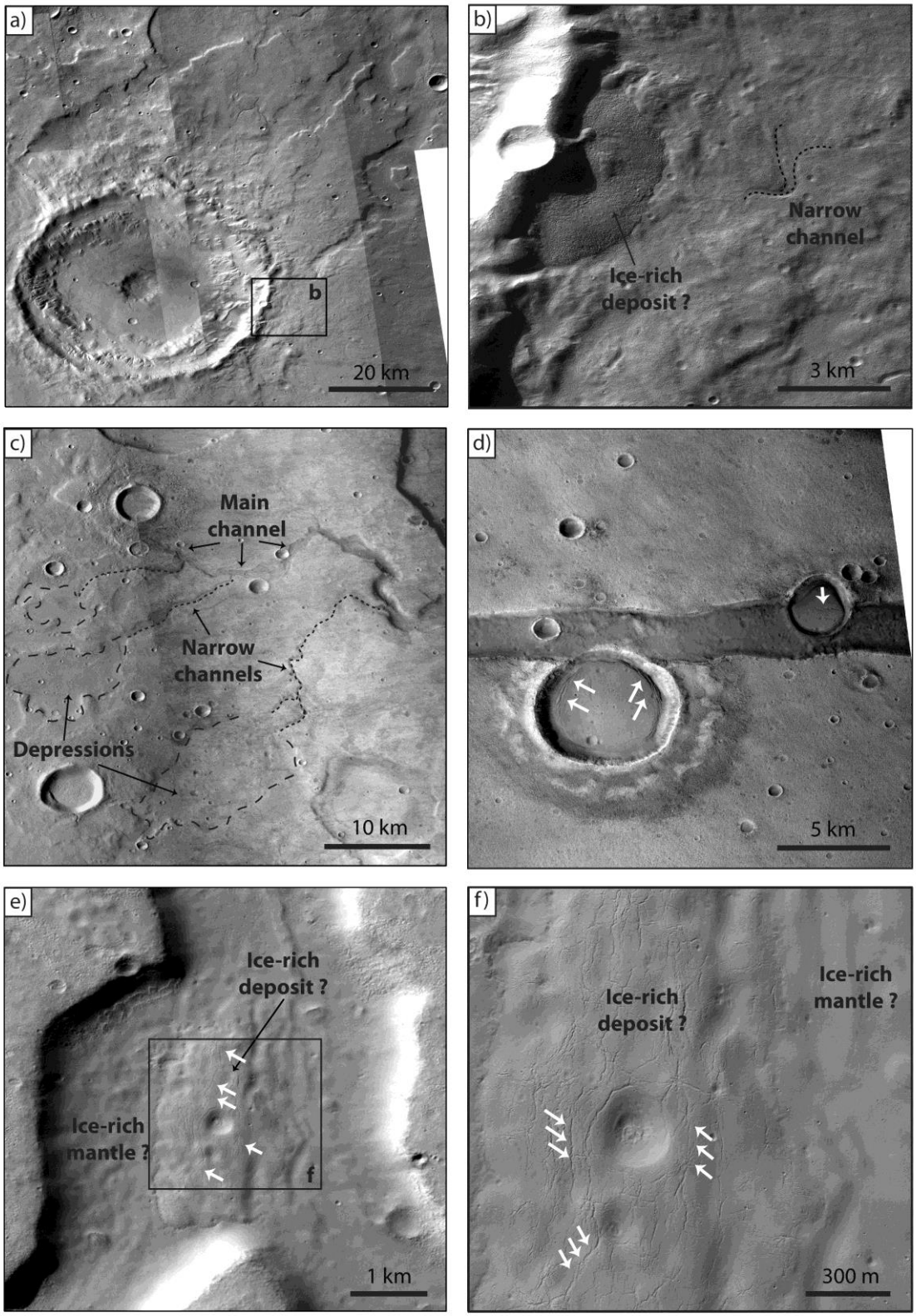

Figure 4.2: Morphologic details of the channels in the upstream section. a) The visible source of the upstream section of the eastern branch. Three channels start at the impact crater and continue toward northeast (detail of CTX P16_007434_1416, G21_026435_1368, P15_006933_1393, D17_033938_1392, and B06_011917_1385). b) [Continue in the next page]

On the floor of the western channel, we observe deposits with convex upward surfaces that are partly covered by a smooth mantle that also covers the channel floor area (Figure 4.2e). The surface of these deposits is longitudinally fractured (Figure 4.2f). These fractures are very common in glacial deposits on Earth, and are called crevasses. They are formed by tensile stresses as response to the ice flow [*Benn and Evans*, 1998]. Next to the northern segment of Sirenum Fossae, two impact craters are filled with smooth-textured materials. The craters rim at the fossae's side is degraded. The filling material is similarly fractured (Figure 4.2d). However, these fractures are concentric, running parallel to the crater rim. Additionally, there are longitudinal cracks on the surface of this material, oriented perpendicular to Sirenum Fossae. They may show the creep of this material toward the lower elevation of the fossae.

The floors of the channels in both the western and eastern branches are partly incised by scour marks. Close to the terminus of the eastern branch, where the streamlined islands are well preserved (Figure 4.3), we observed a ~2km-wide area with a flat surface that does not display any signs of visible erosion (e.g., fluvial incision). The area is limited downstream by a distinct topographic scarp (Figure 4.3). This area may represent a layer of erosion-resistant materials which covers softer materials beneath, a situation which is typical at terrestrial cataracts. Downstream of the scarp we can again follow the channel bed which is characterized by incised erosional features. Another similar feature has also been observed at the north of Sirenum Fossae (Figure 4.4a) which is as well distinguished by a flat surface, and a topographic scarp next to which the channel floor is carved by erosion. We infer that these features are paleo-cataracts and represent former waterfalls. At some places we observe eroded banks and erosional islands in the middle of the channel (Figure 4.3). About 30 km south of the southern segment of Sirenum Fossae, the channel enters an ancient degraded crater of ~9 km in diameter (Figure 4.4b). On the crater floor, there is a fan-shaped deposit with a smooth and flat surface and a distinct frontal scarp, implying a formation as a delta rather than as an alluvial fan, which would be characterized by conical or concave-upward geometry, and a distal margin that grades smoothly into the adjacent plain. An outlet channel leaves the crater on the other side, which is indicative of an open-basin lake [*Fassett and*

[Continue from the previous page-Figure 4.2] b) Close-up of the rim of the impact crater seen in (a), showing a well-preserved and possibly ice-rich deposit and a narrow channel, which may be the result of past melt event(s) (detail of CTX P15_006933_1393). c) Small depressions observed at the head of the narrow channels that fed the main stream (detail of CTX P08_004098_1378 and B06_011851_1397). d) Two impact craters located next to the northern segment of the Sirenum Fossae. These craters are filled with materials that show characteristics (texture, convex-upward margin, concentric fractures) similar to ice-rich deposits (detail of CTX D10_031182_1435). e) The floor of the western branch of the upstream section of the fluvial system. An ice-rich deposit is visible on the floor of the channel; it has been partly covered by an ice-rich mantle. The white arrows point to crevasses (detail of CTX B18_016664_1414). f) Blow up of the surface deposit shown in (e). The limit between the deposit and ice-rich mantle is visible. White arrows point to crevasses (detail of HiRISE ESP_016664_1420). North is up in this and all other figures. See Figure 4.1-b for locations.

Head, 2008]. Thus, it suggests the crater hosted a body of water at the time of the fan delta formation.

North and south of Sirenum Fossae, several fan-shaped deposits are observed. Fan-shaped deposit I and II (Figure 4.4c) are 1 to 3 km across, respectively, with gentle and lobate distal margins, which is indicative for an alluvial fan. On top of the fan-shaped I, however, there is a smaller deposit with a steep front and a relatively flat surface (Figure 4.4c), which may be a fan delta deposited on top of an alluvial fan. Such a mechanism could occur when an initial alluvial fan is deposited on the floor of a dry basin. When the flow of water continues, consequently a fan delta would form on top. This could not have lasted very long, as otherwise the alluvial fan would be totally covered, which is not the case of the fan-shaped deposit I. The narrow channel terminating at the fan–shaped deposit I (Figure 4.4c) incised the Sirenum Fossae's floor, and therefore it formed after the formation of Sirenum Fossae. Here the deposit has been offset vertically rather than laterally, hence the channel dislocated by last activity(s) of the Fossae. The fan–shaped deposit shown in Figure 4.4a north of the Sirenum Fossae is more likely to be a fan delta as it appears to have a sharp distal margin. The surface between this fan delta and the adjacent continuation of the fluvial channel is a few kilometers wide. This area may be a small area flooded by water that overflowed east, and formed a flood plain between the upstream fan–shaped deposit and downstream continuation of channelized flow.

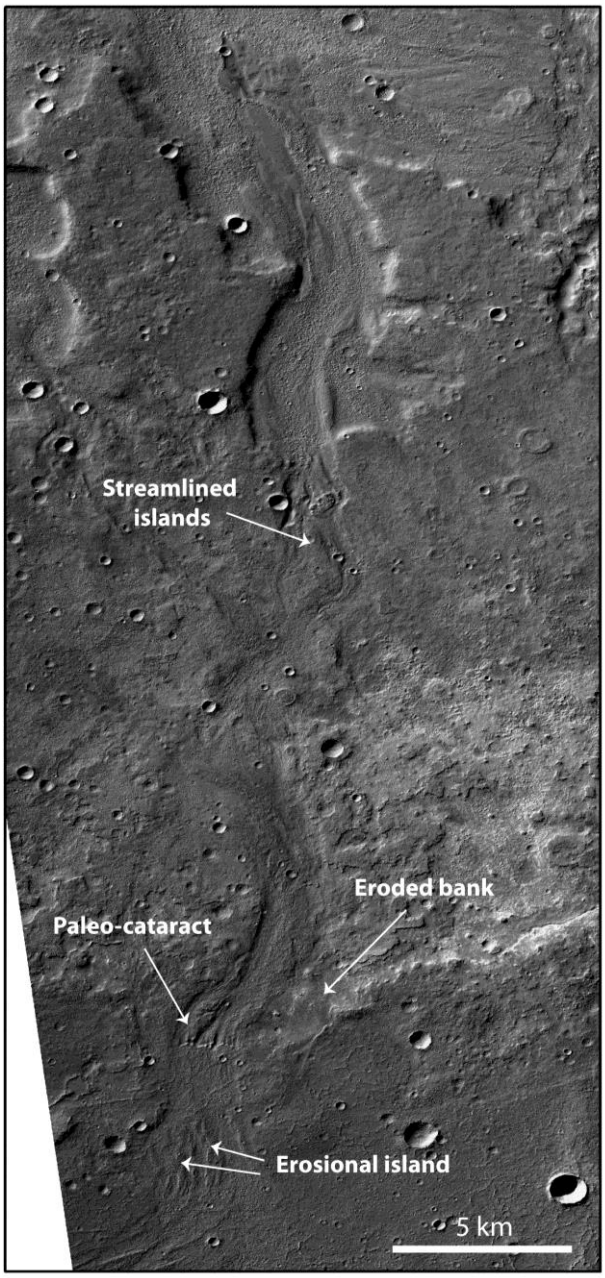

Figure 4.3: An area close to the end of the eastern branch of the upstream section. Erosional features are visible on the floor of the fluvial system (detail of CTX G23_027081_1421). Location of this figure is indicated in Figure 4.1-b.

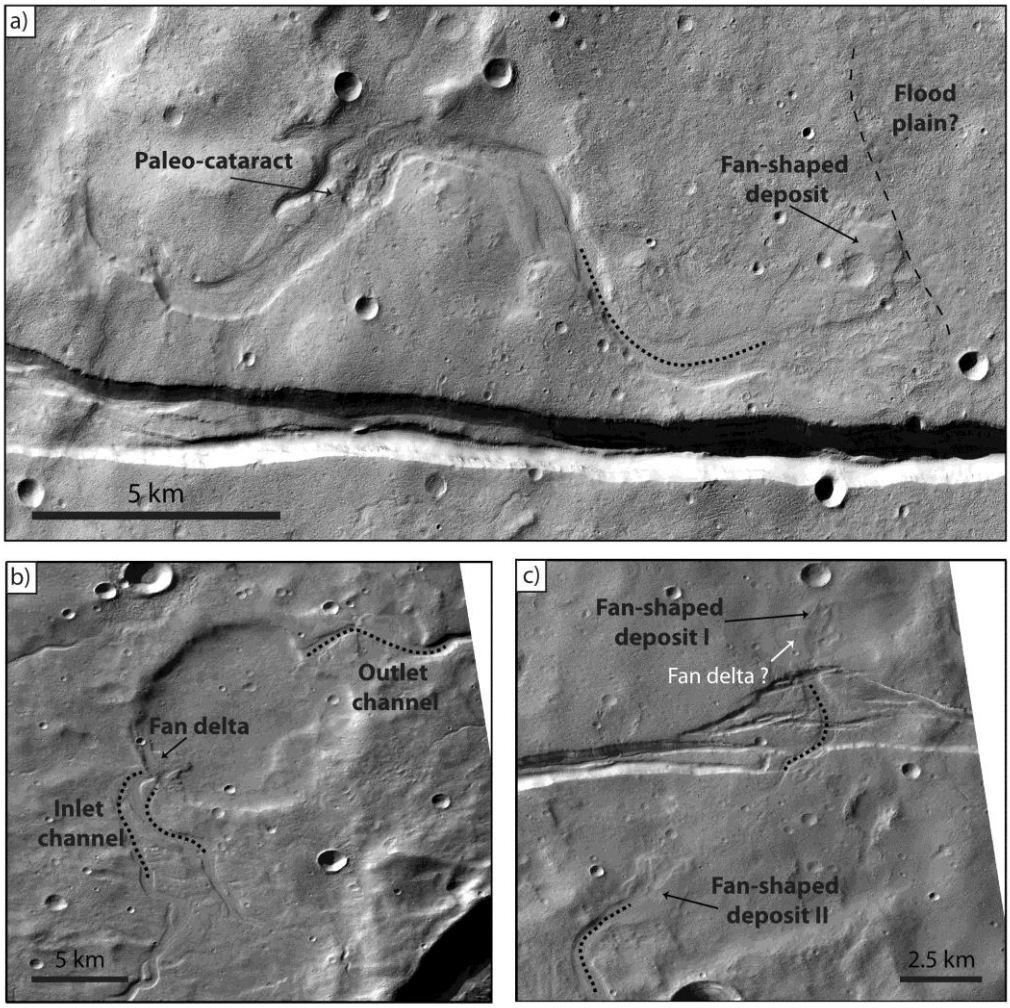

Figure 4.4: Fan-shaped deposits in the eastern branch of the upstream section. a) A part of the eastern fluvial channel that displays a fan-shaped deposit. Note the similarity of the paleo-cataract to the Dry Falls in Channeled Scabland (Washington State, US). A possible flood plain is also shown (detail of CTX F01_036351_1403 and P16_007368_1407). b) Paleo-crater lake within the eastern branch of the fluvial system, displaying an inlet channel with a fan delta and an outlet channel (detail of CTX P17_007869_1399). c) Two fan-shaped deposits within the eastern branch (detail of CTX P16_007368_1407). See Figure 4.1-b for locations.

ii. INTERMEDIATE SECTION

The intermediate section is about ~85 km long and is located between the eastern branch of the upstream section and Kārūn Valles (downstream section). It does not display any fluvial landforms on is surface and is characterized by two geological units: the

bedrock unit south of the northern segment of the Sirenum Fossae, and the mantling unit north of the northern Sirenum Fossae segment which partly overlies the bedrock unit.

1) BEDROCK UNIT

The bedrock unit appears smooth with bright-tone at CTX resolution (Figure 4.5a). It shows several wrinkle ridges that are crosscut by the Sirenum Fossae. The area where the upstream fluvial system terminates is also covered by the bedrock unit, which is clearly incised by the fluvial channel (Figure 4.5b). At the terminus of the fluvial system, the bedrock unit reveals low-albedo and light-toned deposits that are polygonally fractured (Figure 4.5b). The fractures are a few hundred meters long. The light-toned material within the polygonal fractures reveals also smaller cracks with lengths ranging from 1 to 5 m. The absolute model age of the bedrock unit yields an early Amazonian age of $\sim 1.8^{+0.2}_{-0.2}$ Ga (Figure 4.6a) (epoch boundaries are from [*Michael*, 2013]).

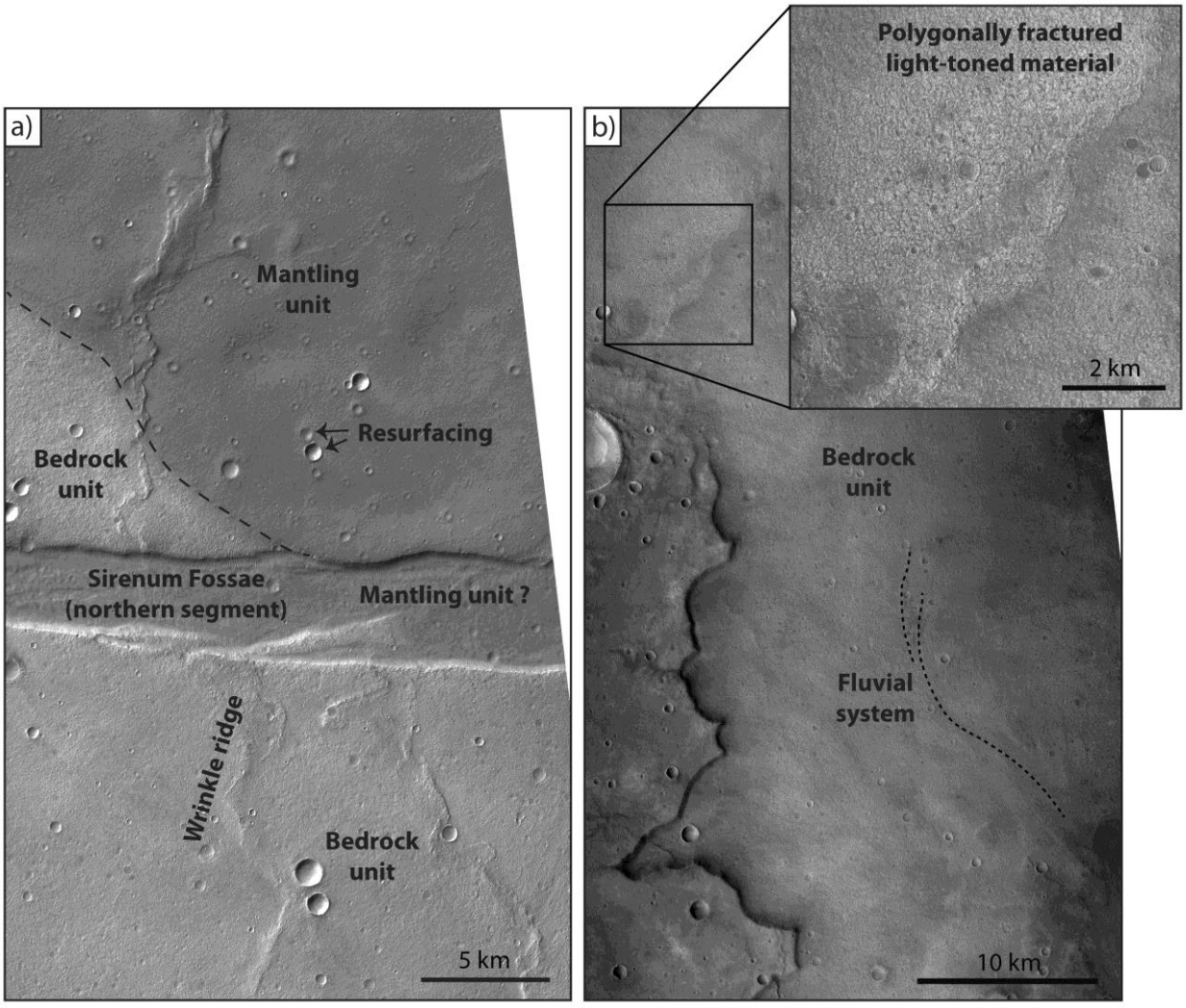

Figure 4.5: Morphology of the intermediate section. a) The two main surface units: bedrock unit and mantling unit. Their contact is indicated by the black dashed line (detail of CTX P17_007658_1420). b) The eastern branch of the upstream section terminates on the bedrock unit. The blow-up image shows light-toned materials, which are polygonally fractured (detail of CTX D09_030826_1423). See Figure 4.1-b for location.

2) MANTLING UNIT

The mantling unit has a darker appearance in CTX images as compared to the bedrock unit (Figure 4.5a). It is ~5 m thick and covers the area in which the Kārūn Valles are incised. Exposed impact craters range in morphology from nearly pristine (fresh) to degraded; some craters are embayed or partially buried (Figure 4.5a). Embayment/burial indicates later resurfacing, which is also notable in our crater size–frequency distribution (CSFD) curve (Figure 4.6b) as distinct kink. The base age of $\sim 3.1^{+0.2}_{-0.4}$ Ga refers to the formation age of the pre-existing geological unit whereas the age of $\sim 730^{+40}_{-40}$ Ma represents the formation age of the mantling unit. The material covering the northern segment of the Sirenum Fossae also has very similar appearance as the mantling unit including a low albedo in visible images. This suggests that the mantling unit also covers the ~3 km-wide graben of the northern segment of the Sirenum Fossae (Figure 4.5a).

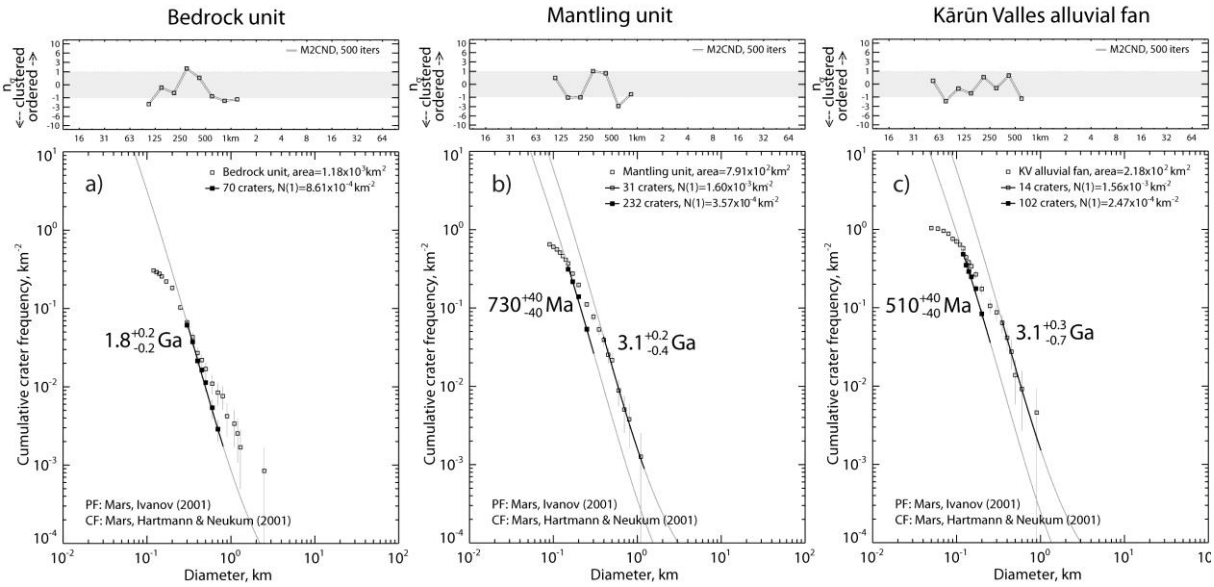

Figure 4.6: Absolute model ages corresponding to a) bedrock unit, b) mantling unit, and c) Kārūn Valles alluvial fan. Crater size distributions, randomness analyses, and isochrons are shown.

iii. DOWNSTREAM SECTION

1) KĀRŪN VALLES

The Kārūn Valles (Figure 4.7a) extend from southeast to northwest, partly through the ejecta blanket of an impact crater that appears to be relatively fresh [e.g., see crater classification in *Mangold et al.*, 2012a]. The Kārūn Valles are the only feature visibly modifying the ejecta blanket, suggesting a recent formation for both; the impact crater and Kārūn Valles. In order to investigate the formative process of the Kārūn Valles, we produced a geomorphological map of these channels and their surrounding area, as shown in Figure 4.8.

The Kārūn Valles have a minimum length of ~63 km. Their maximum length is unclear due to the lack of high resolution images. The upstream part of this channel system seems to emanate northeast and southwest of a ~500 m-high hill, located next to the intermediate section. The head of the SW channel cuts the NE channel (Figure 4.7a), and therefore the SW channel is younger and was incised more recently than the NE channel. Alternatively, both channel heads may have been active simultaneously but the last or last few outflow events occurred only through the SW channel. The average width of the channel is about 3 km, and its depth ranges between 10 and 30 m. Deep grooves (shown by red lines in Figure 4.8) have been observed at the upstream part, as well as along the channel, up to the point where the deposition of the alluvial fan starts. These grooves may indicate scouring of bedrock by high pressure flow in catastrophic floods [*Baker et al.*, 1992].

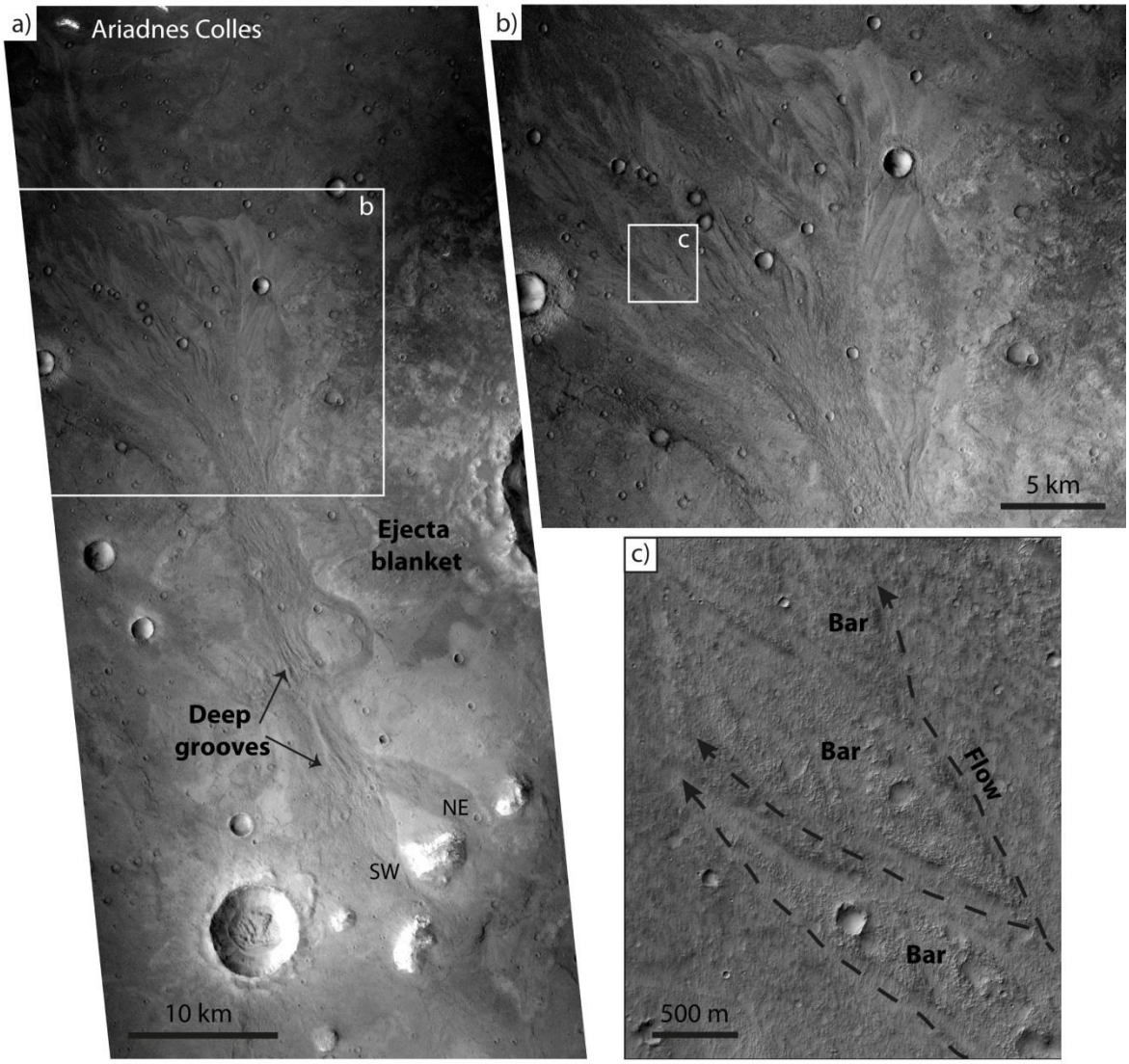

Figure 4.7: a) Morphology of Kārūn Valles located on the rim of the Ariadnes Colles basin. The visible channel head and deep grooves are shown (detail of CTX D10_031182_1435; see Fig. 1-b for location). b) The Kārūn Valles alluvial fan. Note the depositional bars composing the alluvial fan. c) A zoom on one of the braided bars and the flow direction (detail of HiRISE ESP_043261_1440).

Along the channel, the ejecta blanket of the crater has been partly removed. Within the channel some remnants are still visible, which resisted the flow and redirected the stream direction (Figure 4.7 and 4.8). The ejecta blanket's remnants are shaped by the erosional processes into streamlined islands, here called erosional remnant islands (EI, Figure 4.8). Most EI display an impact crater on one of the sides that may have locally formed obstacles by their rims, increasing the resistance against erosion by the flow. The EI have distinct escarpment that are the result of flow erosion. Between EI 1 and EI 2, and slightly to the north of EI 2 on the eastern wall of the channel, we observe two gaps towards east, debouching into small depressions that may have temporarily hosted standing bodies of water, as indicated with a blue hatched pattern on the map (Figure 4.8). Small channels at the head of these gaps show a west-to-east flow direction. These features may indicate bank erosion, which happens when the water level exceeds the channel wall; hence water overflows and erodes the channel wall toward the terrain outside of the channel. Subsequently a small catchment basin may form. On the floor of one of these catchments, a thin layer occurs (Figure 4.8) which may have been deposited while the area was filled with water.

The small EI 3 has an elongated shape, oriented in the flow direction with an impact crater at the upstream end. The highly eroded surface and low relief indicate that this EI had been overflowed and that EI 3 has originally been part of EI 4. The morphology of EI 4 indicates it as the rest of the ejecta blanket (see Figure 4.8). To the west of EI 4 and 5 there may have been a temporary catchment of water as suggested by the low topography and the deep linear erosional features on the western wall of the channel.

At the head of the Kārūn Valles, on the intermediate section, there is a depression, which fits to the contour line of 400 m (MOLA DTM) (Figure 4.1a). It is located north of the Sirenum Fossae and has a close morphological link with the beginning of the outflow channel. This depression could have hosted a body of water, in liquid or frozen state, the overflow of which could have carved the outflow channel. It should as well be considered that the modern morphology may have been modified by potential Sirenum Fossae activity(s) after the outflow event(s), which could have uplifted or depressed the surface.

2) ALLUVIAL FAN

On the downstream part of the Kārūn Valles there is a wide, low–sloping fan–shaped deposit (Figure 4.7 and 4.8). The deposit contains several bars of various sizes that are all elongated in flow direction. The gentle grade of the bars` distal margins and their concave-upward geometry point toward diverging flow with downstream reducing sediment transport capacity, and depositing a splay-like feature with bars. The bars are found mostly in clusters, around which the main channel has been bifurcated and was divided into numerous narrower channels. The smaller bars of each group are also separated by small channels which reconnect on the downstream side of each bar (Figure 4.7c). The complex bars are separated by incisional channels at the larger scale, indicating perhaps a base level drop in the final stages of activity. The bar surfaces show compelling evidence of gradual build-up and migration as multiple scroll bars amalgamated into larger bars. Alternatively, this could also

be interpreted as incision by narrow channels. The comparison with data models and experiments [*Van De Lageweg et al.*, 2013; *Schuurman and Kleinhans*, 2015] shows the former to be more likely. If so, then this, although common in terrestrial rivers, is to our knowledge a unique feature on Mars.

In the main channel, bars are larger but further toward the Ariadnes Colles they become smaller and may have once been part of larger bars and subsequently been divided into smaller ones by erosion. In two locations in the alluvial fan, we observe elongated islands that have sharp scarps and do not exhibit incised channels on their surfaces. Few impact craters are observable on their surfaces (shown by white arrows in Figure 4.8). Our observations suggest that these islands formed by erosion rather than deposition and may represent remnants of the ejecta blanket. The crater size–frequency distribution of the entire alluvial fan surface shows a middle Amazonian age of about 510^{+40}_{-40} Ma (Figure 4.6c) for the alluvial fan. The model age likely refers to the latest stage of fan formation since previous floods and any pre-existing crater populations would have erased, either by erosion or deposition.

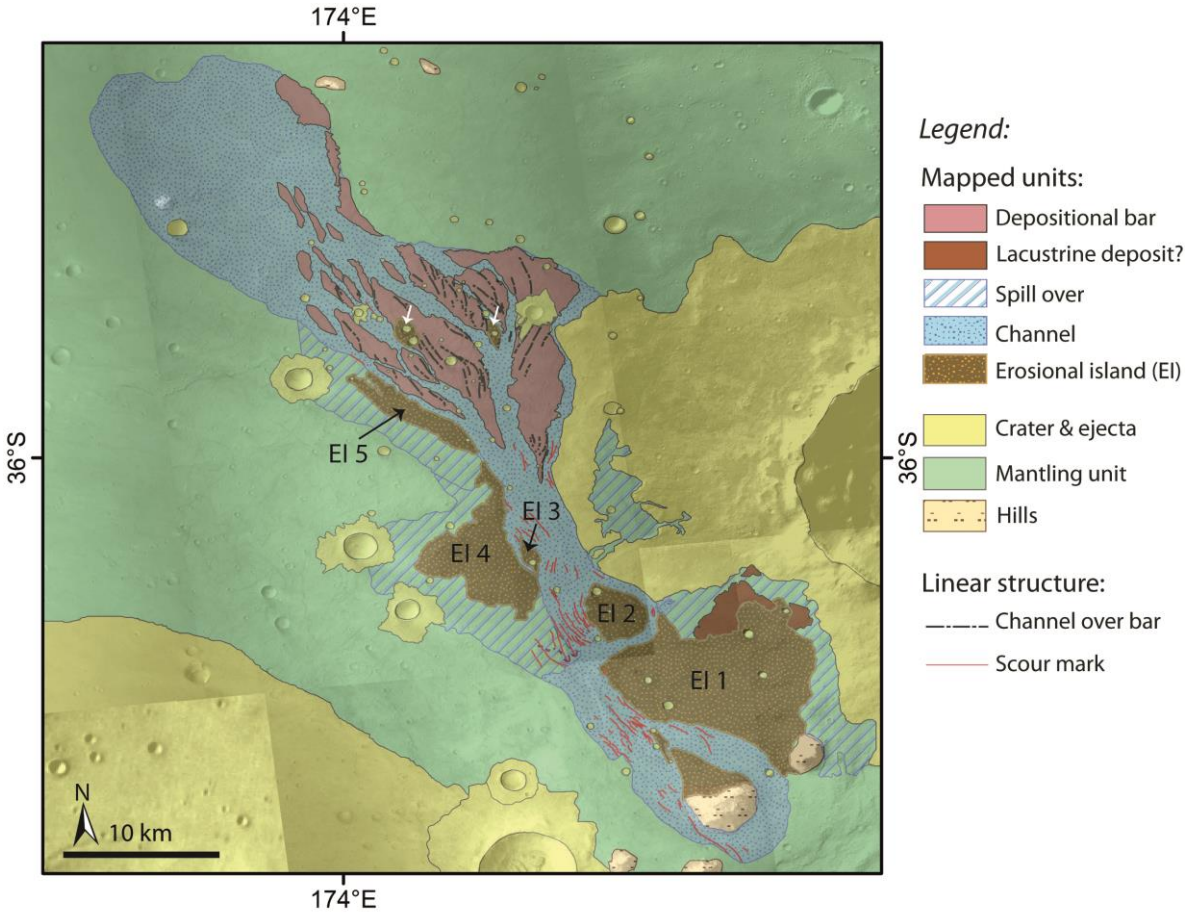

Figure 4.8: Geomorphologic map of the Kārūn Valles overlain on CTX and HRSC images. EI stands for erosional remnant island. The white arrows point to the remnants of the ejecta blanket in the alluvial fan. See Figure 4.1-b for location.

e. HYDRAULIC ANALYSIS

i. FLOW DISCHARGE

The hydraulic analysis is essential in order to better understand the channel formation mechanism and potentially the duration and/or periodicity of the flooding, which in turn increases our knowledge about the source of water. On Mars, however, using orbital data for hydraulic modelling is restricted due to the data resolution constraints. In order to calculate the flow discharge rate, we used the method described extensively in *Kleinhans* [2005] and used in *Kleinhans et al.* [2010] to calculate the flow discharge and sediment flux under Martian conditions. The flow discharge is given as

$$Q = hWu \tag{1}$$

where h is the depth of the channel, which means the thickness of the water column, W is the channel width, and u is flow velocity averaged over the depth and width of the channel. The channel depth and width can be calculated using the topographic data. The average width of the channel is about 3 km (the width of the channel varies locally from ~1,5 km to ~4,5 km), with minimum and maximum depths of 10 m and 30 m, respectively (based on CTX DTM data, Figure 4.9). The flow velocity has to be estimated using a friction law. The most common equations to calculate the flow velocity are the following:

Manning equation:

$$u = \frac{h^{\frac{2}{3}} S^{\frac{1}{2}}}{n} \tag{2}$$

where S is slope of the flow, and n is the Manning roughness coefficient. The Manning equation depends on a dimensional, empirical parameter that includes gravitational acceleration, both of which increase the uncertainty of the results [*Kleinhans*, 2005; *Mangold and Howard*, 2013]. Therefore, the Darcy-Weisbach equation [*Kleinhans*, 2005] (Eq. 3) has been used more often in the recent literature. It has also been used in this study:

$$u = \sqrt{\frac{8ghS}{f}} \tag{3}$$

where g is acceleration due to gravity (3.71 ms^{-2} on Mars), and f is a friction factor that depends on channel bed particle size and bed form.

The friction factor can be calculated from a relation that includes the physics-based boundary layer description, and is here calculated for gravel-bed rivers [*Wilson et al.*, 2004] as:

$$f = 8/(7.515(\frac{h}{D_{50}})^{0.1005} S^{-0.03953} \sigma_g^{-0.1283})^2 \quad (4)$$

where D_{50} is the size at which 50% of clasts are of that size or smaller and σ_g is the geometric standard deviation of the sediment grain size distribution, approximated for logarithmic distributions as:

$$\sigma_g = \frac{1}{2}(\frac{D_{84}}{D_{50}} + \frac{D_{50}}{D_{16}}) \quad (5)$$

The grain size is an important parameter for the hydraulic analysis, but it cannot be determined based on orbital data. Ground-based rover data acquired on the Martian surface, on the other hand, indicate a variety of grain sizes from gravel (~0.01 m) to sand (~0.002 m) down to clay-sized particles (>60-70-µm resolution limit of MAHLI, the microscopic imager on the Curiosity rover [*Grotzinger et al.*, 2015]). It is, however, difficult to find a comparable geological setting among the sites visited by rovers. The grain size distribution in our study area relates to ejected material, which had been later eroded by fluvial activity and deposited in an alluvial fan. We, therefore, used the average grain size of the fluvial sandstone at the Yellowknife Bay formation as measured by the Curiosity rover [*Grotzinger et al.*, 2015] and assumed a median grain size (D_{50}) of 2 mm. In order to constrain the discharge rate with conservative error margins, we have, in addition, calculated the flow discharge and sediment transport volume for three different average grain sizes which are shown in Table 1.Based on the above channel dimensions, equations, and grain size, we obtained values for the discharge rate of $Q_w = 6.9\ km^3/day$ for a channel depth of 10 m and $Q_w = 34\ km^3/day$ for a channel depth of 30 m. It must be noted that these values are order of magnitude estimates given the uncertainty of the friction relation and the chosen particle size. In addition, these values imply bank-full conditions, however, we cannot rule out the possibility of much lower flow depth, at least for a limited time. In order to take this assumption into account, we calculated the discharge rate and other parameters for a case of a 10%–flow–depth, i.e. a flow depth of 1 and 3 m. The results are presented in Table 1-b.

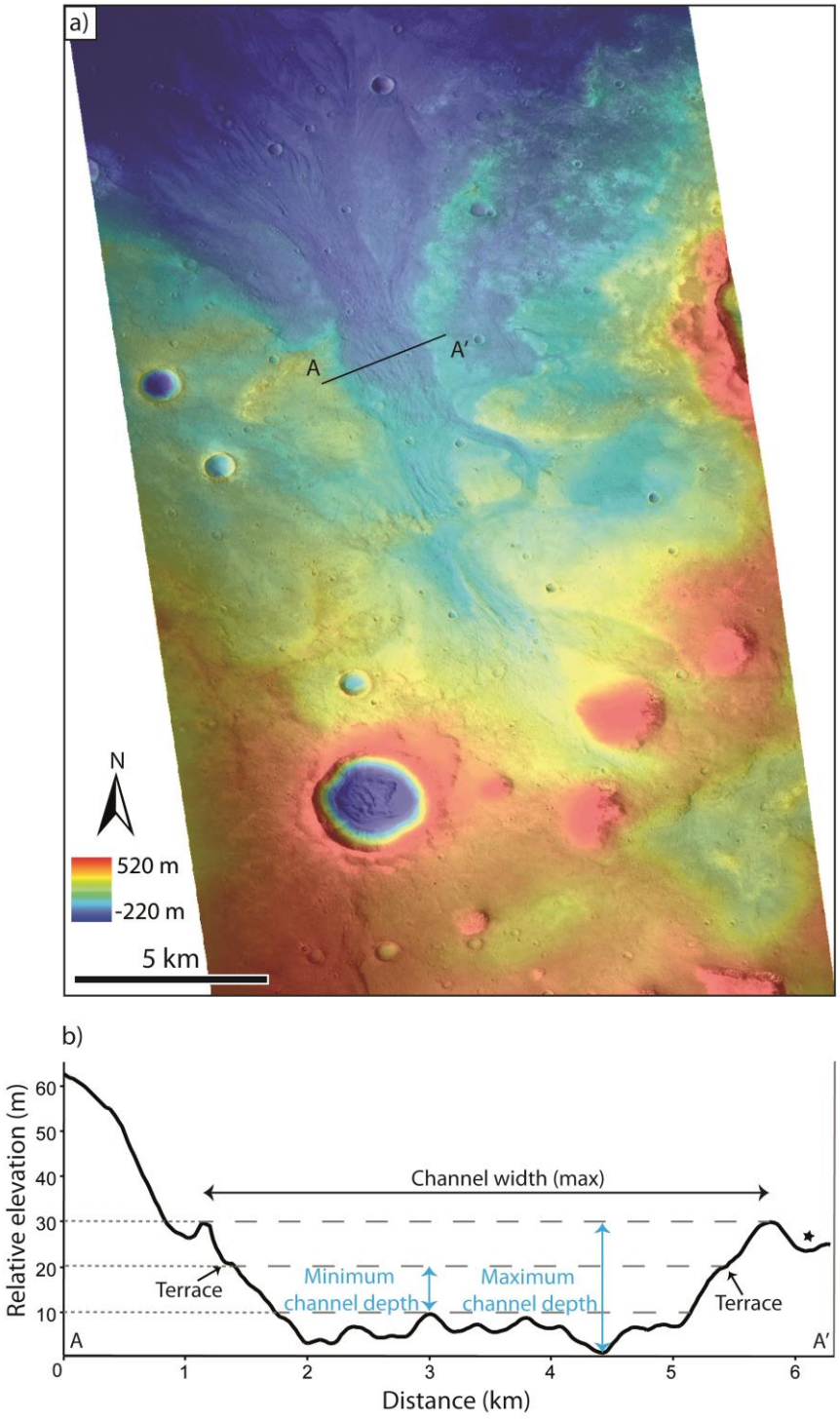

Figure 4.9: a) CTX DEM of Kārūn Valles generated from two CTX images (D10_031182_1435 and D09_030892_1435). The AA' line shows the location of the cross-section presented in (b). b) Cross-section showing an example of the Kārūn Valles channel depth. Note that the channel width value is the maximum value and not the average value used in our hydraulic modelling. The black star shows the location of a depression which has been mapped as a spill-over region in our map in Figure 4.8.

ii. SEDIMENT TRANSPORT

Estimating the sediment transport rates would give an insight into the channel formation mechanism and event(s) duration. It is essential to compare the removed sediment volume with the deposited sediment value of the alluvial fan, in order to understand whether any sediment was washed out of the system or was added into the system from the source area, which could consequently increase our understanding about the source of water. We again note that the values are order of magnitude estimates.

Sediment transport can occur as bedload, suspended bedload, and wash load. The suspended load transport regime is most likely dominant in the larger Martian channels whereas the bedload transport becomes more important in smaller channels [*Kleinhans et al.*, 2010]. In order to assess the sediment transport, we used the method described in *Kleinhans* [2005], and calculated the bedload transport, the suspended load transport, and the total load transport. We used the same values as for flow discharge calculation (see Section 4.e.i), including channel width, depth, slope, and grain size. The total bedload is calculated using the Engelund and Hansen (EH) predictor, as follows:

$$Q_s = \frac{0.1}{f}\theta^{2.5} \tag{6}$$

where Q_s is nondimentional suspended load transport and f is Darcy-Weisbach coefficient related total roughness. The estimated total bedload for 10 m of channel depth is $Q_s = 18.9x10^{-3}\ km^3/day$ and for 30 m of channel depth is $Q_s = 261x10^{-3}\ km^3/day$. These results are summarized in the Table 1-a. We have also calculated the sediment transport rate for a 10%–flow–depth condition as shown in the Table 1-b.

iii. TIME SCALE

When we have an estimate of the amount of eroded material, deposited material, and the flow discharge rate, we can roughly assess a time window in which the channel had been developed or the alluvial fan had been formed. It can be estimated as [*Kleinhans*, 2005]:

$$T_s = \frac{V_s}{(1-\lambda)Q_s} \tag{7}$$

where V_s is the volume of deposited sediment (in the alluvial fan), λ is the porosity of the sediment that is here assumed to be 0.2. This estimate is based on particle measurements in lander images (see *Kleinhans* [2005] and *Kleinhans et al.* [2010] for discussion). This

timescale represents the required time to deposit the Kārūn Valles alluvial fan, which has a volume of ~5.04 km^3. Assuming that the fluvial event took place continuously in a given period of time and a bank–full condition, the alluvial fan would need 19 to 270 days to form, via a channel with 30 m or 10 m of depth, respectively (Table 1-a). In case of a 10%–flow–depth condition, the alluvial fan would form in 4700 to 65000 days, via flow depth of 3 m or 1 m, respectively (Table 1-b). However, we cannot rule out the possibility of several short and repetitive events.

Table 4.1: Estimation of flow discharge rate, bedload transport, and time-scale needed for Kārūn Valles alluvial fan formation, based on various grain sizes cited in literature (see Section 4.e). a) Bank-full condition. b) 10%-flow-depth condition.

(a) Bank-full condition	**Gravel (min)**	**Gravel (max)**	**Sand (min)**	**Sand (max)**	**Fine grain (min)**	**Fine grain (max)**
Channel depth (m)	10	30	10	30	10	30
Grain size (m)	0.01	0.01	0.002	0.002	0.0005	0.0005
Discharge, Q_w (km^3/day)	7.5	36.8	6.9	34	6.4	31
Total bedload, Q_s (km^3/day)	$4.5x10^{-3}$	$62x10^{-3}$	$18.9x10^{-3}$	$261x10^{-3}$	$64x10^{-3}$	$897x10^{-3}$
Alluvial fan formation time-scale (day)	1100	81	270	19	78	5.6
(b) 10%-flow-depth condition						
Channel depth (m)	1	3	1	3	1	3
Grain size (m)	0.01	0.01	0.002	0.002	0.0005	0.0005
Discharge, Q_w (km^3/day)	0.27	1.3	0.25	1.2	0.23	1.1
Total bedload, Q_s (km^3/day)	$0.018x10^{-3}$	$0.25x10^{-3}$	$0.07x10^{-3}$	$1.06x10^{-3}$	$0.26x10^{-3}$	$3.65x10^{-3}$
Alluvial fan formation time-scale (day)	$27x10^4$	$2x10^4$	$6.5x10^4$	$0.47x10^4$	$1.9x10^4$	$0.14x10^4$

f. DISCUSSION

i. THE CATCHMENT SYSTEM FORMATION

The fluvial system in Terra Cimmeria is composed of three sections: upstream section forming the catchment system, intermediate section, and downstream section including Kārūn Valles. The fluvial system in Terra Cimmeria reveals a hydraulic mechanism of different erosional and depositional processes. The model absolute age of the bedrock unit in the intermediate section shows an age of $\sim 1.8^{+0.2}_{-0.2}$ Ga, which corresponds to the early Amazonian, and indicates the maximum age of the fluvial activity. Therefore, the fluvial activity took place at the early Amazonian or at more recent time. Along the main channel path, we observe narrow valleys, which originate from local depressions (Figure 4.2c). The narrow valleys, in our study area, are morphologically very similar (simple morphology, narrow width, few kilometers length, lack of fan deposits) to Amazonian-aged glaciofluvial valleys described by *Fassett et al.* [2010], which are interpreted to be related to ice-rich deposits in mid-latitude regions. These valleys are also observed at the eastern channel head, where a ~5 km-wide deposit appears to be linked with a narrow valley to a wider valley (Figure 4.2b). The link between deposit, narrow channel, and wider channel may suggest that the deposit is a remnant of a wider ice-rich deposit, which partly melted in the past and incised the narrow valleys, which in turn joined and fed the main fluvial system. This ~5 km-deposit is then remained on a crater rim of ~2000 m of elevation. Alternatively, this deposit's current presence may reveal a potentially long history of re-deposition and disappearance of glacial deposits in the past, in which ice accumulation may have occurred several times at the same location. Nevertheless we suggest that the local depressions, which are located at the head of the narrow channels, have hosted ice or snow deposits, which entirely melted and carved the narrow valleys toward the main water stream.

Next to the northern segment of the Sirenum Fossae, there are two craters, which are filled by smooth and concentric crater fill material. Concentric crater fill material elsewhere on Mars has also been previously interpreted as ice-rich [e.g., *Squyres and Carr*, 1986; *Head et al.*, 2005; *Fassett et al.*, 2010]. This fill material seems to creep toward the topographically lower areas of Sirenum Fossae, similar to the downslope-creeping behaviour of viscous ice-rich deposits in other mid-latitude areas on Mars (e.g., an hourglass-shaped deposit on the eastern Hellas basin rim [*Head et al.*, 2005]). Therefore, we infer that the crater filling is remnant of glacial or ice-related material. On the floor of the western fluvial system, there are several deposits with convex-upward cross-sectional profiles that display crevasses on their surfaces (Figure 4.2e and f). These deposits are partly covered by a mantle that may be ice-rich and most likely represent the latitude dependent mantle (LDM [e.g., *Mustard et al.*, 2001; *Conway and Balme*, 2014]). We assume that these deposits are ice-rich, too, due to their prominent morphology, smooth surface and the close link to LDM (Figure 4.2e and f). All these well-preserved ice-rich deposits reinforce the possibility of a prolonged glacial history, including the periodic presence and reappearance of surface water, in particular, snow or ice melt, in Terra Cimmeria, during the early to middle Amazonian.

On the intermediate section's surface we have not observed any direct traces of fluvial activities (i.e. channel incision and/or fan-shaped deposits). The morphology of the intermediate section could have been modified by Amazonian tectonic activity related to the Sirenum Fossae. *Kneissl et al.* [2015] reported that the last tectonic activity of Sirenum Fossae corresponds to $\sim 710^{+140}_{-140}$ Ma, which is almost the age of the mantling unit. Therefore, the intermediate section may have had a different morphology (i.e. surface slope and azimuth) at the time of fluvial activity in Terra Cimmeria, and therefore, it may have been a depression to collect surface runoff. In addition, if the area was glaciated, the Sirenum Fossae-related activity could have been a trigger for collapse and melt of ice, and consequently a catastrophic overflow.

The surface of the bedrock unit is locally polygonally fractured (Figure 4.5b). These polygonal fractures, which are found in bright material of the bedrock unit, may indicate a resurfacing mechanism in which liquid water was involved. They are similar to fractures interpreted as desiccation cracks in Mawrth Vallis [e.g., *Loizeau et al.*, 2010], in Terra Sirenum [*Adeli et al.*, 2015], and in former lacustrine settings [e.g., *El-Maarry et al.*, 2013]. Therefore, the polygonal cracks in bedrock unit suggest liquid water activity similar to lacustrine environment which may be related to the observed fluvial system or to an earlier water activity in the area. The spatial distribution of the mantling unit is more concentrated in the western and northern part of the intermediate section (Figure 4.1b). It is partly covering the bedrock unit at the northern segment of Sirenum Fossae. The Kārūn Valles are incised through the mantling unit and therefore their maximum age is constrained by the age of this unit, which is estimated as $\sim 730^{+40}_{-40}$ Ma, corresponding to the middle Amazonian. The morphological characteristics, distribution, and the Amazonian age suggest that the mantling unit may be a drape of frozen dust. This material has most likely deposited during a middle Amazonian ice age, and reveals one or several recent Amazonian glacial history.

ii. KĀRŪN VALLES FORMATION

The Kārūn Valles are incised through the ejecta blanket of an impact crater (Figure 4.7a). The material removed from the ejecta blanket has been remobilized by the water and was deposited as an alluvial fan. Although the main channel has a straight course (in plan view), there are few islands (EI 1, 2, and 3 in Figure 4.8) that redirected the flow. These islands are remnants of the erosion of the adjacent terrace. We do not observe any depositional material around those islands, which implies a high erosion rate in the main channel that did not allow deposition to take place. A high erosion rate is also supported by the deep scour marks on the channel floor (visible in the cross-section of Figure 4.9b). This indicates a high sediment transport capacity and sufficient flow strength and sediment load to abrade the bed rock.

Most of alluvial fans on Mars show a lobate shape in plan view [e.g., *Moore and Howard*, 2005; *di Achille et al.*, 2012]. However, on the Kārūn Valles alluvial fan, we observe a bifurcating system rather than a continuously deposited alluvial fan. On Earth, bifurcation

occurs in various geological contexts including meandering, anastomosing, and braided rivers, as well as on river deltas with the aforementioned river patterns [*Schumm*, 1977; *Kleinhans et al.*, 2013]. A braided pattern occurs in alleviated conditions when the bars are depositional and shaped inside the river channel by the flow. In such systems, channel migration and instability of channel bifurcations leads to perpetual dynamics with bar growth, bar amalgamation and bar splitting. The Kārūn Valles alluvial fan shows well preserved depositional features, and bars that have been clearly shaped by the flow. The fan is composed of elongated bars and multiple channels that divided and re-joined around the bars. At some places (Figure 4.7b and c) bars are connected with each other laterally, suggesting their migration. A few obstacles, most probably remnants of the ejecta blanket, resisted erosion, and sediment was deposited on their lee side. It is clearly observable that the elongation of these obstacles has a different orientation as compared to that of the bars (Figure 4.8). The Kārūn Valles alluvial fan is a fan-shaped feature built up from a braided system. Such braiding on Mars has been rarely observed [*Matsubara et al.*, 2015] and points to a unique formation mechanism.

The formation time frame for Kārūn Valles can be constrained by the age of the mantling unit where the Kārūn Valles have been incised into, and the age of the alluvial fan itself. Therefore we infer that the Kārūn Valles formation took place between ~730^{+40}_{-40} Ma and 510^{+40}_{-40} Ma, which are the absolute model age estimates of the mantling unit and the alluvial fan, respectively. These ages correspond to the middle Amazonian. The climatic condition (e.g., atmospheric temperature and pressure) during the Amazonian [*Madeleine et al.*, 2009] most probably would not allow liquid water to last or to flow for a long period of time. This fits with our notion that one or several climate changes took place in the recent past and that the appearance of liquid water on the surface may have occurred as a sudden and short event, and water release happened catastrophically.

iii. SOURCE OF WATER

The erosional features of incised channel floors such as groove marks, cataracts, and streamlined islands; and eroded channel banks in eastern and western branches of the upstream section, as well as in Kārūn Valles, point to highly energetic fluvial activity. The morphology of the depositional features of fan deltas and alluvial fans suggests high energetic and short term events. Similar valleys and landforms of Amazonian age have been reported in other areas in mid-latitudes and been interpreted as being formed by a single and short fluvial episode [*Hobley et al.*, 2014; *Salese et al.*, 2016]. The experimental and numerical modelling of *de Villiers et al.* [2013] demonstrates that deltas with simple morphology and no obvious incisions on their surface form most likely during one short-term aqueous event. Our observations of the small deltas, alluvial fans, and fan-shaped deposits in the upstream section (see Figure 4.4) have not shown any incision into their surfaces. The hydraulic modelling of Kārūn Valles also supports a short term event as suggested by our morphological observations and the model of *de Villiers et al.* [2013]. Our calculations point to an event that lasted at least 19 to 270 days in case of bank-full flow condition in the channel. Although our morphological observations point to energetic flow events which would be more plausible in case of a bank-

full or almost bank-full condition, water level variations in the channel are likely, and the flow could have dropped to a fraction of bank-full flow between peaks of high-energy flow events. This would lead to longer flow durations required to carry the sediment, and less dramatic events. In the latter condition the fluvial event could have lasted for tens of thousands of days, e.g., in case of 10% water depth the formative mechanism (in case of a continuous flow) would take only 4,700 to 65,000 days, which is still a geologically short period of time. We do not rule out the possibility of a sequence of multiple episodic short term events. Considering the short duration and catastrophic release of water in combination with our morphological observation of ice-related features, we suggest surface runoff of ice/snow melt as the most likely water source. Obviously, ice and/or snow accumulation and melting would have happened clearly under different climatic conditions than today. Such climate change(s) may have been triggered by obliquity or orbital variations [*Laskar et al.*, 2004] which mobilised polar ice towards the mid-latitude regions of Mars [*Head et al.*, 2003; *Madeleine et al.*, 2014]. An extended ice layer could have covered mid-latitude areas including our study area. This mobilisation and re-deposition of ice could have occurred several times and periodically in the past history of Mars [*Madeleine et al.*, 2014].

The depression at the head of Kārūn Valles (see section 4.3.1. and Figure 4.1a) could have hosted an ice-covered lake or a subglacial lake, which collapsed and initiated a catastrophic outflow. Although we have not observed morphological traces of shore line, erosional or depositional features concerning lake or glacial deposit presence, this assumption cannot be ruled out, considering a lake or a glacial deposit, which lasted over a geologically short time. The liquid water collected by the upstream catchment system may have fed the depression at the head of Kārūn Valles, and formed an ice-covered lake under the middle Amazonian atmospheric condition. Alternatively, the depression may have hosted a glacial deposit, which catastrophically collapsed and melted. Catastrophic outburst of large amounts of water in glacier systems has been widely observed on Earth. These are generally referred to by the Icelandic term Jökulhlaups. Jökulhlaups may originate from subglacial sources of water melted by atmospheric processes, geothermal heat or volcanic eruptions [*Benn and Evans*, 1998; *Björnsson*, 2009]. On Earth, Jökulhlaups generally occur in intervals of weeks to years, and a slightly larger periodicity (e.g., over centuries [*Carling et al.*, 2009]) would also be expected under Martian conditions during the Amazonian. An alternative source of water would be rise of ground water. We have not observed any fissure, opening, or collapse zones, but the Sirenum Fossae could have facilitated the process. Groundwater, however, would not explain the distribution of small depressions and ice-rich deposits on various locations and elevations.

g. CONCLUSION AND IMPLICATIONS

The morphology of a complex channel system in Terra Cimmeria and the presence of ice-rich deposits on the channel floor strongly suggest that the valleys and channels were incised by liquid water during early to middle Amazonian. The narrow valleys originating at small depressions and remnants of ice-rich material indicate ice/snow melt as water source.

The evidence of short term and high energetic event(s), such as deep groove marks, streamlined islands, and morphology of the fan-shaped deposits, enforce the assumption of surface runoff as source of water. Our geologic map and observations of the morphology of the depositional bars in Kārūn Valles alluvial fan show a unique braided depositional pattern typical for terrestrial braided rivers. Our hydraulic and sediment transport modelling is consistent with our morphological observation and suggests that the Kārūn Valles had most likely been carved in one continuous event, which lasted a minimum of few days to few tens of thousands of days, however the possibility of a sequence of several short-term events occurring over a few centuries cannot be ruled out. Kārūn Valles may have been formed by a catastrophic melt of a glacial deposit (i.e., Jökulhlaups) or collapse of an ice-coved lake, which was fed by the upstream catchment and was hosted in the depression that exists at the Kārūn Valles head.

The Amazonian climate is, generally, considered to be globally "cold and dry" [*Head et al.*, 2003] and may have been perturbed by outbursts of water and gas. Observations of significant numbers of Amazonian-aged fluvial channels in the Martian mid-latitudes [e.g., *Howard and Moore*, 2011; *Hobley et al.*, 2014; *Salese et al.*, 2016] reveal the possibility of the presence of liquid water on the Martian surface during the last 3 Ga. Our observations of glacial-like deposits point to past accumulation(s) of ice/snow on the surface, and the narrow valleys confirms the presence of surface water during early and middle Amazonian. Our study shows a maximum age of $\sim 1.8^{+0.2}_{-0.2}$ Ga, corresponding to the early Amazonian and a minimum age of $\sim 510^{+40}_{-40}$ Ma, corresponding to the middle Amazonian, for the fluvial activity in Terra Cimmeria. Based on our results, we conclude that fluvial activity, perhaps episodic, existed throughout the Amazonian. Liquid water was present in Terra Cimmeria in the Amazonian, and it was abundant enough, although during a short period, to carve over 340 km of fluvial channel, transport sediments and deposit them in alluvial fans and fan deltas. Therefore, the existence of liquid water and fluvial activity on the Martian surface did not completely stop at a specific time, and the transition from a warmer and wetter past climate to today´s cold and hyperarid conditions may have been less dramatic than previously thought.

Acknowledgements

This research was supported by the Deutsches Zentrum für Luft- und Raumfahrt (DLR-Berlin). We thank S. Clifford and M.A. de Pablo for their detailed and constructive reviews, which greatly helped to improve the manuscript.

5. GEOMORPHOLOGY OF ICE-RICH VALLEY FILL DEPOSITS IN TERRA CIMMERIA, MARS: IMPLICATIONS FOR AMAZONIAN CLIMATE CHANGES

The following section has been submitted as: **Adeli, S.**, E. Hauber, and R. Jaumann. Geomorphology of ice-rich valley fill deposits in Terra Cimmeria, Mars: Implications for Amazonian climate changes. Submitted to *Geophysical Research Letter (GRL)*. The author contribution is explained in the Section 1.c.

Abstract: In mid-latitude regions of Mars there is clear evidence of ground ice deposits whose formation has been assumed to be a result of Amazonian-aged climate changes, triggered by obliquity variations. This evidence mainly includes several 107 years old lobate debris aprons (LDA), lineated valley fill (LVF), glacier-like forms (GLF), and the recent latitude dependent mantle (LDM). We report here the presence of a new class of deposits which were observed on the floor of an Amazonian-aged valley. These valley fill deposits (VFD) show evidence of shallow ice and are characterized by their convex-upward surface topography, crevasses, ablation moraines, sublimation pits, and ring-mold craters. Our observations suggest that the VFD most probably have been deposited contemporaneously with LDA, LVF, GLF, and have been covered later by LDM, probably during the recent high obliquity period. The observation of VFD reveals that Amazonian glaciation stages may have been more extensive than previously thought.

Keyword:

Mars, Amazonian, Climate change, Ice-rich deposits, Mid-latitudes, LDM

a. INTRODUCTION

In both mid-latitudes regions of Mars, evidence of glaciers [*Head et al.*, 2003; *Holt et al.*, 2008; *Plaut et al.*, 2009; *Hauber et al.*, 2011; *Hubbard et al.*, 2014; *Levy et al.*, 2014] and widespread ground-ice mantle [*Mustard et al.*, 2001; *Kreslavsky and Head*, 2002; *Head and Marchant*, 2003; *Levy et al.*, 2010] have been widely observed. Global circulation models (GCM) suggest that obliquity oscillations caused the mobilization of ice from polar regions and its re-deposition at lower latitudes [*Mischna et al.*, 2003; *Forget et al.*, 2006; *Madeleine et al.*, 2009]. They show that during high obliquity periods, ice can be deposited almost anywhere in the mid-latitudes and during low obliquity ice is transported back to the poles [*Levrard et al.*, 2007; *Greve et al.*, 2010; *Madeleine et al.*, 2012; *Smith et al.*, 2016]. Over the past 20 Myr, Mars' obliquity variations caused significant changes in the seasonal cycles [*Laskar et al.*, 2004]. *Head et al.* [2003] hypothesizes an ice age between 2.1 to 0.4 Ma ago, when the obliquity exceeded 30° and water-ice was removed from the polar regions and transported to mid-latitudes, where a mantle of icy dust covered the surface. The end of this ice age is been evidenced by rapid accumulation of north polar layered deposits which is the result of degradation and retreat of ice-rich deposits in the mid-latitudes [*Smith et al.*, 2016]. Although the obliquity variations are not predictable for periods more than 20 Ma ago [*Laskar et al.*, 2004], it is likely that the surface of Mars have been repeatedly undergone such climate changes leading to deposition and sublimation/evaporation of ice-rich material [e.g., *Head et al.*, 2005; *Smith et al.*, 2016].

Geomorphological investigation of the remnants of ice-rich deposits in the mid-latitudes offers a better insight into their formation process and timespan, as well as the Amazonian paleoclimate and its transit into the current climatic condition. We report, here, the presence of very well preserved and unreported glacial-like deposits, which are defined as valley fill deposit (VFD) and are observed in Terra Cimmeria (Figure 5.1). They are located on the floor of valleys, which show Amazonian-aged fluvial activities and glacial landscapes [*Adeli et al.*, 2016]. Our investigation of these mid-latitude glacial deposits, preserved under the current condition, offer an insight into the earlier and recent Amazonian climate. We performed our geomorphological investigation using the High Resolution Stereo Camera (HRSC) [*Neukum et al.*, 2004; *Jaumann et al.*, 2007] from the Mars Express (MEX) orbiter, Context Camera images (CTX) [*Malin et al.*, 2007] from the Mars Reconnaissance Orbiter (MRO), which have typical ground pixel sizes of 10 to 40 m and ~6 m, respectively. Several images acquired through the High Resolution Imaging Science Experiment (HiRISE, 25 cm/pixel [*McEwen et al.*, 2007]) were also used to study the detailed surface texture of the deposits, with higher resolution.

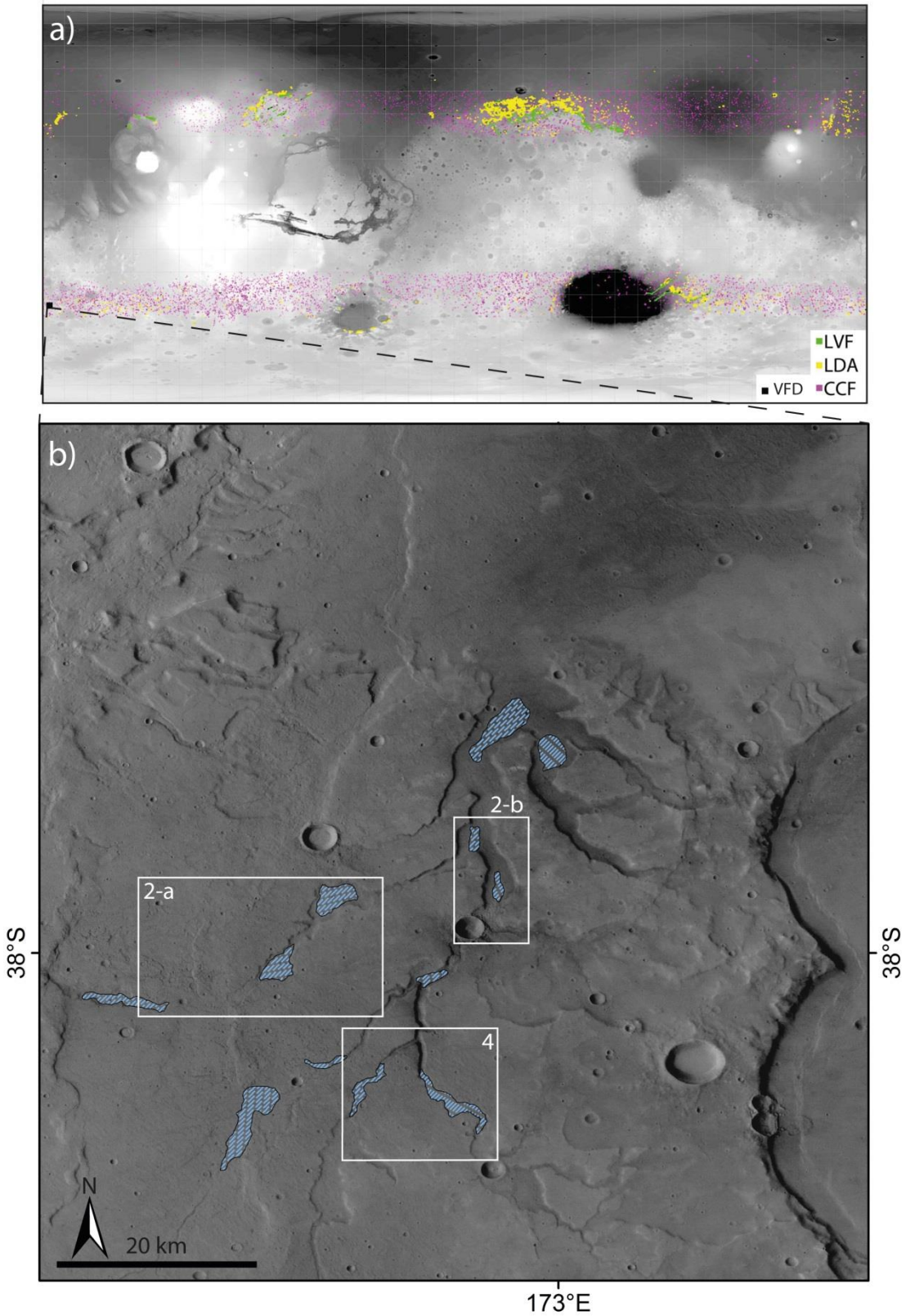

Figure 5.1: Study area. a) Global distribution of LVF, LDA, and CCF shown on a MOAL map [modified after Levy et al., 2014] in addition to the VFD's location reported in this study. b) the valley system in Terra Cimmeria with VFDs indicated in hachured blue lines (detail of HRSC nadir image, orbit number 4198). The location is some figures in this study are marked.

b. GEOLOGIC BACKGROUND

Recent glacial-related landforms are widespread in mid-latitude regions on Mars which extends between ~30-60° latitude ([*Levy et al.*, 2014] and Figure 5.1a), and mainly include: lobate debris aprons (LDA) [*Mangold*, 2003], lineated valley fill (LVF) [*Head et al.*, 2006], concentric crater fill (CCF) [*Levy et al.*, 2010], glacier-like forms (GLF) [*Hubbard et al.*, 2011]. Lobate debris aprons (LDA) originate at mesas and escarpment walls, have a convex-upward shape, represent unconfined mass wasting processes, and are indicators of ice-rich deposits that had been mantled and their surfaces have been modified and degraded by sublimation of near-surface ice [*Squyres*, 1978; *Malin and Edgett*, 2000b; *Mangold*, 2003], a process that is more likely still going on [*Mangold*, 2003]. Lineated valley fill (LVF) and concentric crater fill (CCF) consist of the same kind of material as LDA but are confined and restricted to the floors and walls of valleys and craters, respectively [*Squyres*, 1978]. Glacier-like forms (GFL) are mainly composed of ice-dust mixtures and show signs of downhill viscous deformation [*Hubbard et al.*, 2014]. There is no clear evidence of the formation time of these features, and their formation has been assumed in literature as middle to late Amazonian (e.g., minimum age of around 40 Ma [*Head et al.*, 2005], around 60 Ma [*Parsons and Holt*, 2016], between 1 Ga and ~300 Ma [*Berman et al.*, 2015], or more generally, several hundreds of million years [*Mangold*, 2003]). These ice-related features are believed to be the result of climate changes due to shifts in the obliquity and eccentricity of Mars' orbital rotation [*Mellon and Jakosky*, 1993].

Latitude dependent mantle (LDM) formed in the last few million years (e.g., around 3-5 Ma [*Willmes et al.*, 2012], around 2.1-0.4 Ma [*Head et al.*, 2003] , and less than 1.5 Ma [*Mustard et al.*, 2001]) and is an ice-rich dust deposit which partly covers the surface of the mid-latitude areas [*Mustard et al.*, 2001; *Kreslavsky and Head*, 2002; *Head et al.*, 2003; *Kostama et al.*, 2006; *Conway and Balme*, 2014] and is currently undergoing degradation and retreat [*Head et al.*, 2003]. The LDM consists of different layers indicating a repeated emplacement mechanism, which is believed to be caused by obliquity cycles [*Mustard et al.*, 2001; *Kreslavsky and Head*, 2002; *Head et al.*, 2003; *Kostama et al.*, 2006].

The study area is located in the southern mid-latitude area of the Terra Cimmeria region centered at about 38°S and 173°E (Figure 5.1), where a part of the Eridania paleolake was present during late Noachian-early Hesperian epoch [*Irwin et al.*, 2002]. South of this area, there is the Sirenum Fossae graben system. Around 100 km southward of Sirenum Fossae there is a valley system, which displays evidence for Amazonian activity and terminates at the floor of the Ariadnes Colles basin with an outflow channel named Kārūn Valles [*Adeli et al.*, 2016]. The features of interest of this study are located on the floor of this fluvial system.

c. VALLEY FILL DEPOSIT (VFD) MORPHOLOGICAL CHARACTERISTICS

Several deposits on the flat floors of S-N trending valleys south of Ariadnes Colles are characterized by (1) widths and lengths of a few kilometers, (2) convex-upward surface topography, and (3) crevasses on their surface (Figure 5.1). The main trunks of the host valleys are joined by narrow channels, which suggests that these valleys are of fluvial origin and were fed by occasional surface runoff due to ice/snow melt [*Adeli et al.*, 2016]. The valley floors as well as the areas surrounding the deposits are partly covered by a thin, smooth-textured mantle. This draping material shows similar characteristics as the LDM. These characteristics are a smooth surface, widespread and latitude dependent distribution, thin thickness (up to 10 m thick [*Mustard et al.*, 2001]), and very few and small superposed impact craters, implying a recent age [e.g., *Mustard et al.*, 2001; *Willmes et al.*, 2012].

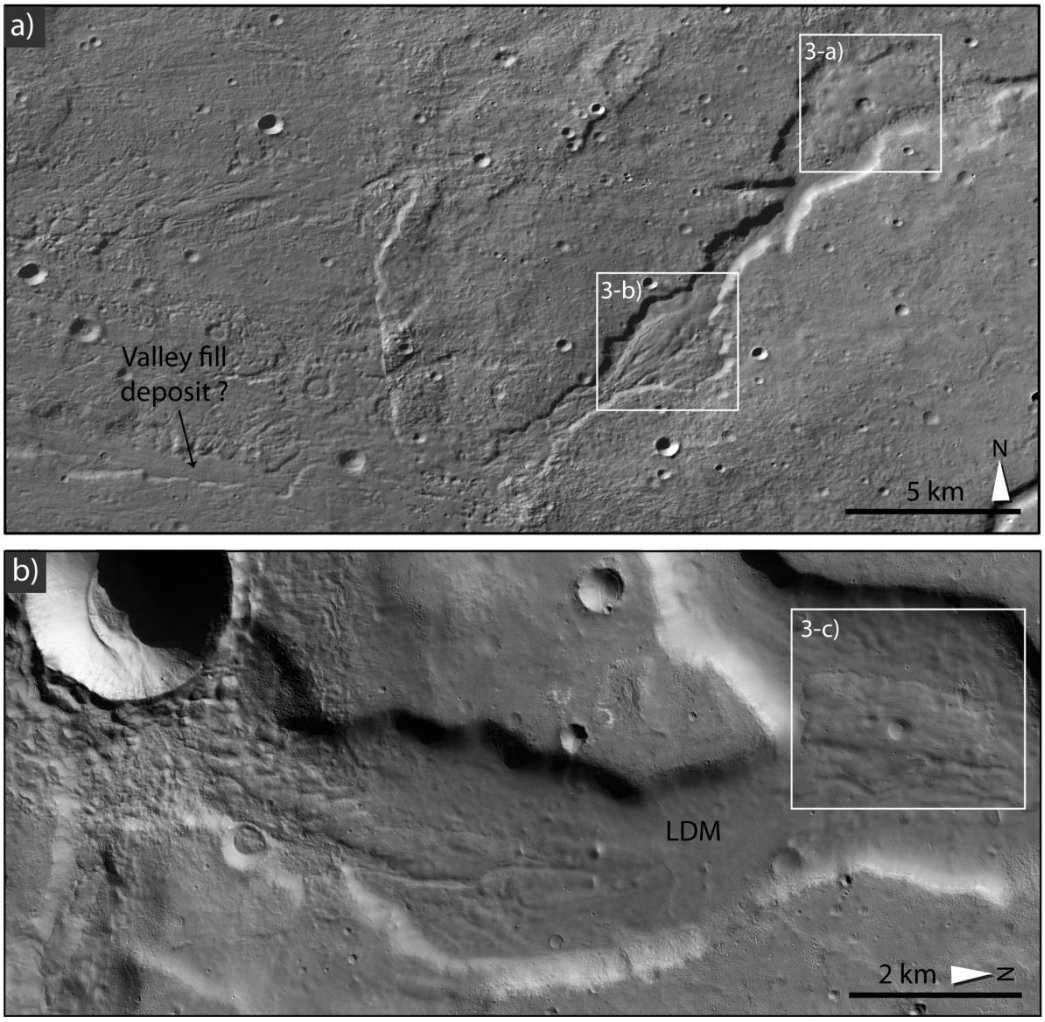

Figure 5.2 Valley fill deposit (VFD) distribution in the study area. a) The VFD has almost filled the width of the valley. The valley is a part of a fluvial system located in Terra Cimmeria. The valley floor is partly covered by the VFDs and partly by the ice-rich LDM (CTX image B21_017798_1416). b) VFD observed in the center of the valley width, exposed beneath the LDM (HiRISE image ESP 016664_1420). Locations of figures are shown in Figure 5.1.

The valley floor deposits (VFD) in some cases cover the width of the host valley (Figure 5.2a) which indicates their post-valley formation. In other cases they are exposed in the center of the valley, from beneath of the ice-rich latitude dependent mantle (LDM) which is partly covering the VFD (Figure 5.2b). The surface of VFD shows only few impact craters with diameters equal or smaller than ~700 m. Craters larger than 70 m are mostly degraded, their rims show almost no positive relief (in CTX resolution) and they have flat floors. Smaller modified craters have been observed, but there are also a few small fresh impact craters (smaller than 70 m in diameter) which do not show any modification on their rim and wall. On the surface of the deposit shown in Figure 5.3a, a feature with a circular shape may represent a crater which is highly degraded and filled with material. The surface areas of the VFD are only a few square kilometers to a few tens of square kilometers, hence they are not large enough to enable applying the crater size–frequency method with a confident result [*Warner et al.*, 2015].

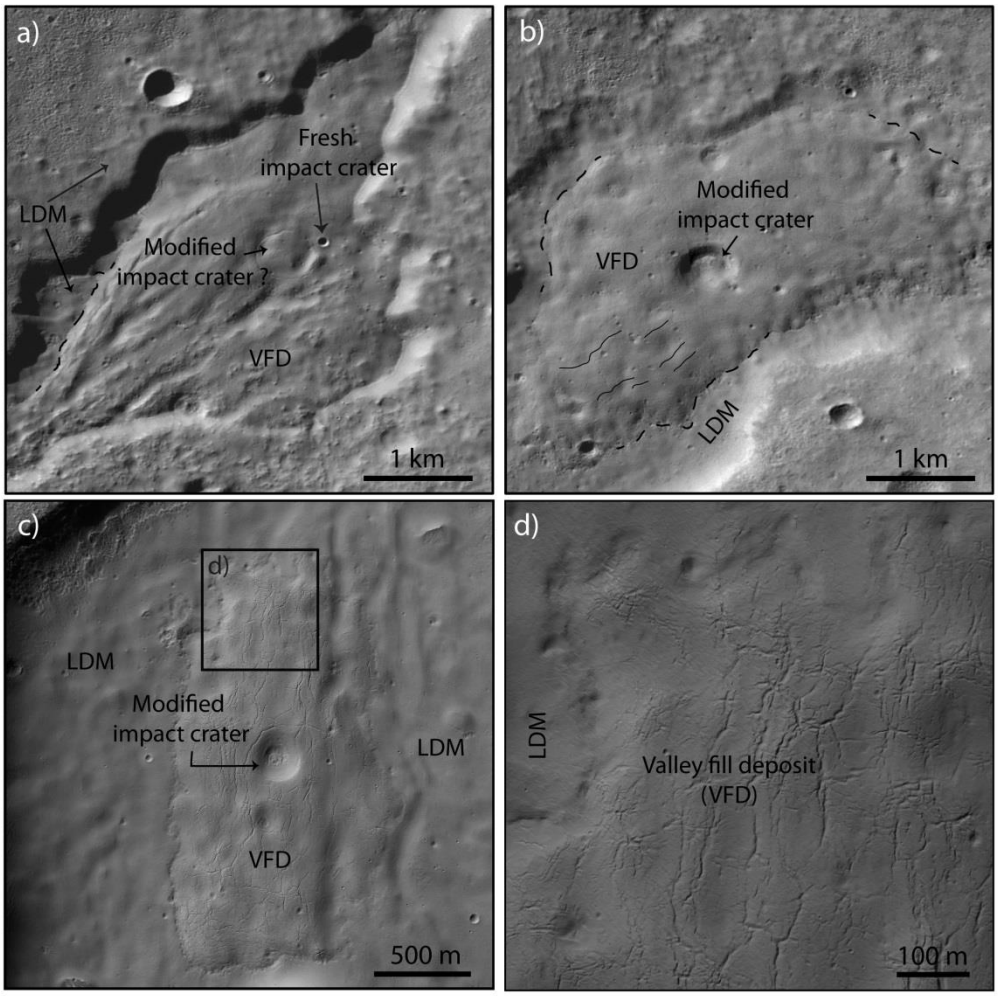

Figure 5.3: Valley fill deposit (VFD). a) VFD with longitudinal furrows. Note the circular feature which may represent a filled impact crater, and the small unmodified and fresh impact crater. b) VFD with a modified impact crater on its surface. The dashed line represents the limit between the LDM and VFD. The solid line shows some crevasses. c) VFD with clear crevasses on its surface, and a modified impact crater. d) A blow-up on the surface of the VFD in (c). The thin LDM was deposited on top of the VFD. Location of the figures and image credits are indicated in Figure 5.2.

Where higher resolution data are available, we can observe cracks and crevasses on surface of VFD (Figure 5.3). The VFD in Figure 5.3a shows a more modified surface as compared to other VFDs in the area. In the southwestern part of the VFD, there are linear features that are wider than the crevasses in other VFD. A circular feature, which may be an impact crater, is almost fully filled and covered. The presence of LDM on the southwestern part of the VFD in Figure 5.3a is less pronounced than in the northeastern part. In all VFD cases, in this area, the LDM is stratigraphically above the VFD and covers the valley floor and partly the VFDs. In the Figure 5.3d we can clearly see the contact between the mantle (LDM) and the VFD.

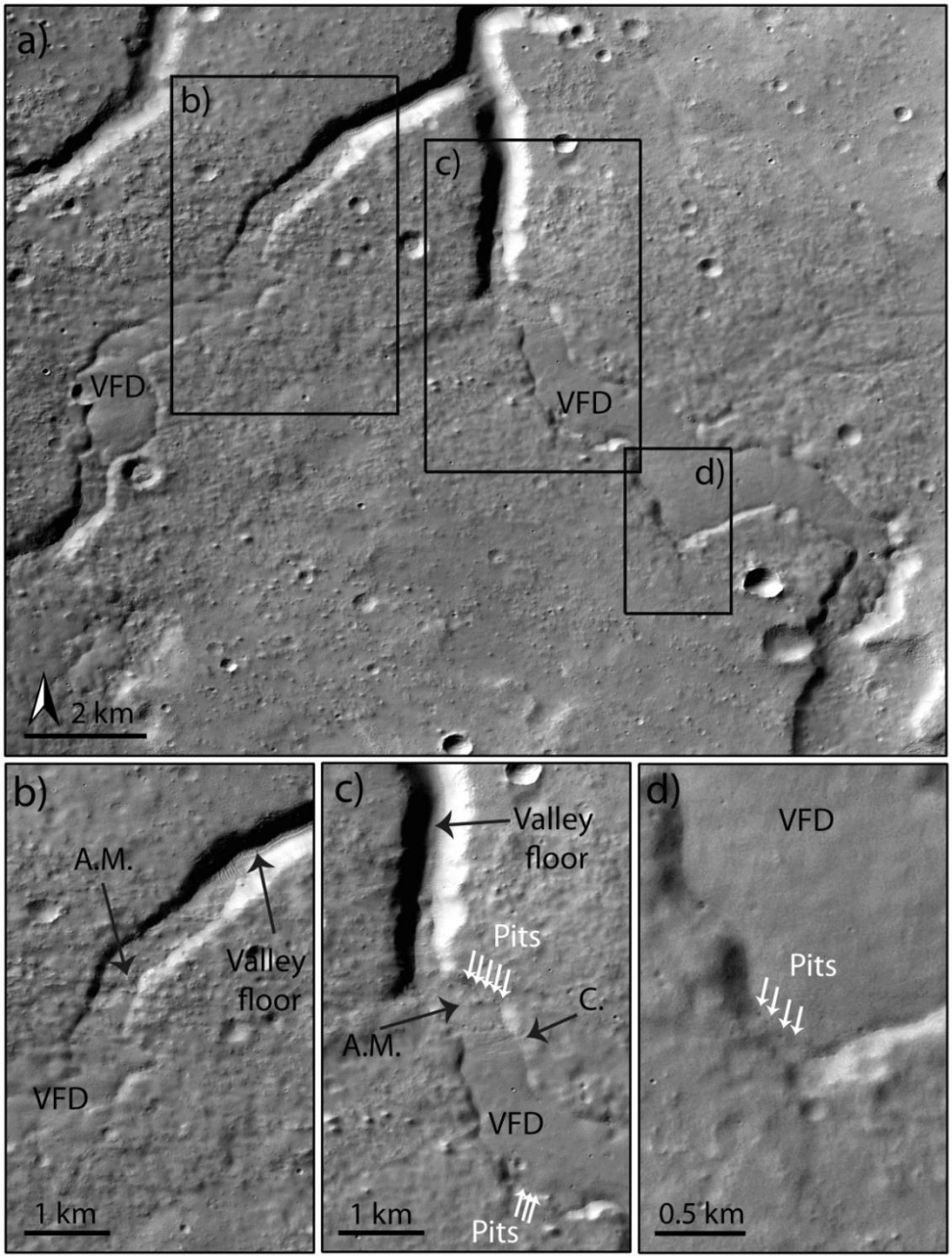

Figure 5.4: Two few kilometers long VFDs on the floor of a valley system. b and c) Blow-ups of the head of the glacier, showing the transvers crevasses (C.), the ablation moraine (A.M.), the valley floor and the sublimation pits (white arrows). d) Few ten of meters large pits on the border of the VFD (CTX image B18_016664_1414). Locations of figures are shown in Figure 5.1.

On the floor of two valleys, we observed two VFDs which completely cover the host valleys (Figure 5.4a). They have several crevasses on the surface as well as lateral or transverse crevasses at their head (Figure 5.4b). Transverse crevasses indicate tensile stress caused by viscous flow of the deposit. In front of these VFDs in both valleys, the valley floors are rougher adjacent to the VFD (Figure 5.4b and c) which may be due to sediments accumulation with a higher concentration closer to the VFD. The accumulation of sediments reduces gently toward north until the valley floor is visible (Figure 5.4b and c). The sediment accumulation in both valleys has a length of around 1-3 km. At the contact between the VFD and valley walls, we observed several pits a few tens of meters large and oriented along a preferential direction on the border of the VFD (Figure 5.4b). Pits due to ice sublimation have often been observed at the mid-latitude ice-related features [*Mangold*, 2003; *Mangold*, 2011].

d. INTERPRETATION AND IMPLICATIONS

Our detailed observation and investigation of valley fill deposits (VFD) allow analyzing the possible formation mechanism of the valley fill deposits (VFD) in Terra Cimmeria, and their implication for the Amazonian climate. Given the morphological characteristics of the VFD, such as their convex-upward shape, transverse crevasses, and moraine-like deposits, it is unlikely that VFD represent sediments transported and deposited due to fluvial or aeolian activities in the valleys. In case of sediments deposited due to fluvial activities, the VFDs would have a fan-like shape; however we observe the VFD in the middle of the valleys. In addition, fluvial deposits would not fill the entire valley depth, however we observed a few VFDs (e.g., in Figure 5.4) which fill the valley in depth and width. In case of the aeolian infilling, we would most probably observe more homogenous and widespread distribution, as it is the case for the LDM which also covers the surrounding area. Instead, it seems more likely that ice-rich material and glacial-like processes filled the valleys after their incision. The VFD reveals features typical of terrestrial glacial settings, such as convex-upward morphology, accumulated deposits at the deposit's head, and crevasses. Figure 5.4 shows that the accumulated sediments (A.M. in Figure 5.4b and c) have a rough surface textures and different morphology as compared to the VFD. These sediments could, most likely, be remnant deposits of the glacier retreat which may be due to rapid ice sublimation, known as ablation moraines. The transverse crevasses (C in Figure 5.4c) show that the principle stresses are parallel to the direction of the glacier flow, so that transverse crevasses open up at right angles to the center-line and curve downstream which is influenced by the drag of the valley walls [*Benn and Evans*, 1998]. Considering these observations, we suggest that the sublimation of the glacier head caused the glacier surface to curve downward, inducing tensile stress and opening of the crevasses. Sublimation is also indicated here by pits that are observed at the border of the VFD (Figure 5.4c and d).

The impact craters observed on the surface of some of the VFDs are few hundred meters in diameter, bowl-shaped, rimless, and have a flat floor (Figure 5.3b and c). Very similar characteristics have been observed for impact craters on LDA and LVF surfaces in mid-latitudes, which are termed ring-mold craters (RMC) by *Kress and Head* [2008] and are

thought to be a result of impacts into shallow buried ice. The circular feature in Figure 5.3a may alternatively represent a pre-VDF impact crater, the shape of which is reflected on the VFD surface as a result of differential material deposition or collapse. The thin ice-dust mixture of LDM drapes the valley floor and partly the VFD. Its degradation on the higher elevated portions of the VFD allows the surface of the VFD to become exposed from beneath the degrading LDM. In some parts where the LDM is less pronounced (e.g., in SW of Figure 5.3a), the VFD is more degraded as in other cases. Therefore, the LDM layer may have preserved the VFDs from erosion and degradation. The LDM surface is very smooth and lacks fresh and unmodified impact craters with diameters larger than 100 m. These characterizations are similar to what has been observed elsewhere on Mars and been interpreted as a sign for a surface age of less than ~1.5×10^5 years [*Mustard et al.*, 2001 and references within].

The VFD have been observed on the floor of a valley system with traces of early to middle Amazonian fluvial activities [*Adeli et al.*, 2016]. Our observations point to a post-valley formation for the VFD. The lineated valley fill (LVF) is another ice-rich feature which is observed on the floor of valleys, mainly in the so-called Fretted Terrain at the dichotomy boundary [*Squyres and Carr*, 1986; *Head et al.*, 2006]. LVF has also been interpreted as a glacial landform due to its similarities to terrestrial valley glaciers, including crevasses and lateral and medial moraines [see *Head et al.*, 2006]. Although these similarities have been observed as well in VFD, we did not observe the lineated pattern in the surface of the VFD.

The accumulation of ice/snow at mid-latitudes cannot be explained by the current climatic condition of Mars, as the atmosphere does not sustain snow/ice accumulation and surface ice is unstable at mid-latitudes [*Mellon and Jakosky*, 1995]. Therefore, the glaciation and deposition of VFD should have taken place under different climatic conditions in the past. The stability of ice at the surface is sensitive to the insolation which varies with the obliquity cycle. During periods of high obliquity ice would be driven from the polar regions to be deposited at lower latitudes [*Mellon and Jakosky*, 1995]. The obliquity variation happened quasi-periodic [*Laskar et al.*, 2004] in the past, and Mars is currently in a relatively low obliquity phase of 25 degree. The VFD is partly covered by LDM, whose emplacement occurred a few millions years ago. Collectively, LDA, LVF, GLF, and CCF represent ice-rich deposits that are related to a much older emplacement phase, a few hundred million years ago [*Mangold*, 2003; *Head et al.*, 2005; *Parsons and Holt*, 2016], indicating the possibility of obliquity oscillations and consequently climate changes in the last few hundred million years. *Levy et al.* [2014] estimated the volume of the remnant glacial deposits in both mid-latitudes, and derived a global equivalent ice layer thickness of 0.9 to 2.6 m. The VFD in our study area is exposed where the thin blanket of LDM is eroded. This suggests that under the LDM on the valley floor of our study area and elsewhere in the mid-latitudes, there may be additional deposits of ice from previous accumulation phases that cannot be clearly observed, thus the amount of near surface water ice reported on the current surface of Mars may be more extensive and greater than previously thought. This needs further investigation using wider coverage of high resolution imagery and topographic data such as the upcoming imaging

experiment, CaSSIS (Colour and Stereo Surface Imaging System), on the ExoMars Trace Gas Orbiter mission.

The sequence of VFD beneath LDM refers to an earlier emplacement of VFD as compared to the LDM. Therefore we infer that the VFD formation took place before the last stage of LDM emplacement, and it is likely that it occurred by a similar mechanism which formed LDA, LVF, GLF, and CCF during a similar climate change phase, or even by the same mechanism and contemporaneously with those deposits. The presence of ice-rich VFD underneath the young LDM is an evidence of an episodic and multi-event process of ice emplacement in the mid-latitudes of Mars during the Amazonian.

Acknowledgements

This research was supported by the Deutsches Zentrum für Luft- und Raumfahrt (DLR-Berlin). Data to support this paper are from the PDS Geosciences Node archive (http://pds-geosciences.wustl.edu/).

6. DISCUSSION AND CONCLUSION

a. HISTORY OF LIQUID WATER IN TERRA SIRENUM-TERRA CIMMERIA

Did the liquid water disappear in Terra Sirenum-Terra Cimmeria with the desiccation of the large Eridania lake? What happened in the Terra Sirenum–Terra Cimmeria after the late Noachian? How are the current surface conditions for the presence of water (liquid or ice) in this area? These are the main questions which will be addressed in this section by summarizing the major results and findings reported in Chapter 3, 4, and 5. At the end of this chapter, a timeline of the surface water presence in the Terra Sirenum–Terra Cimmeria region, from the late Noachian until current time, has been presented. In order to tackle these questions, a multi-datasets and multi-methodical approach has been taken into account to have a wide overview on the past, recent, and current geological history of the area and processes which formed the surface. Thus this chapter mainly focuses on a timeline of geological events, in the study area, with a focus on the water abundance, and its implication on the aqueous processes and the climate of Mars.

i. EARLY MARS PALEOLAKE

In the southern cratered highlands, there is widespread and clear morphological and mineralogical evidence of more than two hundred paleolakes in the form of closed, open, and lake chain systems [*Cabrol and Grin*, 1999; 2001; *Fassett and Head*, 2008; *Hauber et al.*, 2009; *Goudge et al.*, 2012]. Surface runoff and groundwater aquifers are the likely water sources, and both have been important for the Martian hydrology system [e.g., *Cabrol and Grin*, 2010]. The Eridania lake is one of the largest lake, on Mars, with a volume of ~480,000 km^3 which occupied an area of ~1,100,000 km^2. This paleolake existed, most probably, between middle to late Noachian [*Irwin et al.*, 2002; 2004; *de Pablo et al.*, 2004] and later drained through the Ma'adim Vallis [*Irwin et al.*, 2002]. After several drainage phases, the Eridania lake transformed into isolated lakes hosted by pre-existing depressions, which have most likely an impact origin [*Irwin and Howard*, 2002; *Irwin et al.*, 2002; *de Pablo and Fairén*, 2004; *Howard and Moore*, 2004; *Irwin et al.*, 2004; *Wray et al.*, 2011]. The duration of these isolated lakes is poorly constrained and they are hypothesized to have existed sometimes during the late Noachian and early Hesperian [*Irwin et al.*, 2004; this work].

The climate at the time of the Eridania lake formation and later its transformation into smaller lakes must have been different and warmer than current conditions. The paleoclimate could sustain a recharged and stable water table for a considerably long time. However, it is still under debate how warm such a paleoclimate was. Although the findings in this work strongly support large-scale and long-time presence of liquid water on the surface, there is no evidence against the possibility of ice-covered lakes which would nonetheless mean warmer climate than the current one. The long-term presence of bodies of water in this area is evidenced not only by the complex morphology of the basins and stratigraphy of deposited

material (see Chapter 3.d and f), but also by the existence of a thick layer (up to 600 m of thickness) of light-toned material rich in Fe/Mg-phyllosilicates on the basin's floors, in form of knobs (see Chapter 3.e and f). The Fe/Mg-phyllosilicates in this area correspond to Fe/Mg-smectite (see Chapter 3.e.i) which generally forms in neutral to alkaline environments [*McKeown et al.*, 2009]. On the basins rim, on top of the Fe/Mg-smectite, a thin layer of Al-phyllosilicates-rich material has been observed (Chapter 3.e.ii). The sequence of Al-phyllosilicate on top of Fe/Mg-phyllosilicate is characteristic for an alteration by up-down leaching of limited amounts of water [*Poulet et al.*, 2005; *McKeown et al.*, 2009]. This alteration is also known as pedogenesis and normally occurs in (slightly) acidic environments ([*Poulet et al.*, 2005] and Chapter 3.f.ii.2). These hydrated minerals and their stratigraphic relation reveal an environment change in this area, which may be related to a decrease of liquid water abundance and the chemical environment oscillation. The change of chemical environment has happened at the end of the lakes life span, or during their desiccation phase. The decrease of the amount of water had also occurred in other areas of the highlands, as there is no significant evidence of a large body of water (e.g., as large as the Eridania paleolake) in the southern hemisphere during the Hesperian period.

In several shallow depressions, the phyllosilicate-rich sediments are partly covered by a thin layer of chloride-bearing material (Chapter 3.e.iii). The detection of chloride reveals an evaporitic condition which differs from a phyllosilicate-forming environment. Therefore the formation of chloride salt may correspond to a playa environment which prevailed during the last stage of the lakes existence, or later due to potential reoccurrence of small amounts of liquid water in the area (Chapter 3.f.ii.3). In the studied basins, there are three geologic units which partly cover the phyllosilicate-rich materials (Chapter 3.d). These units are dated as early Amazonian and indicate that deposition, alteration, and erosion of material deposited in bodies of water took place before the formation of the early Amazonian units (Chapter 3.f.iii). Two of these units show evidence of volcanic activities and potential lava flow emplacement (Chapter 3.f.iii.3). The third unit formative mechanism is interpreted as airfall material cemented by a limited amount of liquid water originated from rainfall and/or ice/snow melt (Chapter 3.f.iii.2). This interpretation points to the presence of liquid water, in the Terra Sirenum-Terra Cimmeria region, during the early Amazonian epoch.

ii. AMAZONIAN-AGED VALLEY AND CHANNEL SYSTEM

Amazonian climate is globally considered as cold and hyperarid [e.g., *Marchant and Head*, 2007], however, morphological evidence of Amazonian liquid water has been recently identified in high-resolution images returned by the Mars Odyssey (MO), Mars Reconnaissance Orbiter (MRO), and Mars Express (MEX) missions. These observations revealed the presence of tens to hundreds of kilometers long Amazonian-aged fluvial channels [*Howard and Moore*, 2011; *Hobley et al.*, 2014; *Salese et al.*, 2016], alluvial fans and fan deltas [*Hauber et al.*, 2013]. In Terra Cimmeria, south of the Eridania paleolake shoreline, the existence of a fluvial system has been reported (Chapter 4). The fluvial system has an early to middle Amazonian age as estimated by crater size–frequency distribution (Chapter 4.d). The main channel at the upstream section of this fluvial system seems to be fed by surface runoff

via narrow glaciofluvial valleys. These narrow valleys are located adjacent to the small and local depressions, which are interpreted to have hosted ice or snow deposits (Chapter 4.f.i). These deposits have entirely melted and carved the narrow valleys toward the main water stream. Several fan-delta and fan-shaped deposits have been observed on the upstream section, suggesting a relatively short and energetic fluvial activity (Chapter 4.f.iii) which is also evidenced by groove marks, cataracts, and streamlined islands on the valley floors (Chapter 4.f.iii).

The downstream section of the fluvial system is composed of more than 63 km Kārūn Valles which has a wide, low–sloping, and fan–shaped deposit at its terminus (Chapter 4.d.iii). The morphology of this deposit, such as its gentle grade of the distal margins and a concave-upward geometry, points toward an alluvial fan (Chapter 4.d.iii.2). Closer observations revealed the braided nature of this alluvial fan, which has been rarely observed on Mars [*Matsubara et al.*, 2015]. The hydraulic modelling for the Kārūn Valles reveals a geologically short formation time of few days to few tens of thousands days (Chapter 4.e.iii). Kārūn Valles, the correspondence fluvial system, and other fluvial features reported elsewhere on Mars [e.g., *Howard and Moore*, 2011; *Hobley et al.*, 2014; *Salese et al.*, 2016] clearly show the presence of a limited amount of liquid water during the Amazonian. Fluvial activity, perhaps episodic, existed throughout the Amazonian, and it could be best explained by surface run off of snow or ice melt, due to climate change caused by obliquity variations (see *Laskar et al.* [2004] and Chapter 4.f.iii for discussion).

iii. RECENT GLACIAL-LIKE DEPOSITS

Landforms of glacial origin have been observed in both mid-latitude regions [e.g., *Levy et al.*, 2010] including lobate debris aprons (LDA), lineated valley fill (LVF) [*Head et al.*, 2006], concentric crater fill (CCF) [*Levy et al.*, 2010], and glacier-like forms (GLF) [*Hubbard et al.*, 2011] which are several hundred million years old ice-rich deposits [e.g., *Mangold*, 2003] and dust-ice drape of latitude dependent mantle (LDM) which formed in the last few million years [*Mustard et al.*, 2001; *Head et al.*, 2003; *Willmes et al.*, 2012]. During periods of high obliquity, ice can be deposited almost anywhere in the mid-latitudes and during low obliquity ice is transported back to the poles [*Smith et al.*, 2016]. In Terra Cimmeria several glacial-like and ice-rich deposits have been observed (Chapter 5.c) on the floor of the fluvial valley system reported in the Chapter 4. These deposits are characterized by their convex-upward surface topography, crevasses, ablation moraines, sublimation pits, and ring-mold craters (Chapter 5.c). They are partly covered by the thin LDM.

The ice accumulation of VFD have most probably taken place during a stage of high obliquity, the same mechanism that caused the deposition of LDA, LVF, CCF, and GLF in the mid-latitude regions of Mars (Chapter 5.d). The VFD have later been covered by the LDM, most likely during the recent climate change phase. This indicates that beneath the LDM on the valley floor of our study area and elsewhere in the mid-latitudes, there may be additional deposits of ice from previous accumulation phases that cannot be clearly observed,

thus the amount of near surface water ice reported on the current surface of Mars may be greater and more extensive than previously thought. Therefore, the Amazonian climate, although not currently favorable for ice to accumulate, underwent climate change phase(s) which caused widespread deposition of ice in the mid latitude regions.

The liquid water abundance on the surface of Mars has significantly decreased from late Noachian-early Hesperian large bodies of water, however, in the early-middle Amazonian there are, again, traces of fluvial activities, along with evidence of ice/snow melt. In the late Amazonian under a cold and hyperarid climate, there are ice-rich and glacial-like deposits preserved under a drape of frozen dust. All these observations show that the liquid water presence on the Martian surface has not completely ceased. Thus, the Terra Sirenum-Terra Cimmeria region with a diverse collection of water-related features which occurred in various time frames and in different geomorphological and chemical environments, is a prime candidate for an in-situ investigation by a future lander on the red planet and needs to be considered in the future.

b. GEOLOGIC TIMELINE

The results of Chapter 3, 4, and 5, suggest a sequence of geologic events in the study area from the late Noachian to the current late Amazonian epoch. Geomorphologic observations, geologic mapping results, mineralogical analysis, hydraulic modelling, and crater size–frequency distribution results are carefully combined, in order to reconstruct the timeline of the major geological processes occurred in the Terra Sirenum and Terra Cimmeria regions. Here we summarize the sequence of events (Figure 6.1):

Step 1) during the middle to late Noachian, the large Eridania lake covered the entire area, and its drainage to the north carved Ma'adim Vallis. Later, the water level decreased, and the Eridania lake split into smaller isolated lakes (ice-covered or liquid). Airfall deposits accumulated light-toned and altered material (phyllosilicate-bearing) on the plateaus, floors, and rims of the lakes, (Figure 6.1-step 1).

Step 2) during late Noachian-early Hesperian the water level decreased, and therefore the environment on the basin rims changed from subaqueous to subaerial. Surficial Fe/Mg-phyllosilicates-rich sediments were partly altered to Al-phyllosilicates by pedogenesis. In several shallow depressions the Al-phyllosilicates is partly covered by chloride-bearing material, suggesting a playa environment after the formation of Al-phyllosilicates (Figure 6.1-step 2).

Step 3) after desiccation of the lakes during the Hesperian, dewatering cracks appeared on the basin floors and weakened and weathered materials along the cracks were removed by wind erosion and/or episodic aqueous activity and were re-shaped into the current knobby topography (Figure 6.1-step 3).

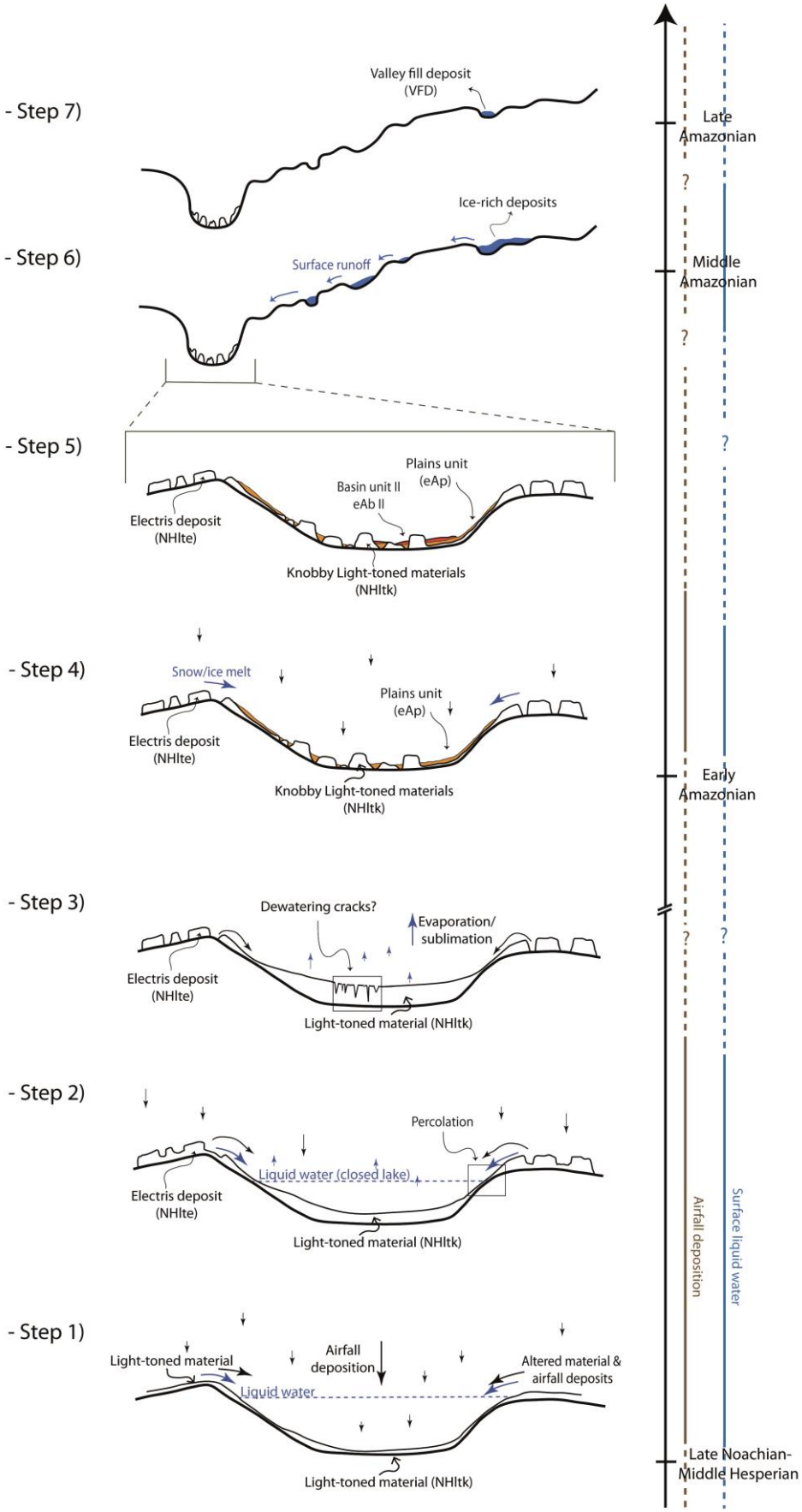

Figure 6.1: Geologic timeline of the major geologic events in the Terra Sirenum-Terra Cimmeria, from late Noachian to the current late Amazonian epoch.

Step 4) airfall deposition re-occurred in the early Amazonian and covered the floors of all basins with a thin layer. This deposited material, especially at the basin rims, was partly indurated by late aqueous activity probably linked to rainfall and/or ice/snow melt (Figure 6.1-step 4).

Step 5) thin lava flows partly covered the basin floors, suggesting that volcanism may have been episodically active during the early Amazonian in Terra Sirenum (Figure 6.1-step 5).

Step 6) during early to middle Amazonian fluvial activity due to surface runoff of ice/snow melt took place in the area, and deposited fan-shaped deposits and particularly the braided Kārūn Valles alluvial fan. This fluvial activity lasted a minimum of few days to few tens of thousands of days (Figure 6.1-step 6).

Step 7) currently ice-rich and glacial-like valley fill deposits are present on the surface of the study area. Their formation may be due to the past (few 10^7 year ago) obliquity variations (Figure 6.1-step 7).

c. FUTURE WORK

The sequence of Al-phyllosilicates and Fe/Mg-phyllosilicates was an important observation, leading to the assumption of pedogenesis alteration in the presence of limited amount of water. Analysing new CRISM data from the light-toned material in Atlantis, Simois, Caralis, and northern basins, would help to understand whether there is a stratigraphic relation between the various Fe/Mg-phyllosilicates. Additionally searching for other minerals in a dust-free outcrop, would as well offer a better insight into the chemical environment during those minerals formation.

New HiRISE stereo pair images of the fluvial system in Terra Cimmeria have been proposed to be acquired with the aim of investigating the morphological features in higher resolution and studying the geometry of the valleys, which would bring us closer to infer the formation process, particularly in case of the Kārūn Valles, which is, to our knowledge, a unique braiding alluvial fan on Mars.

Additional mapping of the distribution of the Amazonian-aged fluvial system in the southern mid-latitudes is essential to comprehend the Amazonian climate and climate change phase(s) on a regional scale, as well as in a global scale.

The detection of VFDs in Terra Cimmeria revealed that the preserved ice-rich material from the most recent climate change(s) is more widespread than previously assumed. Although what was presented here corresponds to a small amount of deposits, but considering a wider presence of similar features in the both mid-latitudes would mean a considerably large amount of ice-bearing material. Their distribution, geometry, and stratigraphic relation with other layers, would crucially increase our current understanding of the Amazonian climate change phase(s).

The last but not least on my future work objectives, I will be trying to bring planetary science into non-planetary scientists' daily life, to make it more accessible and easier to understand, with the hope of getting more attention from public for other planets which may in future, perhaps not very far future, be home(s) to our species.

REFERENCES

Adeli, S., L. Le Deit, E. Hauber, A. Molina, and R. Jaumann (2012), Phyllosilicate-rich Knobs in the Atlantis Chaos Basin, Terra Sirenum, in *European Planetary Science Congress 2012*, edited, p. 291.

Adeli, S., E. Hauber, L. Le Deit, and R. Jaumann (2013), Different Phylloslicate-Rich Materials on the Terra Sirenum Region, Mars, *LPI Contributions*, *1719*, 2752.

Adeli, S., E. Hauber, L. Le Deit, and R. Jaumann (2015), Geologic evolution of the eastern Eridania basin: Implications for aqueous processes in the southern highlands of Mars, *Journal of Geophysical Research: Planets*, *120*(11), 1774-1799. doi: 10.1002/2015je004898

Adeli, S., E. Hauber, M. Kleinhans, L. Le Deit, T. Platz, P. Fawdon, and R. Jaumann (2016), Amazonian-aged fluvial system and associated ice-related features in Terra Cimmeria, Mars, *Icarus*, *277*, 286-299. doi: 10.1016/j.icarus.2016.05.020

Andrews-Hanna, J. C., M. T. Zuber, and R. J. Phillips (2008), Early Mars Hydrology: Valley Networks and Evaporites, in *Lunar and Planetary Science Conference*, edited, p. 1993.

Annex, A. M., and A. D. Howard (2011), Phyllosilicates Related to Exposed Knobs in Sirenum Fossae, Ariadnes Colles, in *Lunar and Planetary Science Conference*, edited, p. 1577.

Aydin, A., and J. M. DeGraff (1988), Evoluton of Polygonal Fracture Patterns in Lava Flows, *Science*, *239*(4839), 471-476. doi: 10.1126/science.239.4839.471

Baker, V. R., M. H. Carr, V. C. Gulick, C. R. Williams, and M. S. Marley (1992), Channels and valley networks, in *Mars*, edited by Kieffer H., Jakosky B., Snyder C. and M. M., pp. 493-522, University of Arizona Press, Tuscon.

Baker, V. R. (2001), Water and the martian landscape, *Nature*, *412*, 228-236.

Balme, M., N. Mangold, D. Baratoux, F. Costard, M. Gosselin, P. Masson, P. Pinet, and G. Neukum (2006), Orientation and distribution of recent gullies in the southern hemisphere of Mars: Observations from High Resolution Stereo Camera/Mars Express (HRSC/MEX) and Mars Orbiter Camera/Mars Global Surveyor (MOC/MGS) data, *Journal of Geophysical Research: Planets*, *111*(E5). doi: 10.1029/2005je002607

Benn, D. I., and D. J. A. Evans (1998), *Glaciers and Glaciation*, Arnold, London, Great Britain.

Berman, D. C., D. A. Crown, and E. C. S. Joseph (2015), Formation and mantling ages of lobate debris aprons on Mars: Insights from categorized crater counts, *Planetary and Space Science*, *111*, 83-99.

Bibring, J.-P., Y. Langevin, J. F. Mustard, F. Poulet, R. Arvidson, A. Gendrin, B. Gondet, N. Mangold, P. Pinet, F. Forget, O. Team, M. Berthé, C. Gomez, D. Jouglet, A. Soufflot, M. Vincendon, M. Combes, P. Drossart, T. Encrenaz, T. Fouchet, R. Merchiorri, G. Belluci, F. Altieri, V. Formisano, F. Capaccioni, P. Cerroni, A. Coradini, S. Fonti, O. Korablev, V. Kottsov, N. Ignatiev, V. Moroz, D.

Titov, L. Zasova, D. Loiseau, P. Pinet, S. Doute, B. Schmitt, C. Sotin, E. Hauber, H. Hoffmann, R. Jaumann, U. Keller, R. Arvidson, T. Duxbury, and G. Neukum (2006), Global Mineralogical and Aqueous Mars History Derived from OMEGA/Mars Express Data, *Science*, *312*, 400-404.

Bishop, J. L., M. D. Dyar, and A. J. Brown (2008a), Reflectance and emission spectroscopy study of four groups of phyllosilicates: smectites, kaolinite-serpentines, chlorites and micas, *Clay Minerals*, *43*(1), 35-54. doi: 10.1180/claymin.2008.043.1.03

Bishop, J. L., E. Z. N. Dobrea, N. K. McKeown, M. Parente, B. L. Ehlmann, J. R. Michalski, R. E. Milliken, F. Poulet, G. A. Swayze, J. F. Mustard, S. L. Murchie, and J.-P. Bibring (2008b), Phyllosilicate Diversity and Past Aqueous Activity Revealed at Mawrth Vallis, Mars, *Science*, *321*, 830-.

Björnsson, H. (2009), Jökulhlaups in Iceland: sourcces, release and drainage, *In Burr, D.M. et al., eds. Megaflooding on Earth and Mars: Cambridge*, 50-65.

Brož, P., E. Hauber, T. Platz, and M. Balme (2015), Evidence for Amazonian highly viscous lavas in the southern highlands on Mars, *Earth and Planetary Science Letters*, *415*(0), 200-212. doi: 10.1016/j.epsl.2015.01.033

Cabrol, N., R. Landheim, R. Greeley, and J. Farmer (1994), Fluvial processes in Ma'adim Vallis and the potential of Gusev crater as a high priority site, in *Lunar and Planetary Institute Science Conference Abstracts*, edited, pp. 213-214.

Cabrol, N. A., E. A. Grin, and G. Dawidowicz (1996), Ma'adim Vallis Revisited through New Topographic Data: Evidence for an Ancient Intravalley Lake, *Icarus*, *123*, 269-283.

Cabrol, N. A., E. A. Grin, R. Landheim, R. O. Kuzmin, and R. Greeley (1998), Duration of the Ma'adim Vallis/Gusev Crater Hydrogeologic System, Mars, *Icarus*, *133*, 98-108.

Cabrol, N. A., and E. A. Grin (1999), Distribution, Classification, and Ages of Martian Impact Crater Lakes, *Icarus*, *142*, 160-172.

Cabrol, N. A., and E. A. Grin (2001), The Evolution of Lacustrine Environments on Mars: Is Mars Only Hydrologically Dormant?, *Icarus*, *149*, 291-328.

Cabrol, N. A., E. A. Grin, M. H. Carr, B. Sutter, J. M. Moore, J. D. Farmer, R. Greeley, R. O. Kuzmin, D. J. DesMarais, M. G. Kramer, H. Newsom, C. Barber, I. Thorsos, K. L. Tanaka, N. G. Barlow, D. A. Fike, M. L. Urquhart, B. Grigsby, F. D. Grant, and O. de Goursac (2003), Exploring Gusev Crater with Spirit: Review of science objectives and testable hypotheses, *Journal of Geophysical Research (Planets)*, *108*, 8076.

Cabrol, N. A., and E. A. Grin (2010), 1 - Searching for lakes on Mars: Four decades of exploration, in *Lakes on Mars*, edited by A. C. Nathalie and A. G. Edmond, pp. 1-29, Elsevier, Amsterdam.

Carling, P. A., D. M. Burr, T. F. Johnsen, and T. A. Brennand (2009), *A review of open-channel megaflood depositional landforms on Earth and Mars in Megaflooding on Earth and Mars*, Cambridge University Press.

Carr, M. H. (1995), The Martain drainage system and the origin of valley networks and fretted channels, *Journal of Geophysical Research*, *100*, 7479-7507.

Carr, M. H. (2007), *The Surface of Mars*, Cambridge University Press.

Carr, M. H., and J. W. Head (2010), Geologic history of Mars, *Earth and Planetary Science Letters*, *294*, 185-203.

Carter, J., and F. Poulet (2012), Orbital identification of clays and carbonates in Gusev crater, *Icarus*, *219*(1), 250-253. doi: 10.1016/j.icarus.2012.02.024

Carter, J., F. Poulet, J.-P. Bibring, N. Mangold, and S. Murchie (2013), Hydrous minerals on Mars as seen by the CRISM and OMEGA imaging spectrometers: Updated global view, *Journal of Geophysical Research (Planets)*, *118*, 831-858.

Christensen, P. R., J. L. Bandfield, V. E. Hamilton, S. W. Ruff, H. H. Kieffer, T. N. Titus, M. C. Malin, R. V. Morris, M. D. Lane, R. L. Clark, B. M. Jakosky, M. T. Mellon, J. C. Pearl, B. J. Conrath, M. D. Smith, R. T. Clancy, R. O. Kuzmin, T. Roush, G. L. Mehall, N. Gorelick, K. Bender, K. Murray, S. Dason, E. Greene, S. Silverman, and M. Greenfield (2001), Mars Global Surveyor Thermal Emission Spectrometer experiment: Investigation description and surface science results, *Journal of Geophysical Research*, *106*, 23823-23872.

Christensen, P. R., M. B. Wyatt, T. D. Glotch, A. D. Rogers, S. Anwar, R. E. Arvidson, J. L. Bandfield, D. L. Blaney, C. Budney, W. M. Calvin, A. Fallacaro, R. L. Fergason, N. Gorelick, T. G. Graff, V. E. Hamilton, A. G. Hayes, J. R. Johnson, A. T. Knudson, H. Y. McSween, G. L. Mehall, L. K. Mehall, J. E. Moersch, R. V. Morris, M. D. Smith, S. W. Squyres, S. W. Ruff, and M. J. Wolff (2004a), Mineralogy at Meridiani Planum from the Mini-TES Experiment on the Opportunity Rover, *Science*, *306*, 1733-1739.

Christensen, P. R., B. M. Jakosky, H. H. Kieffer, M. C. Malin, H. Y. McSween, Jr., K. Nealson, G. L. Mehall, S. H. Silverman, S. Ferry, M. Caplinger, and M. Ravine (2004b), The Thermal Emission Imaging System (THEMIS) for the Mars 2001 Odyssey Mission, *Space Science Reviews*, *110*, 85-130.

Christensen, P. R., E. Engle, S. Anwar, S. Dickenshied, D. Noss, N. Gorelick, and M. Weiss-Malik (2009), JMARS - A Planetary GIS, *AGU Fall Meeting Abstracts*, *22*.

Clark, R. N., T. V. V. King, M. Klejwa, G. A. Swayze, and N. Vergo (1990), High spectral resolution reflectance spectroscopy of minerals, *Journal of Geophysical Research*, *95*, 12653-12680.

Clark, R. N., G. A. Swayze, R. Wise, E. Livo, T. Hoefen, R. Kokaly, and S. J. Sutley (2007), *USGS digital spectral library splib06a: U.S. Geological Survey, Digital Data Series 231*.

Conway, S. J., and M. R. Balme (2014), Decameter thick remnant glacial ice deposits on Mars, *Geophysical Research Letters*, *41*(15), 5402-5409. doi: 10.1002/2014gl060314

Craddock, R. A., and A. D. Howard (2002), The case for rainfall on a warm, wet early Mars, *Journal of Geophysical Research (Planets)*, *107*, 21-21-21-36.

Curtis, C. D., and D. A. Spears (1971), Diagenetic Development of Kaolinite *Clays and Clay Minerals*, *19*, 219-227.

Davila, A. F., C. Gross, G. A. Marzo, A. G. Fairén, T. Kneissl, C. P. McKay, and J. M. Dohm (2011), A large sedimentary basin in the Terra Sirenum region of the southern highlands of Mars, *Icarus*, *212*(2), 579-589. doi: 10.1016/j.icarus.2010.12.023

de Pablo, M. A. (2003), MOLA Topographic Data Analysis of the Atlantis Paleolake Basin, Sirenum Terrae, Mars, in *Sixth International Conference on Mars*, edited by A. L. Albee, p. 3037.

de Pablo, M. A., A. G. Fairén, A. Márquez, and E. Stansbery (2004), The Geology of Atlantis Basin, Mars, and Its Astrobiological Interest, in *Lunar and Planetary Institute Science Conference Abstracts*, edited by S. Mackwell, p. 1223.

de Pablo, M. A., and A. G. Fairén (2004), Atlantis basin, Sirenum Terrae, Mars: geological setting and astrobiological implications, *International Journal of Astrobiology*, *3*, 257-263.

de Pablo, M. A., A. Márquez, J. D. Centeno, and E. Stansbery (2005), Geomorphologic Map of the Atlantis Basin, Terra Sirenum, Mars, in *36th Annual Lunar and Planetary Science Conference*, edited by S. Mackwell, p. 1297.

de Villiers, G., M. G. Kleinhans, and G. Postma (2013), Experimental delta formation in crater lakes and implications for interpretation of Martian deltas, *Journal of Geophysical Research (Planets)*, *118*, 651-670.

di Achille, G., M. R. T. Hoke, A. P. Rossi, B. M. Hynek, F. Esposito, E. W. H. Hutton, and A. J. Kettner (2012), Process-Response Sedimentary Modeling of Ancient Martian Deltas 1: Introduction and Case Studies, in *Lunar and Planetary Science Conference*, edited.

Dundas, C. M., S. Diniega, and A. S. McEwen (2015), Long-term monitoring of martian gully formation and evolution with MRO/HiRISE, *Icarus*, *251*, 244-263. doi: 10.1016/j.icarus.2014.05.013

Edgett, K. S., and M. C. Malin (2000), New views of Mars eolian activity, materials, and surface properties: Three vignettes from the Mars Global Surveyor Mars Orbiter Camera, *Journal of Geophysical Research: Planets*, *105*(E1), 1623-1650. doi: 10.1029/1999je001152

Ehlmann, B. L., J. F. Mustard, C. I. Fassett, S. C. Schon, J. W. Head, III, D. J. Des Marais, J. A. Grant, and S. L. Murchie (2008), Clay minerals in delta deposits and organic preservation potential on Mars, *Nature Geoscience*, *1*, 355-358.

Ehlmann, B. L., J. F. Mustard, G. A. Swayze, R. N. Clark, J. L. Bishop, F. Poulet, D. J. Des Marais, L. H. Roach, R. E. Milliken, J. J. Wray, O. Barnouin-Jha, and S. L. Murchie (2009), Identification of hydrated silicate minerals on Mars using MRO-CRISM: Geologic context near Nili Fossae and implications for aqueous alteration, *Journal of Geophysical Research*, *114*. doi: 10.1029/2009je003339

Ehlmann, B. L., J. F. Mustard, S. L. Murchie, J. P. Bibring, A. Meunier, A. A. Fraeman, and Y. Langevin (2011), Subsurface water and clay mineral formation during the early history of Mars, *Nature*, *479*(7371), 53-60. doi: 10.1038/nature10582

El-Maarry, M. R., A. Pommerol, and N. Thomas (2013), Analysis of polygonal cracking patterns in chloride-bearing terrains on Mars: Indicators of ancient playa settings, *Journal of Geophysical Research: Planets*, *118*(11), 2263-2278. doi: 10.1002/2013je004463

El-Maarry, M. R., W. Watters, N. K. McKeown, J. Carter, E. Noe Dobrea, J. L. Bishop, A. Pommerol, and N. Thomas (2014), Potential desiccation cracks on Mars: A synthesis from modeling, analogue-field studies, and global observations, *Icarus*, *241*(0), 248-268. doi: 10.1016/j.icarus.2014.06.033

ESRI (2013), Arcgis resource center, edited, URL http://resources.arcgis.com/en/help/.

Fairén, A. G. (2010), A cold and wet Mars, *Icarus*, *208*, 165-175.

Fassett, C. I., and J. W. Head (2007), Valley formation on martian volcanoes in the Hesperian: Evidence for melting of summit snowpack, caldera lake formation, drainage and erosion on Ceraunius Tholus, *Icarus*, *189*, 118-135.

Fassett, C. I., and J. W. Head (2008), Valley network-fed, open-basin lakes on Mars: Distribution and implications for Noachian surface and subsurface hydrology, *Icarus*, *198*, 37-56.

Fassett, C. I., J. L. Dickson, J. W. Head, J. S. Levy, and D. R. Marchant (2010), Supraglacial and proglacial valleys on Amazonian Mars, *Icarus*, *208*(1), 86-100. doi: 10.1016/j.icarus.2010.02.021

Fergason, R. L., P. R. Christensen, and H. H. Kieffer (2006), High-resolution thermal inertia derived from the Thermal Emission Imaging System (THEMIS): Thermal model and applications, *Journal of Geophysical Research (Planets)*, *111*, 12004.

Forget, F., R. M. Haberle, F. Montmessin, B. Levrard, and J. W. Head (2006), Formation of Glaciers on Mars by Atmospheric Precipitation at High Obliquity, *Science*, *311*, 368-371.

Frey, H. V. (2006), Impact constraints on, and a chronology for, major events in early Mars history, *Journal of Geophysical Research: Planets*, *111*(E8), n/a-n/a. doi: 10.1029/2005je002449

Gallagher, C., and M. Balme (2015), Eskers in a complete, wet-based glacial system in the Phlegra Montes region, Mars, *Earth and Planetary Science Letters*, *431*, 96-109.

Gillespie, A. R., A. B. Kahle, and R. E. Walker (1986), Color enhancement of highly correlated images. I. Decorrelation and HSI contrast stretches, *Remote Sensing of Environment*, *20*(3), 209-235. doi: 10.1016/0034-4257(86)90044-1

Glotch, T. D., J. L. Bandfield, L. L. Tornabene, H. B. Jensen, and F. P. Seelos (2010), Distribution and formation of chlorides and phyllosilicates in Terra Sirenum, Mars, *Geophysical Research Letters*, *37*(16). doi: 10.1029/2010gl044557

Goudge, T. A., J. F. Mustard, J. W. Head, and C. I. Fassett (2012), Constraints on the history of open-basin lakes on Mars from the composition and timing of volcanic resurfacing, *Journal of Geophysical Research (Planets), 117*.

Gradstein, F. M. (2012), Chapter 1 - Introduction, in *The Geologic Time Scale*, edited, pp. 1-29, Elsevier, Boston.

Grant, J. A., and P. H. Schultz (1990), Gradational epochs on Mars - Evidence from west-northwest of Isidis Basin and Electris, *Icarus, 84*, 166-195. doi: 10.1016/0019-1035(90)90164-5

Grant, J. A., R. P. Irwin, J. P. Grotzinger, R. E. Milliken, L. L. Tornabene, A. S. McEwen, C. M. Weitz, S. W. Squyres, T. D. Glotch, and B. J. Thomson (2008), HiRISE imaging of impact megabreccia and sub-meter aqueous strata in Holden Crater, Mars, *Geology*, *36*(3), 195. doi: 10.1130/g24340a.1

Grant, J. A., S. A. Wilson, E. Noe Dobrea, R. L. Fergason, J. L. Griffes, J. M. Moore, and A. D. Howard (2010), HiRISE views enigmatic deposits in the Sirenum Fossae region of Mars, *Icarus, 205*(1), 53-63. doi: 10.1016/j.icarus.2009.04.009

Greeley, R., R. N. Leach, S. H. Williams, B. R. White, J. B. Pollack, D. H. Krinsley, and J. R. Marshall (1982), Rate of wind abrasion on Mars, *Journal of Geophysical Research: Solid Earth, 87*(B12), 10009-10024. doi: 10.1029/JB087iB12p10009

Greeley, R., and B. D. Schneid (1991), Magma Generation on Mars: Amounts, Rates, and Comparisons with Earth, Moon, and Venus, *Science*, *254*(5034), 996-998. doi: 10.1126/science.254.5034.996

Greeley, R., B. H. Foing, H. Y. McSween, G. Neukum, P. Pinet, M. van Kan, S. C. Werner, D. A. Williams, and T. E. Zegers (2005), Fluid lava flows in Gusev crater, Mars, *Journal of Geophysical Research (Planets), 110*, 5008.

Greve, R., B. Grieger, and O. J. Stenzel (2010), MAIC-2, a latitudinal model for the Martian surface temperature, atmospheric water transport and surface glaciation, *Planetary and Space Science, 58*(6), 931-940. doi: 10.1016/j.pss.2010.03.002

Grotzinger, J. P., S. Gupta, M. C. Malin, D. M. Rubin, J. Schieber, K. Siebach, D. Y. Sumner, K. M. Stack, A. R. Vasavada, R. E. Arvidson, F. Calef, L. Edgar, W. F. Fischer, J. A. Grant, J. Griffes, L. C. Kah, M. P. Lamb, K. W. Lewis, N. Mangold, M. E. Minitti, M. Palucis, M. Rice, R. M. E. Williams, R. A. Yingst, D. Blake, D. Blaney, P. Conrad, J. Crisp, W. E. Dietrich, G. Dromart, K. S. Edgett, R. C. Ewing, R. Gellert, J. A. Hurowitz, G. Kocurek, P. Mahaffy, M. J. McBride, S. M. McLennan, M. Mischna, D. Ming, R. Milliken, H. Newsom, D. Oehler, T. J. Parker, D. Vaniman, R. C. Wiens, and S. A. Wilson (2015), Deposition, exhumation, and paleoclimate of an ancient lake deposit, Gale crater, Mars, *Science, 350*(aac7575-1 - aac7575-12). doi: 10.1126/science.aac7575

Gwinner, K., F. Scholten, F. Preusker, S. Elgner, T. Roatsch, M. Spiegel, R. Schmidt, J. Oberst, R. Jaumann, and C. Heipke (2010), Topography of Mars from global mapping by HRSC high-resolution digital terrain models and orthoimages: Characteristics and performance, *Earth and Planetary Science Letters, 294*, 506-519.

Hartmann, W. K. (1971), Martian cratering III: Theory of crater obliteration, *Icarus*, *15*(3), 410-428. doi: 10.1016/0019-1035(71)90119-9

Hartmann, W. K., and G. Neukum (2001), Cratering Chronology and the Evolution of Mars, *Space Science Reviews*, *96*, 165-194.

Hartmann, W. K. (2005), Martian cratering 8: Isochron refinement and the chronology of Mars, *Icarus*, *174*(2), 294-320. doi: 10.1016/j.icarus.2004.11.023

Hauber, E., K. Gwinner, M. Kleinhans, D. Reiss, G. Di Achille, G.-G. Ori, F. Scholten, L. Marinangeli, R. Jaumann, and G. Neukum (2009), Sedimentary deposits in Xanthe Terra: Implications for the ancient climate on Mars, *Planetary and Space Science*, *57*, 944-957.

Hauber, E., D. Reiss, M. Ulrich, F. Preusker, and F. Trauthan (2011), Landscape evolution in Martian mid-latitude regions: insights from analogous periglacial landforms in Svalbard, *Geological Society of London Special Publications*, *356*, 111-131.

Hauber, E., T. Platz, D. Reiss, L. Le Deit, M. G. Kleinhans, W. A. Marra, T. Haas, and P. Carbonneau (2013), Asynchronous formation of Hesperian and Amazonian-aged deltas on Mars and implications for climate, *Journal of Geophysical Research (Planets)*, *118*, 1529-1544.

Head, J. W., and D. R. Marchant (2003), Cold-based mountain glaciers on Mars: Western Arsia Mons, *Geology*, *31*, 641-644.

Head, J. W., J. F. Mustard, M. A. Kreslavsky, R. E. Milliken, and D. R. Marchant (2003), Recent ice ages on Mars, *Nature*, *426*, 797-802.

Head, J. W., G. Neukum, R. Jaumann, H. Hiesinger, E. Hauber, M. Carr, P. Masson, B. Foing, H. Hoffmann, M. Kreslavsky, S. Werner, S. Milkovich, S. van Gasselt, and H. C.-I. Team (2005), Tropical to mid-latitude snow and ice accumulation, flow and glaciation on Mars, *Nature*, *434*, 346-351.

Head, J. W., D. R. Marchant, M. C. Agnew, C. I. Fassett, and M. A. Kreslavsky (2006), Extensive valley glacier deposits in the northern mid-latitudes of Mars: Evidence for Late Amazonian obliquity-driven climate change, *Earth and Planetary Science Letters*, *241*, 663-671.

Hobley, D. E. J., A. D. Howard, and J. M. Moore (2014), Fresh shallow valleys in the Martian midlatitudes as features formed by meltwater flow beneath ice, *Journal of Geophysical Research (Planets)*, *119*, 128-153.

Holt, J. W., A. Safaeinili, J. J. Plaut, J. W. Head, R. J. Phillips, R. Seu, S. D. Kempf, P. Choudhary, D. A. Young, N. E. Putzig, D. Biccari, and Y. Gim (2008), Radar Sounding Evidence for Buried Glaciers in the Southern Mid-Latitudes of Mars, *Science*, *322*(5905), 1235-1238. doi: 10.1126/science.1164246

Howard, A. D., and J. M. Moore (2004), Scarp-bounded benches in Gorgonum Chaos, Mars: Formed beneath an ice-covered lake?, *Geophysical Research Letters*, *31*, 1702.

Howard, A. D., and J. M. Moore (2011), Late Hesperian to early Amazonian midlatitude Martian valleys: Evidence from Newton and Gorgonum basins, *Journal of Geophysical Research (Planets)*, *116*, E05003. doi: 10.1029/2010JE003782

Hubbard, B., R. E. Milliken, J. S. Kargel, A. Limaye, and C. Souness (2011), Geomorphological characterisation and interpretation of a mid-latitude glacier-like form: Hellas Planitia, Mars, *Icarus*, *211*, 330-346.

Hubbard, B., C. Souness, and S. Brough (2014), Glacier-like forms on Mars, *The Cryosphere*, *8*(6), 2047-2061. doi: 10.5194/tc-8-2047-2014

Hynek, B. M., M. Beach, and M. R. T. Hoke (2010), Updated global map of Martian valley networks and implications for climate and hydrologic processes, *Journal of Geophysical Research (Planets)*, *115*, E09008. doi: 10.1029/2009JE003548

Irwin, R. P., T. A. Maxwell, A. D. Howard, R. A. Craddock, and D. W. Leverington (2002), A Large Paleolake Basin at the Head of Ma'adim Vallis, Mars, *Science*, *296*, 2209-2212.

Irwin, R. P., A. D. Howard, and T. A. Maxwell (2004), Geomorphology of Ma'adim Vallis, Mars, and associated paleolake basins, *Journal of Geophysical Research (Planets)*, *109*, 12009.

Irwin, R. P., III, and A. D. Howard (2002), Drainage basin evolution in Noachian Terra Cimmeria, Mars, *J. Geophys. Res.*, *107*(E7), 5056. doi: 10.1029/2001je001818

Irwin, R. P., III, and J. R. Zimbelman (2012), Morphometry of Great Basin pluvial shore landforms: Implications for paleolake basins on Mars, *Journal of Geophysical Research (Planets)*, *117*, 7004.

Ivanov, B. A. (2001), Mars/Moon Cratering Rate Ratio Estimates, *Space Science Reviews*, *96*, 87-104.

Jaumann, R., G. Neukum, T. Behnke, T. C. Duxbury, K. Eichentopf, J. Flohrer, S. v. Gasselt, B. Giese, K. Gwinner, E. Hauber, H. Hoffmann, A. Hoffmeister, U. Köhler, K.-D. Matz, T. B. McCord, V. Mertens, J. Oberst, R. Pischel, D. Reiss, E. Ress, T. Roatsch, P. Saiger, F. Scholten, G. Schwarz, K. Stephan, M. Wählisch, and t. H. C.-I. Team (2007), The high-resolution stereo camera (HRSC) experiment on Mars Express: Instrument aspects and experiment conduct from interplanetary cruise through the nominal mission, *Planetary and Space Science*, *55*, 928-952. doi: 10.1016/j.pss.2006.12.003

Jaumann, R., A. Nass, D. Tirsch, D. Reiss, and G. Neukum (2010), The Western Libya Montes Valley System on Mars: Evidence for episodic and multi-genetic erosion events during the Martian history, *Earth and Planetary Science Letters*, *294*, 272-290.

Jaumann, R., D. Tirsch, E. Hauber, G. Erkeling, H. Hiesinger, L. Le Deit, M. Sowe, S. Adeli, A. Petau, and D. Reiss (2014), Water and Martian habitability: Results of an integrative study of water related processes on Mars in context with an interdisciplinary Helmholtz research alliance "Planetary Evolution and Life", *Planetary and Space Science*, *98*, 128-145. doi: 10.1016/j.pss.2014.02.013

Kerber, L., F. Forget, J.-B. Madeleine, R. Wordsworth, J. W. Head, and L. Wilson (2013), The effect of atmospheric pressure on the dispersal of pyroclasts from martian volcanoes, *Icarus*, *223*(1), 149-156. doi: 10.1016/j.icarus.2012.11.037

Kieffer, H. H., S. C. Chase, Jr., E. Miner, G. Münch, and G. Neugebauer (1973), Preliminary report on infrared radiometric measurements from the Mariner 9 spacecraft, *Journal of Geophysical Research*, *78*, 4291-4312.

Kirk, R. L., E. Howington-Kraus, M. R. Rosiek, J. A. Anderson, B. A. Archinal, K. J. Becker, D. A. Cook, D. M. Galuszka, P. E. Geissler, T. M. Hare, I. M. Holmberg, L. P. Keszthelyi, B. L. Redding, W. A. Delamere, D. Gallagher, J. D. Chapel, E. M. Eliason, R. King, and A. S. McEwen (2008), Ultrahigh resolution topographic mapping of Mars with MRO HiRISE stereo images: Meter-scale slopes of candidate Phoenix landing sites, *Journal of Geophysical Research (Planets)*, *113*(E3), E00A24. doi: 10.1029/2007JE003000

Kleinhans, M. G. (2005), Flow discharge and sediment transport models for estimating a minimum timescale of hydrological activity and channel and delta formation on Mars, *Journal of Geophysical Research (Planets)*, *110*, E12003. doi: 10.1029/2005JE002521

Kleinhans, M. G., H. E. van de Kasteele, and E. Hauber (2010), Palaeoflow reconstruction from fan delta morphology on Mars, *Earth and Planetary Science Letters*, *294*(3-4), 378-392. doi: 10.1016/j.epsl.2009.11.025

Kleinhans, M. G., R. I. Ferguson, S. N. Lane, and R. J. Hardy (2013), Splitting rivers at their seams: bifurcations and avulsion, *Earth Surface Processes and Landforms*, *38*(1), 47-61. doi: 10.1002/esp.3268

Kneissl, T., S. van Gasselt, and G. Neukum (2011), Map-projection-independent crater size-frequency determination in GIS environments—New software tool for ArcGIS, *Planetary and Space Science*, *59*, 1243-1254. doi: 10.1016/j.pss.2010.03.015

Kneissl, T., G. G. Michael, T. Platz, and S. H. G. Walter (2015), Age determination of linear surface features using the Buffered Crater Counting approach - Case studies of the Sirenum and Fortuna Fossae graben systems on Mars, *Icarus*, *250*, 384-394.

Kostama, V.-P., M. A. Kreslavsky, and J. W. Head (2006), Recent high-latitude icy mantle in the northern plains of Mars: Characteristics and ages of emplacement, *Geophysical Research Letters*, *33*, L11201. doi: 10.1029/2006GL025946

Kreslavsky, M. A., and J. W. Head (2002), Mars: Nature and evolution of young latitude-dependent water-ice-rich mantle, *Geophysical Research Letters*, *29*, 14-11–14-14. doi: 10.1029/2002GL015392

Kress, A. M., and J. W. Head (2008), Ring-mold craters in lineated valley fill and lobate debris aprons on Mars: Evidence for subsurface glacial ice, *Geophysical Research Letters*, *35*.

Lammer, H., E. Chassefière, Ö. Karatekin, A. Morschhauser, P. B. Niles, O. Mousis, P. Odert, U. V. Möstl, D. Breuer, V. Dehant, M. Grott, H. Gröller, E. Hauber, and L. B. S. Pham (2013), Outgassing

History and Escape of the Martian Atmosphere and Water Inventory, *Space Science Reviews*, *174*, 113-154.

Laskar, J., A. C. M. Correia, M. Gastineau, F. Joutel, B. Levrard, and P. Robutel (2004), Long term evolution and chaotic diffusion of the insolation quantities of Mars, *Icarus*, *170*, 343-364.

Le Deit, L., S. Le Mouélic, O. Bourgeois, J.-P. Combe, D. Mège, C. Sotin, A. Gendrin, E. Hauber, N. Mangold, and J.-P. Bibring (2008), Ferric oxides in East Candor Chasma, Valles Marineris (Mars) inferred from analysis of OMEGA/Mars Express data: Identification and geological interpretation, *Journal of Geophysical Research: Planets*, *113*(E7), n/a-n/a. doi: 10.1029/2007je002950

Le Deit, L., J. Flahaut, C. Quantin, E. Hauber, D. Mège, O. Bourgeois, J. Gurgurewicz, M. Massé, and R. Jaumann (2012), Extensive surface pedogenic alteration of the Martian Noachian crust suggested by plateau phyllosilicates around Valles Marineris, *Journal of Geophysical Research*, *117*. doi: 10.1029/2011je003983

Léveillé, R. J., J. Bridges, R. C. Wiens, N. Mangold, A. Cousin, N. Lanza, O. Forni, A. Ollila, J. Grotzinger, S. Clegg, K. Siebach, G. Berger, B. Clark, C. Fabre, R. Anderson, O. Gasnault, D. Blaney, L. Deflores, L. Leshin, S. Maurice, and H. Newsom (2014), Chemistry of fracture-filling raised ridges in Yellowknife Bay, Gale Crater: window into past aqueous activity and habitability on Mars, *Journal of Geophysical Research: Planets*, 2014JE004620. doi: 10.1002/2014je004620

Leverington, D. W. (2004), Volcanic rilles, streamlined islands, and the origin of outflow channels on Mars, *Journal of Geophysical Research: Planets*, *109*(E10), n/a-n/a. doi: 10.1029/2004je002311

Levrard, B., F. Forget, F. Montmessin, and J. Laskar (2007), Recent formation and evolution of northern Martian polar layered deposits as inferred from a Global Climate Model, *Journal of Geophysical Research: Planets*, *112*(E6), n/a-n/a. doi: 10.1029/2006je002772

Levy, J., J. Head, and D. Marchant (2008), Thermal Contraction Crack Polygon Classification and Distribution: Morphological Variations in Northern Hemisphere Patterned Ground, in *European Planetary Science Congress 2008*, edited, p. 459.

Levy, J., J. Head, and D. Marchant (2009), Thermal contraction crack polygons on Mars: Classification, distribution, and climate implications from HiRISE observations, *Journal of Geophysical Research: Planets*, *114*(E1), E01007. doi: 10.1029/2008je003273

Levy, J., J. W. Head, and D. R. Marchant (2010), Concentric crater fill in the northern mid-latitudes of Mars: Formation processes and relationships to similar landforms of glacial origin, *Icarus*, *209*, 390-404.

Levy, J. S., C. I. Fassett, J. W. Head, C. Schwartz, and J. L. Watters (2014), Sequestered glacial ice contribution to the global Martian water budget: Geometric constraints on the volume of remnant, midlatitude debris-covered glaciers, *Journal of Geophysical Research: Planets*, *119*(10), 2188-2196. doi: 10.1002/2014je004685

Loizeau, D., N. Mangold, F. Poulet, V. Ansan, E. Hauber, J.-P. Bibring, B. Gondet, Y. Langevin, P. Masson, and G. Neukum (2010), Stratigraphy in the Mawrth Vallis region through OMEGA, HRSC color imagery and DTM, *Icarus*, *205*, 396-418.

Loizeau, D., S. C. Werner, N. Mangold, J.-P. Bibring, and J. L. Vago (2012), Chronology of deposition and alteration in the Mawrth Vallis region, Mars, *Planetary and Space Science*, *72*, 31-43.

Madeleine, J.-B., F. Forget, J. W. Head, B. Levrard, F. Montmessin, and E. Millour (2009), Amazonian northern mid-latitude glaciation on Mars: A proposed climate scenario, *Icarus*, *203*, 390-405.

Madeleine, J.-B., J. W. Head, F. Forget, T. Navarro, E. Millour, A. Spiga, A. Colaïtis, A. Määttänen, F. Montmessin, and J. L. Dickson (2014), Recent Ice Ages on Mars: The role of radiatively active clouds and cloud microphysics, *Geophysical Research Letters*, *41*, 4873-4879.

Madeleine, J. B., F. Forget, E. Millour, T. Navarro, and A. Spiga (2012), The influence of radiatively active water ice clouds on the Martian climate, *Geophysical Research Letters*, *39*(23), n/a-n/a. doi: 10.1029/2012gl053564

Malin, M. C., and K. S. Edgett (2000a), Sedimentary Rocks of Early Mars, *Science*, *290*, 1927-1937.

Malin, M. C., and K. S. Edgett (2000b), Evidence for Recent Groundwater Seepage and Surface Runoff on Mars, *Science*, *288*, 2330-2335.

Malin, M. C., M. A. Caplinger, and S. D. Davis (2001), Observational Evidence for an Active Surface Reservoir of Solid Carbon Dioxide on Mars, *Science*, *294*(5549), 2146-2148. doi: 10.1126/science.1066416

Malin, M. C., and K. S. Edgett (2001), Mars Global Surveyor Mars Orbiter Camera: Interplanetary cruise through primary mission, *Journal of Geophysical Research: Planets*, *106*(E10), 23429-23570. doi: 10.1029/2000je001455

Malin, M. C., and K. S. Edgett (2003), Evidence for Persistent Flow and Aqueous Sedimentation on Early Mars, *Science*, *302*, 1931-1934.

Malin, M. C., J. F. Bell, III, B. A. Cantor, M. A. Caplinger, W. M. Calvin, R. T. Clancy, K. S. Edgett, L. Edwards, R. M. Haberle, P. B. James, S. W. Lee, M. A. Ravine, P. C. Thomas, and M. J. Wolff (2007), Context Camera Investigation on board the Mars Reconnaissance Orbiter, *J. Geophys. Res.*, *112*(E5), E05S04. doi: 10.1029/2006je002808

Mangold, N. (2003), Geomorphic analysis of lobate debris aprons on Mars at Mars Orbiter Camera scale: Evidence for ice sublimation initiated by fractures, *Journal of Geophysical Research (Planets)*, *108*.

Mangold, N., F. Poulet, J. F. Mustard, J.-P. Bibring, B. Gondet, Y. Langevin, V. Ansan, P. Masson, C. Fassett, J. W. Head, H. Hoffmann, and G. Neukum (2007), Mineralogy of the Nili Fossae region with OMEGA/Mars Express data: 2. Aqueous alteration of the crust, *Journal of Geophysical Research (Planets)*, *112*.

Mangold, N. (2011), Ice sublimation as a geomorphic process: A planetary perspective, *Geomorphology*, *126*, 1-17. doi: 10.1016/j.geomorph.2010.11.009

Mangold, N., S. Adeli, S. Conway, V. Ansan, and B. Langlais (2012a), A chronology of early Mars climatic evolution from impact crater degradation, *Journal of Geophysical Research (Planets)*, *117*(E4), E04003. doi: 10.1029/2011JE004005

Mangold, N., J. Carter, F. Poulet, E. Dehouck, V. Ansan, and D. Loizeau (2012b), Late Hesperian aqueous alteration at Majuro crater, Mars, *Planetary and Space Science*, *72*, 18-30.

Mangold, N., and A. D. Howard (2013), Outflow channels with deltaic deposits in Ismenius Lacus, Mars, *Icarus*, *226*, 385-401.

Marchant, D. R., and J. W. Head (2007), Antarctic dry valleys: Microclimate zonation, variable geomorphic processes, and implications for assessing climate change on Mars, *Icarus*, *192*(1), 187-222. doi: 10.1016/j.icarus.2007.06.018

Marzo, G. A., A. F. Davila, L. L. Tornabene, J. M. Dohm, A. G. Fairén, C. Gross, T. Kneissl, J. L. Bishop, T. L. Roush, and C. P. McKay (2010), Evidence for Hesperian impact-induced hydrothermalism on Mars, *Icarus*, *208*, 667-683.

Matsubara, Y., A. D. Howard, D. M. Burr, R. M. E. Williams, W. E. Dietrich, and J. M. Moore (2015), River meandering on Earth and Mars: A comparative study of Aeolis Dorsa meanders, Mars and possible terrestrial analogs of the Usuktuk River, AK, and the Quinn River, NV, *Geomorphology*, *240*, 102-120. doi: 10.1016/j.geomorph.2014.08.031

McEwen, A. S., E. M. Eliason, J. W. Bergstrom, N. T. Bridges, C. J. Hansen, W. A. Delamere, J. A. Grant, V. C. Gulick, K. E. Herkenhoff, L. Keszthelyi, R. L. Kirk, M. T. Mellon, S. W. Squyres, N. Thomas, and C. M. Weitz (2007), Mars Reconnaissance Orbiter's High Resolution Imaging Science Experiment (HiRISE), *J. Geophys. Res.*, *112*(E5), E05S02. doi: 10.1029/2005je002605

McEwen, A. S., L. Ojha, C. M. Dundas, S. Mattson, and M. Masse (2011a), Recent Observations of Recurring Slope Lineae on Mars, *AGU Fall Meeting Abstracts*, *21*.

McEwen, A. S., L. Ojha, C. M. Dundas, S. S. Mattson, S. Byrne, J. J. Wray, S. C. Cull, S. L. Murchie, N. Thomas, and V. C. Gulick (2011b), Seasonal Flows on Warm Martian Slopes, *Science*, *333*, 740-743. doi: 10.1126/science.1204816

McGuire, P. C., J. L. Bishop, A. J. Brown, A. A. Fraeman, G. A. Marzo, M. Frank Morgan, S. L. Murchie, J. F. Mustard, M. Parente, S. M. Pelkey, T. L. Roush, F. P. Seelos, M. D. Smith, L. Wendt, and M. J. Wolff (2009), An improvement to the volcano-scan algorithm for atmospheric correction of CRISM and OMEGA spectral data, *Planetary and Space Science*, *57*, 809-815. doi: 10.1016/j.pss.2009.03.007

McKeown, N. K., J. L. Bishop, E. Z. Noe Dobrea, B. L. Ehlmann, M. Parente, J. F. Mustard, S. L. Murchie, G. A. Swayze, J.-P. Bibring, and E. A. Silver (2009), Characterization of phyllosilicates observed in the central Mawrth Vallis region, Mars, their potential formational processes, and implications for past climate, *Journal of Geophysical Research*, *114*. doi: 10.1029/2008je003301

McKeown, N. K., J. L. Bishop, and E. A. Silver (2013), Variability of rock texture and morphology correlated with the clay-bearing units at Mawrth Vallis, Mars, *Journal of Geophysical Research (Planets)*, *118*, 1245-1256.

McLennan, S. M., J. F. Bell, W. M. Calvin, P. R. Christensen, B. C. Clark, P. A. de Souza, J. Farmer, W. H. Farrand, D. A. Fike, R. Gellert, A. Ghosh, T. D. Glotch, J. P. Grotzinger, B. Hahn, K. E. Herkenhoff, J. A. Hurowitz, J. R. Johnson, S. S. Johnson, B. Jolliff, G. Klingelhöfer, A. H. Knoll, Z. Learner, M. C. Malin, H. Y. McSween, J. Pocock, S. W. Ruff, L. A. Soderblom, S. W. Squyres, N. J. Tosca, W. A. Watters, M. B. Wyatt, and A. Yen (2005), Provenance and diagenesis of the evaporite-bearing Burns formation, Meridiani Planum, Mars, *Earth and Planetary Science Letters*, *240*, 95-121.

Mellon, M. T., and B. M. Jakosky (1993), Geographic variations in the thermal and diffusive stability of ground ice on Mars, *Journal of Geophysical Research: Planets*, *98*(E2), 3345-3364. doi: 10.1029/92je02355

Mellon, M. T., and B. M. Jakosky (1995), The distribution and behavior of Martian ground ice during past and present epochs, *Journal of Geophysical Research*, *100*, 11781-11799.

Melosh, H. J., and A. M. Vickery (1989), Impact erosion of the primordial atmosphere of Mars, *Nature*, *338*(6215), 487-489. doi: 10.1038/338487a0

Michael, G. G., and G. Neukum (2010), Planetary surface dating from crater size-frequency distribution measurements: Partial resurfacing events and statistical age uncertainty, *Earth and Planetary Science Letters*, *294*, 223-229. doi: 10.1016/j.epsl.2009.12.041

Michael, G. G., T. Platz, T. Kneissl, and N. Schmedemann (2012), Planetary surface dating from crater size–frequency distribution measurements: Spatial randomness and clustering, *Icarus*, *218*(1), 169-177. doi: 10.1016/j.icarus.2011.11.033

Michael, G. G. (2013), Planetary surface dating from crater size–frequency distribution measurements: Multiple resurfacing episodes and differential isochron fitting, *Icarus*, *226*(1), 885-890. doi: 10.1016/j.icarus.2013.07.004

Milton, D. J. (1973), Water and processes of degradation in the Martian landscape, *Journal of Geophysical Research*, *78*(20), 4037-4047. doi: 10.1029/JB078i020p04037

Mischna, M. A., M. I. Richardson, R. J. Wilson, and D. J. McCleese (2003), On the orbital forcing of Martian water and CO2 cycles: A general circulation model study with simplified volatile schemes, *Journal of Geophysical Research (Planets)*, *108*, 16-11.

Molina, A., E. Hauber, L. Le Deit, S. Adeli, D. C. Fernández-Remolar, and M. A. de Pablo (2012), Geologic analysis of knob fields and sedimentary deposits in Ariadnes Colles, Terra Sirenum, Mars, in *European Planetary Science Congress 2012*, edited, p. 213.

Moore, J. M., A. D. Howard, W. E. Dietrich, and P. M. Schenk (2003a), Martian Layered Fluvial Deposits: Implications for Noachian Climate Scenarios, *Geophysical Research Letters*, *30*, 2292.

Moore, J. M., A. D. Howard, and E. Stansbery (2003b), Ariadnes-Gorgonum Knob Fields of North-Western Terra Sirenum, Mars, in *Lunar and Planetary Institute Science Conference Abstracts*, edited by S. Mackwell, p. 1402.

Moore, J. M., and A. D. Howard (2005), Large alluvial fans on Mars, *Journal of Geophysical Research: Planets*, *110*(E4), E04005. doi: 10.1029/2004je002352

Murchie, S., R. Arvidson, P. Bedini, K. Beisser, J. P. Bibring, J. Bishop, J. Boldt, P. Cavender, T. Choo, R. T. Clancy, E. H. Darlington, D. Des Marais, R. Espiritu, D. Fort, R. Green, E. Guinness, J. Hayes, C. Hash, K. Heffernan, J. Hemmler, G. Heyler, D. Humm, J. Hutcheson, N. Izenberg, R. Lee, J. Lees, D. Lohr, E. Malaret, T. Martin, J. A. McGovern, P. McGuire, R. Morris, J. Mustard, S. Pelkey, E. Rhodes, M. Robinson, T. Roush, E. Schaefer, G. Seagrave, F. Seelos, P. Silverglate, S. Slavney, M. Smith, W. J. Shyong, K. Strohbehn, H. Taylor, P. Thompson, B. Tossman, M. Wirzburger, and M. Wolff (2007), Compact Reconnaissance Imaging Spectrometer for Mars (CRISM) on Mars Reconnaissance Orbiter (MRO), *Journal of Geophysical Research*, *112*(E5), E05S03. doi: 10.1029/2006je002682

Murchie, S. L., F. P. Seelos, C. D. Hash, D. C. Humm, E. Malaret, J. A. McGovern, T. H. Choo, K. D. Seelos, D. L. Buczkowski, M. F. Morgan, O. S. Barnouin-Jha, H. Nair, H. W. Taylor, G. W. Patterson, C. A. Harvel, J. F. Mustard, R. E. Arvidson, P. McGuire, M. D. Smith, M. J. Wolff, T. N. Titus, J.-P. Bibring, and F. Poulet (2009), Compact Reconnaissance Imaging Spectrometer for Mars investigation and data set from the Mars Reconnaissance Orbiter's primary science phase, *Journal of Geophysical Research (Planets)*, *114*.

Mustard, J. F., C. D. Cooper, and M. K. Rifkin (2001), Evidence for recent climate change on Mars from the identification of youthful near-surface ground ice, *Nature*, *412*, 411-414.

Mustard, J. F., S. L. Murchie, S. M. Pelkey, B. L. Ehlmann, R. E. Milliken, J. A. Grant, J. P. Bibring, F. Poulet, J. Bishop, E. N. Dobrea, L. Roach, F. Seelos, R. E. Arvidson, S. Wiseman, R. Green, C. Hash, D. Humm, E. Malaret, J. A. McGovern, K. Seelos, T. Clancy, R. Clark, D. D. Marais, N. Izenberg, A. Knudson, Y. Langevin, T. Martin, P. McGuire, R. Morris, M. Robinson, T. Roush, M. Smith, G. Swayze, H. Taylor, T. Titus, and M. Wolff (2008a), Hydrated silicate minerals on Mars observed by the Mars Reconnaissance Orbiter CRISM instrument, *Nature*, *454*(7202), 305-309.

Mustard, J. F., S. L. Murchie, S. M. Pelkey, B. L. Ehlmann, R. E. Milliken, J. A. Grant, J. P. Bibring, F. Poulet, J. Bishop, E. N. Dobrea, L. Roach, F. Seelos, R. E. Arvidson, S. Wiseman, R. Green, C. Hash, D. Humm, E. Malaret, J. A. McGovern, K. Seelos, T. Clancy, R. Clark, D. D. Marais, N. Izenberg, A. Knudson, Y. Langevin, T. Martin, P. McGuire, R. Morris, M. Robinson, T. Roush, M. Smith, G. Swayze, H. Taylor, T. Titus, and M. Wolff (2008b), Hydrated silicate minerals on Mars observed by the Mars Reconnaissance Orbiter CRISM instrument, *Nature*, *454*(7202), 305-309. doi: 10.1038/nature07097

Nazarian, A. H., and A. D. Rogers (2013), Thermal Infrared Spectral Characterization of the Gorgonum-Atlantis Subregion of Mars' Eridania Basin, in *Lunar and Planetary Institute Science Conference Abstracts*, edited, p. 2628.

Neukum, G., and H. Dietzel (1971), On the development of the crater population on the moon with time under meteoroid and solar wind bombardment, *Earth and Planetary Science Letters*, *12*(1), 59-66. doi: 10.1016/0012-821X(71)90055-0

Neukum, G., B. Koenig, and J. Arkani-Hamed (1975), A study of lunar impact crater size-distributions, *Moon*, *12*, 201-229.

Neukum, G., R. Jaumann, and The HRSC Science and Experiment Team (2004), The High Resolution Stereo Camera of Mars Express, *ESA Special Publication*, *1240*, 17-35.

Nimmo, F., and K. Tanaka (2005), Early Crustal Evolution of Mars, *Annual Review of Earth and Planetary Sciences*, *33*, 133-161.

Noe Dobrea, E. Z., and G. Swayze (2010), Acid Pedogenesis on Mars? Evidence for Top-Down Alteration on Mars from CRISM and HiRISE Data, in *Lunar and Planetary Institute Science Conference Abstracts*, edited, p. 2620.

Nyquist, L. E., D. D. Bogard, C.-Y. Shih, A. Greshake, D. Stöffler, and O. Eugster (2001), Ages and Geologic Histories of Martian Meteorites, *Space Science Reviews*, *96*(1), 105-164. doi: 10.1023/a:1011993105172

Ojha, L., A. McEwen, C. Dundas, S. Byrne, S. Mattson, J. Wray, M. Masse, and E. Schaefer (2014), HiRISE observations of Recurring Slope Lineae (RSL) during southern summer on Mars, *Icarus*, *231*, 365-376.

Osterloo, M. M., V. E. Hamilton, J. L. Bandfield, T. D. Glotch, A. M. Baldridge, P. R. Christensen, L. L. Tornabene, and F. S. Anderson (2008), Chloride-Bearing Materials in the Southern Highlands of Mars, *Science*, *319*, 1651-.

Osterloo, M. M., F. S. Anderson, V. E. Hamilton, and B. M. Hynek (2010), Geologic context of proposed chloride-bearing materials on Mars, *Journal of Geophysical Research*, *115*(E10). doi: 10.1029/2010je003613

Parsons, R., and J. Holt (2016), Constraints on the formation and properties of a Martian lobate debris apron: Insights from high-resolution topography, SHARAD radar data, and a numerical ice flow model, *Journal of Geophysical Research: Planets*, *121*(3), 2015JE004927. doi: 10.1002/2015je004927

Plaut, J. J., A. Safaeinili, J. W. Holt, R. J. Phillips, J. W. Head, R. Seu, N. E. Putzig, and A. Frigeri (2009), Radar evidence for ice in lobate debris aprons in the mid-northern latitudes of Mars, *Geophysical Research Letters*, *36*(2), n/a-n/a. doi: 10.1029/2008gl036379

Poulet, F., J. P. Bibring, J. F. Mustard, A. Gendrin, N. Mangold, Y. Langevin, R. E. Arvidson, B. Gondet, C. Gomez, M. Berthe, S. Erard, O. Forni, N. Manaud, G. Poulleau, A. Soufflot, M. Combes, P. Drossart, T. Encrenaz, T. Fouchet, R. Melchiorri, G. Bellucci, F. Altieri, V. Formisano, S. Fonti, F. Capaccioni, P. Cerroni, A. Coradini, O. Korablev, V. Kottsov, N. Ignatiev, D. Titov, L. Zasova, P. Pinet, B. Schmitt, C. Sotin, E. Hauber, H. Hoffmann, R. Jaumann, U. Keller, and F. Forget (2005), Phyllosilicates on Mars and implications for early martian climate, *Nature*, *438*(7068), 623-627. doi: 10.1038/nature04274

Ruesch, O., F. Poulet, M. Vincendon, J.-P. Bibring, J. Carter, G. Erkeling, B. Gondet, H. Hiesinger, A. Ody, and D. Reiss (2012), Compositional investigation of the proposed chloride-bearing materials on

Mars using near-infrared orbital data from OMEGA/MEx, *Journal of Geophysical Research*, *117*. doi: 10.1029/2012je004108

Salese, F., G. Di Achille, A. Neesemann, G. G. Ori, and E. Hauber (2016), Hydrological and sedimentary analyses of well-preserved paleofluvial-paleolacustrine systems at Moa Valles, Mars, *Journal of Geophysical Research (Planets)*, *121*, 194-232. doi: 10.1002/2015JE004891

Saper, L., and J. F. Mustard (2013), Extensive linear ridge networks in Nili Fossae and Nilosyrtis, Mars: implications for fluid flow in the ancient crust, *Geophysical Research Letters*, *40*, 245-249.

Scholten, F., K. Gwinner, T. Roatsch, K.-D. Matz, M. Waehlisch, B. Giese, J. Oberst, R. Jaumann, G. Neukum, and T. H. C.-I. Team (2005), Mars Express HRSC Data Processing-Methods and Operational Aspects, *Photogrammetric Engineering & Remote Sensing*, *71*, 1143-1152.

Schumm, S. A. (1977), *The fluvial system*, The Blackburn Press.

Schuurman, F., and M. G. Kleinhans (2015), Bar dynamics and bifurcation evolution in a modelled braided sand-bed river, *Earth Surface Processes and Landforms*, *40*(10), 1318-1333. doi: 10.1002/esp.3722

Scott, D. H. (1978), Mars, highlands-lowlands: Viking contributions to mariner relative age studies, *Icarus*, *34*(3), 479-485. doi: 10.1016/0019-1035(78)90039-8

Scott, D. H. (1985), Global geologic mapping of Mars: The western equatorial region, *Advances in Space Research*, *5*(8), 71-82. doi: 10.1016/0273-1177(85)90243-1

Smith, D., Neumann G. , Arvidson R. E., Guinness E. A., and S. S. (2003), Mars Global Surveyor Laser Altimeter Mission Experiment Gridded Data Record, *NASA Planetary Data System*, *MGS-M-MOLA-5-MEGDR-L3-V1.0*.

Smith, D. E., M. T. Zuber, H. V. Frey, J. B. Garvin, J. W. Head, D. O. Muhleman, G. H. Pettengill, R. J. Phillips, S. C. Solomon, H. J. Zwally, W. B. Banerdt, T. C. Duxbury, M. P. Golombek, F. G. Lemoine, G. A. Neumann, D. D. Rowlands, O. Aharonson, P. G. Ford, A. B. Ivanov, C. L. Johnson, P. J. McGovern, J. B. Abshire, R. S. Afzal, and X. Sun (2001), Mars Orbiter Laser Altimeter: Experiment summary after the first year of global mapping of Mars, *Journal of Geophysical Research*, *106*, 23689-23722.

Smith, I. B., N. E. Putzig, J. W. Holt, and R. J. Phillips (2016), An ice age recorded in the polar deposits of Mars, *Science*, *352*(6289), 1075-1078. doi: 10.1126/science.aad6968

Souness, C., B. Hubbard, R. E. Milliken, and D. Quincey (2012), An inventory and population-scale analysis of martian glacier-like forms, *Icarus*, *217*, 243-255.

Squyres, S. W. (1978), Martian fretted terrain: Flow of erosional debris, *Icarus*, *34*(3), 600-613. doi: 10.1016/0019-1035(78)90048-9

Squyres, S. W., and M. H. Carr (1986), Geomorphic evidence for the distribution of ground ice on Mars, *Science*, *231*, 249-252.

Squyres, S. W., R. E. Arvidson, J. F. Bell, J. Brückner, N. A. Cabrol, W. Calvin, M. H. Carr, P. R. Christensen, B. C. Clark, L. Crumpler, D. J. Des Marais, C. d'Uston, T. Economou, J. Farmer, W. Farrand, W. Folkner, M. Golombek, S. Gorevan, J. A. Grant, R. Greeley, J. Grotzinger, L. Haskin, K. E. Herkenhoff, S. Hviid, J. Johnson, G. Klingelhöfer, A. Knoll, G. Landis, M. Lemmon, R. Li, M. B. Madsen, M. C. Malin, S. M. McLennan, H. Y. McSween, D. W. Ming, J. Moersch, R. V. Morris, T. Parker, J. W. Rice, L. Richter, R. Rieder, M. Sims, M. Smith, P. Smith, L. A. Soderblom, R. Sullivan, H. Wänke, T. Wdowiak, M. Wolff, and A. Yen (2004), The Spirit Rover's Athena Science Investigation at Gusev Crater, Mars, *Science*, *305*, 794-800.

Tanaka, K. L. (2005), Geology and insolation-driven climatic history of Amazonian north polar materials on Mars, *Nature*, *437*(7061), 991-994.

Tanaka, K. L., J. A. Skinner, L. S. Crumpler, and J. M. Dohm (2009), Assessment of planetary geologic mapping techniques for Mars using terrestrial analogs: The SP Mountain area of the San Francisco Volcanic Field, Arizona, *Planetary and Space Science*, *57*, 510-532.

Tanaka, K. L., J. A. Skinner, Jr.;, and T. M. Hare (2010), Planetary geologic mapping handbook, in *Abstracts of the Annual Meeting of Planetary Geologic Mappers*, edited by L. F. I. Bleamaster, K. L. Tanaka, M. S. Kelley and eds, NASA Conference Publication CP-2010-217041, Falgstaff, AZ, 2010: Washington DC.

Tanaka, K. L., and W. K. Hartmann (2012), Chapter 15 - The Planetary Time Scale, in *The Geologic Time Scale*, edited, pp. 275-298, Elsevier, Boston.

Tanaka, K. L., J. A. Skinner, Jr., J. M. Dohm, R. P. Irwin, III, E. J. Kolb, C. M. Fortezzo, T. Platz, G. G. Michael, and T. M. Hare (2014), Geologic map of Mars: U.S. Geological Survey Scientific Investigations Map 3292, scale 1:20,000,000, *pamphlet* 43. doi: 10.3133/sim3292

Tirsch, D., R. Jaumann, A. Pacifici, and F. Poulet (2011), Dark aeolian sediments in Martian craters: Composition and sources, *Journal of Geophysical Research: Planets*, *116*(E3), n/a-n/a. doi: 10.1029/2009je003562

Tosca, N. J., and S. M. McLennan (2006), Chemical divides and evaporite assemblages on Mars, *Earth and Planetary Science Letters*, *241*, 21-31.

Van De Lageweg, W. I., W. M. Van Dijk, and M. G. Kleinhans (2013), Morphological and Stratigraphical Signature of Floods In A Braided Gravel-Bed River Revealed From Flume Experiments, *Journal of Sedimentary Research*, *83*(11), 1032-1045. doi: 10.2110/jsr.2013.70

Warner, N. H., S. Gupta, F. Calef, P. Grindrod, N. Boll, and K. Goddard (2015), Minimum effective area for high resolution crater counting of martian terrains, *Icarus*, *245*, 198-240.

Weaver, C. E. (1989), *Clays, muds, and shales: C.E. Weaver. Developments in Sedimentology, 44, Elsevier, Amsterdam, 1989, 819 pp., ISBN 0-444-87381-3.*

Wendt, L., J. L. Bishop, G. Neukum, and N. Giesen (2012), Phyllosilcates in the Knob Fields around Ariadnes Colles on Mars: Stratigraphy, Mineralogy and Morphology, in *EGU General Assembly Conference Abstracts*, edited by A. Abbasi, p. 9105.

Wendt, L., J. L. Bishop, and G. Neukum (2013), Knob fields in the Terra Cimmeria/Terra Sirenum region of Mars: Stratigraphy, mineralogy and morphology, *Icarus*, *225*, 200-215.

Willmes, M., D. Reiss, H. Hiesinger, and M. Zanetti (2012), Surface age of the ice-dust mantle deposit in Malea Planum, Mars, *Planetary and Space Science*, *60*, 199-206.

Wilson, L., and J. W. Head (2002), Tharsis-radial graben systems as the surface manifestation of plume-related dike intrusion complexes: Models and implications, *Journal of Geophysical Research*, *107*(E8), 1-1–1-24. doi: 10.1029/2001je001593

Wilson, L., G. J. Ghatan, J. W. Head, and K. L. Mitchell (2004), Mars outflow channels: A reappraisal of the estimation of water flow velocities from water depths, regional slopes, and channel floor properties, *Journal of Geophysical Research (Planets)*, *109*, E09003. doi: 10.1029/2004JE002281

Wordsworth, R. D., L. Kerber, R. T. Pierrehumbert, F. Forget, and J. W. Head (2015), Comparison of "warm and wet" and "cold and icy" scenarios for early Mars in a 3-D climate model, *Journal of Geophysical Research: Planets*, *120*(6), 1201-1219. doi: 10.1002/2015je004787

Wray, J. J., R. E. Milliken, C. M. Dundas, G. A. Swayze, J. C. Andrews-Hanna, A. M. Baldridge, M. Chojnacki, J. L. Bishop, B. L. Ehlmann, S. L. Murchie, R. N. Clark, F. P. Seelos, L. L. Tornabene, and S. W. Squyres (2011), Columbus crater and other possible groundwater-fed paleolakes of Terra Sirenum, Mars, *Journal of Geophysical Research*, *116*(E1). doi: 10.1029/2010je003694

Curriculum Vitae Solmaz Adeli

For reasons of data protection, the curriculum vitae is not published in the electronic version. The reader is kindly referred to the printed version of this dissertation.